

MAXIMUM ENTROPY SPECTRAL ANALYSIS
OF FREE OSCILLATIONS OF THE EARTH:
THE 1964 ALASKA EVENT

by

John C. Davies

B.Sc., University of British Columbia, 1973

A THESIS SUBMITTED IN PARTIAL FULFILMENT OF
THE REQUIREMENTS FOR THE DEGREE OF
MASTER OF SCIENCE

in the Department
of
Geophysics and Astronomy

We accept this thesis as conforming to the
required standard

The University Of British Columbia

March, 1976

© John C. Davies

In presenting this thesis in partial fulfilment of the requirements for an advanced degree at the University of British Columbia, I agree that the Library shall make it freely available for reference and study.

I further agree that permission for extensive copying of this thesis for scholarly purposes may be granted by the Head of my Department or by his representatives. It is understood that copying or publication of this thesis for financial gain shall not be allowed without my written permission.

Department of

Geophysics

The University of British Columbia
2075 Wesbrook Place
Vancouver, Canada
V6T 1W5

Date

March 30/76

ABSTRACT

The UCLA gravimeter recording obtained after the 1964 Alaska earthquake, has been subjected to various, recently developed data processing techniques. In particular, the maximum entropy method (MEM) of spectral estimation and filter design was utilised.

Prediction filters were used to extend the original tidal gravimeter recording, so as to avoid information loss caused by tapering the record prior to filtering. Time adaptive prediction error filters were then used to locate noise bursts, or 'glitches', which are present in the filtered record. The record was then deglitched using two methods, one a predictive approach, and the other involving a division of the record by a weighted envelope function.

Power spectra using the classical periodogram approach, as well as MEM, were calculated for the filtered records, both before and after deglitching.

This analysis resulted in new values for the splitting parameter ' β ', and the centre frequency, for various free oscillation modes. A dramatic increase in the signal to noise ratio was also observed after the filtered records were deglitched. The presence of core mode oscillations was also

investigated, but no evidence for these undertones was found. Instead, numerous peaks attributed to either instrument non-linearities, or barometric pressure effects, were found in the frequency range 0.12 to 1.20 cycles per hour.

TABLE OF CONTENTS

	Page
ABSTRACT	i
TABLE OF CONTENTS	iii
LIST OF TABLES	v
LIST OF FIGURES	vi
ACKNOWLEDGEMENTS	viii
CHAPTER I. INTRODUCTION	
I-1. Purpose	1
I-2. Data Description	2
I-3. Free Oscillations	7
I-4. Spectral Splitting	10
I-5. Core Undertones	12
CHAPTER II. THEORETICAL BACKGROUND	
II-1. Classical Spectral Estimation	
A. Periodogram	14
B. Autocorrelation Function	15
II-2. Maximum Entropy Method	
A. Information and Entropy	16
B. Maximum Entropy Solution	18
C. Analytical Integration	19
D. Z-transform Approach	22
E. Heuristic Solution	24
II-3. Levinson Recursion	26
II-4. Autoregressive Models and MEM	28
II-5. Time Adaptive MEM	31
CHAPTER III. DATA ANALYSIS PROCEDURES	
III-1. Necessity of Tapering	35
III-2. Prediction	36
III-3. Filtering	36

III-4.	Deglitching	
A.	Identification	46
B.	Prediction into Gaps	47
C.	Deglitching by Envelope	52
III-5.	Power Spectral Analysis	
A.	Periodogram and MEM Spectra	61
B.	Complex Demodulation	64
CHAPTER IV. RESULTS		
IV-1.	Free Oscillation Mode Frequencies	
A.	$\circ S_2$ mode	68
B.	$\circ S_3$ mode	78
C.	$\circ S_4$ mode	86
D.	$\circ S_5$ mode	93
E.	$\circ S_6$ mode	99
IV-2.	Core Undertones	100
CHAPTER V	SUMMARY	110
REFERENCES		112
APPENDIX 1		115

LIST OF TABLES

		PAGE
Table 1.	$\circ S_2$ Frequencies	69
Table 2.	$\circ S_3$ Frequencies	79
Table 3.	$\circ S_4$ Frequencies	87
Table 4.	$\circ S_5$ Frequencies	94
Table 5.	$\circ S_6$ Frequencies	99

LIST OF FIGURES

	Page	
Figure 1.	Unprocessed gravimeter data	4
Figure 2.	Periodogram power of unprocessed data	6
Figure 3.	Predicted gravimeter data	38
Figure 4.	High pass filtered predicted data	41
Figure 5.	Band pass filtered predicted data	43
Figure 6.	High pass filtered unpredicted data	45
Figure 7.	Prediction error trace of high passed record	49
Figure 8.	Prediction error trace of band passed record	51
Figure 9.	Gap prediction test case	54
Figure 10.	Deglitched high passed record	56
Figure 11.	Deglitched band passed record	57
Figure 12.	Prediction error trace of deglitched high passed record	59
Figure 13.	Prediction error trace of deglitched band passed record	60
Figure 14.	Deglitched high passed record using envelope squared	63
Figure 15.	Power spectra of ${}_0S_2$ mode	73
Figure 16.	Power spectra of ${}_0S_3$ mode	82
Figure 17.	Power spectra of ${}_0S_4$ mode	89
Figure 18.	Power spectra of ${}_0S_5$ mode	96

Figure 19.	Power spectra of oS_6 mode	102
Figure 20.	Periodogram of undeglitched band passed record	107
Figure 21.	Periodogram of deglitched band passed record	108

ACKNOWLEDGEMENTS

I would like to thank Dr. T. J. Ulrych for many valuable discussions that took place during the course of this research project. Dr. Ulrych also devoted time and effort in the critical appraisal of this thesis, as well as provided the necessary financial support to see this project to an end.

My thanks also go to Dr. R. M. Clowes who gave a second opinion of this thesis and to Rob Clayton and George Spence who dropped several useful programming hints my way.

Much use was made of the University of British Columbia computing centre and the computing costs were born by a National Research Council of Canada grant made to Dr. T. J. Ulrych (#67-1804).

I. INTRODUCTION

1. PURPOSE

This research project was undertaken in order to investigate earth free oscillation data utilising relatively new techniques in time series analysis. The investigation focused on the well known UCLA gravimeter data obtained by Dr. L. Slichter after the Alaska earthquake of March 27, 1964 (Slichter 1967b). Maximum entropy techniques were used for two purposes in this study:

1. To compute power spectra of fundamental spheroidal oscillation modes, and to use the improved resolution features of the maximum entropy method to study the associated spectral splitting.
2. To design filter operators necessary to identify and predict sections of the record which were made untenable by noise glitches.

The deglitching of the data set was an important step in reducing the noise power of this record, so that the presence and detectability of core undertones could be investigated.

2. DATA DESCRIPTION

The data used in this study originated from UCLA gravimeter #4, one of two Lacoste-Romberg tidal gravimeters that were in operation in Los Angeles at the time of the 1964 Alaska earthquake. This seismic event is the largest to be extensively recorded with long-period instruments, and is the primary source for much of the present information on normal modes. The data has a sampling rate of 1/12 of an hour and extends for 18.5 days. Free oscillation information is superimposed on high amplitude earth tide data, and, in the unprocessed form, the normal mode data is not observable when the record is plotted (Figure #1).

The data set was recorded on a Lacoste-Romberg tidal gravimeter, which in simple terms, is a mass on the end of a spring-supported beam. A photo-electric cell detects motions in the mass, relays the information to a servomechanism, which in turn raises or lowers the upper end of the spring by means of a screw. The angular position of the screw is recorded digitally in units of 0.1 microgals. Lacoste-Romberg gravimeters generally have drift rates of between 1 and 20 microgals per day. The noise power for this data set increases 28 db. from 0.4 cycles per hour to 0.0 cycles per hour (Figure #2).

The first step in the data processing was to eliminate the tidal frequencies from the record using a filtering scheme. However, since the free oscillation information starts at the beginning of the tidal record, any frequency

FIGURE 1.

Original unprocessed gravimeter data recorded at Los Angeles during the 1964 Alaska earthquake. The record consists of 5320 points with a sampling rate of 1/12th of an hour.

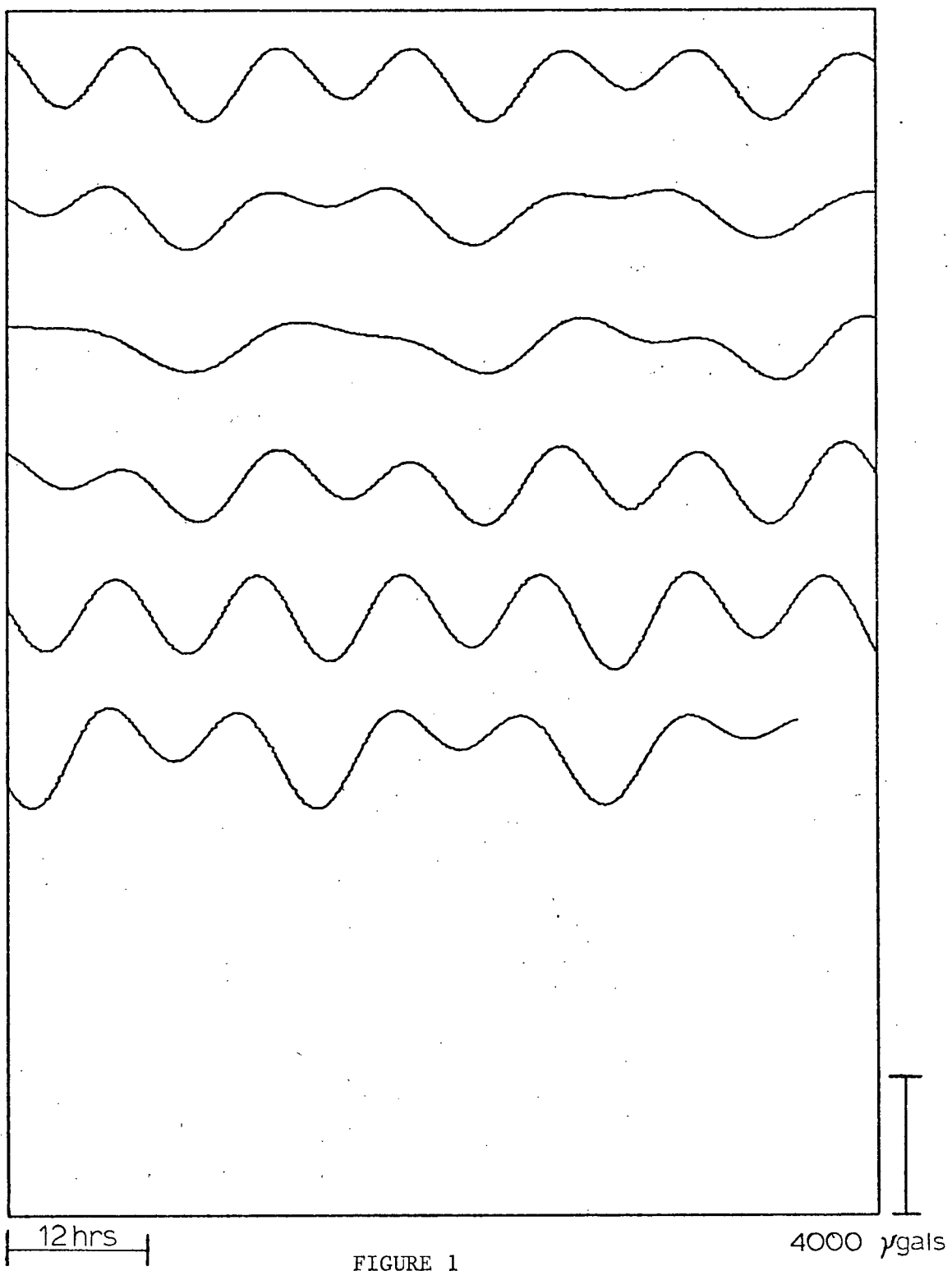


FIGURE 1

FIGURE 2.

Unsmoothed periodogram power spectrum of the unprocessed gravimeter data. The Nyquist frequency is at 6.0 cycles per hour. The location of some of the fundamental spheroidal oscillation modes is indicated. Also shown are the basic diurnal and semi-diurnal tides.

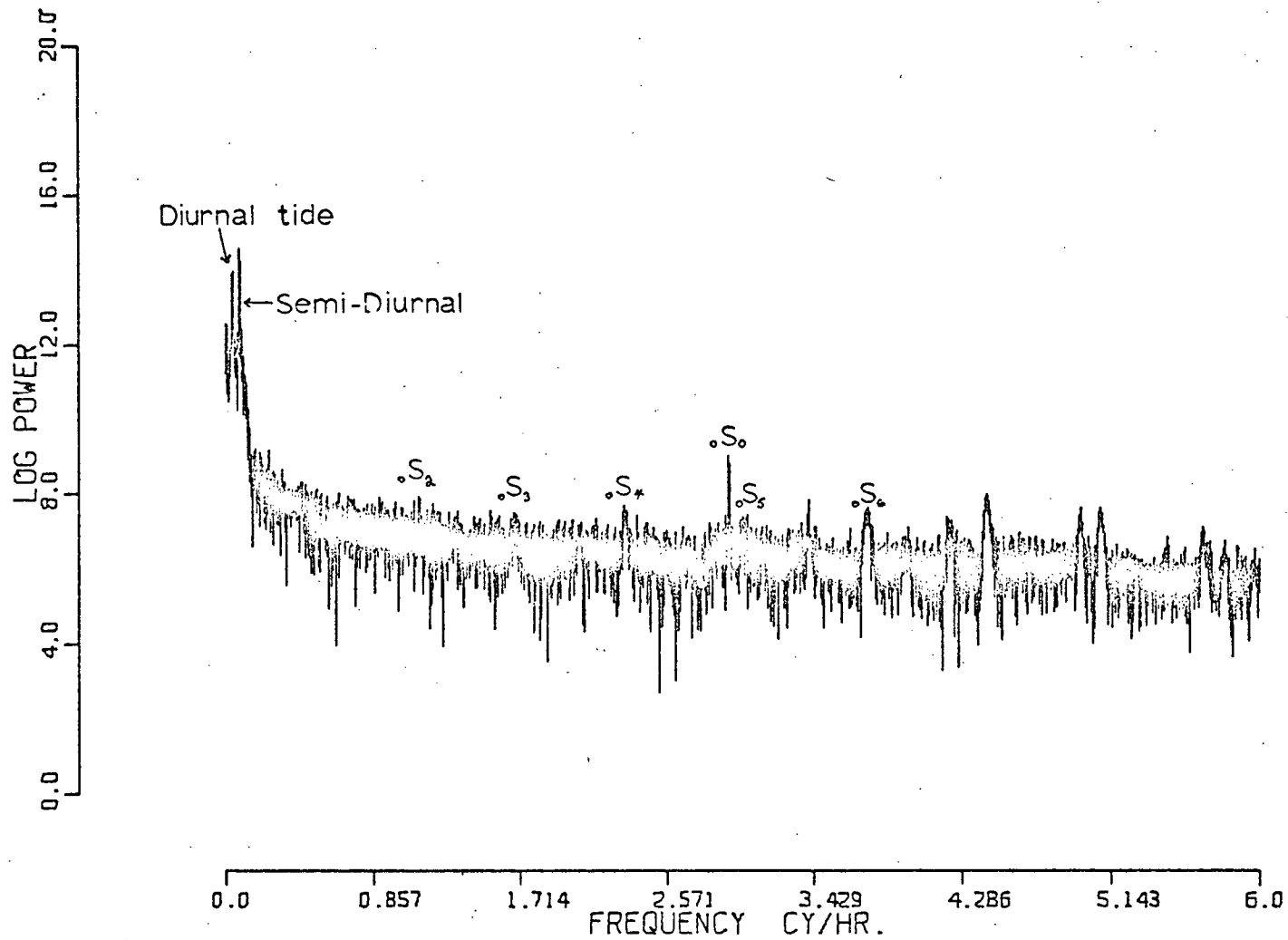


FIGURE 2

domain filtering method will result in tapering of the front and tail end of the data set. It is particularly important not to taper the record in this manner, as high amplitude normal mode information at the onset of the record, will be lost. To circumvent this problem, a scheme based on predictive filtering was used (Ulrych et al. 1973).

Another problem with the data becomes immediately evident when low-pass tidal filtering is accomplished. The filtered record is contaminated by noise bursts or glitches which are caused by digitization errors and aftershock features (Wiggins and Miller 1972). To eliminate these unwanted noise features, a method of data prediction was used to fill in reasonable data values (Ulrych and Clayton 1975).

3. FREE OSCILLATIONS

Free oscillations have their theoretical beginning with Lamb (1882), who first considered the problem of normal modes of a uniform sphere. Love (1911) then extended the development to include a self-gravitating uniform sphere. Benioff et al. (1954) first reported earth free oscillations after observing a normal mode with a period of 57 minutes. In 1961 various groups reported observing a number of normal modes excited by the Chilean earthquake of 1960 (Alsop et al. 1961; Benioff et al. 1961; Bogert 1961; and Ness et al. 1961). Theoretical interest increased greatly at this point, and the mathematical theory for a heterogeneous earth model was developed, allowing a comparison between

experimental and theoretical results. Inversion schemes were developed, which when utilised, yielded velocity-depth models for the earth, which in turn enabled separation of Lamé's parameters as a function of depth (Press 1968; Haddon and Bullen 1967; Backus and Gilbert 1967; and Dziewonski and Gilbert 1973).

There are two fundamental types of free oscillations of a sphere:

1. Spheroidal: radial displacements always exist.
2. Toroidal: displacements are entirely tangential.

Spherical geometry can be broken down into three components, latitude (Θ), longitude (φ), and radius (r). Slichter (1967a) gives the displacements for these three components for toroidal modes as:

1. $U_r = 0$
2. $U_\Theta = v_\eta(r, l, m) \cos(\Theta)^{-1} P_l^m(\sin \Theta)$
 $\times \frac{\partial \exp(-i\omega_\gamma \{t \mp m\omega_\gamma^{-1}\varphi\})}{\partial \varphi}$
3. $U_\varphi = -v_\eta(r, l, m) \frac{\partial P_l^m(\sin \Theta)}{\partial \Theta}$
 $\times \exp(-i\omega_\gamma \{t \mp m\omega_\gamma^{-1}\varphi\})$

For spheroidal modes the displacement components are:

$$1. \quad U_r = U_n(r, l, m) P_l^m(\sin \theta) \\ \times \exp(-i \omega_s \{t \mp m \omega_s^{-1} \varphi\})$$

$$2. \quad U_\theta = W_n(r, l, m) \frac{\partial P_l^m(\sin \theta)}{\partial \theta} \\ \times \exp(-i \omega_s \{t \mp m \omega_s^{-1} \varphi\})$$

$$3. \quad U_\varphi = W_n(r, l, m) (\cos \theta)^{-1} P_l^m(\sin \theta) \\ \times \frac{\partial \exp(-i \omega_s \{t \mp m \omega_s^{-1} \varphi\})}{\partial \varphi}$$

P_l^m : spherical surface harmonic of degree ' l ' and order ' m ' ($m=0, 1, 2, \dots, l$).

For the radial functions V_n, U_n , and W_n , ' n ' denotes the overtone number, where the fundamental overtone is ' $n=0$ '.

Spheroidal free oscillations are represented by the symbols ${}_n S_l^m$ and toroidal oscillations are represented by ${}_n T_l^m$. The ${}_0 S_0$ mode is entirely a radial motion of the earth, expanding and contracting much as if a balloon were being inflated and deflated periodically. Another spheroidal mode, ${}_0 S_2$, is nicknamed the football mode and represents a change of shape of the earth from prolate to oblate and back again. Nodal points do exist and it is possible some modes will not be observed when the recording station is located at one of these points of minimum amplitude. Some free oscillation modes are not possible for the earth. ${}_0 S_1^m$ is a

rigid body oscillation and is not observable. ${}_0T_0^0$ is a rigid body translation about the polar axis and has not yet been observed, and for the mode ${}_nT_0^0$ all the displacements are equal to zero.

4. SPECTRAL SPLITTING

After the records from the 1960 Chilean earthquake were examined, splitting of some of the fundamental spheroidal modes was observed. An analogous phenomenon in nuclear physics is the Zeeman effect where atomic spectral lines show splitting in the presence of a magnetic field. Rotation and ellipticity of the earth were believed to be two possible causes for this behaviour. Suitable theory was developed and it was found that rotation would cause the splitting of the central peak into $2\ell + 1$ peaks, and ellipticity would cause a splitting into $\ell + 1$ peaks. Only spheroidal modes have been observed to show splitting, as torsional modes attenuate too quickly, resulting in dissipative broadening of the spectral lines. The following formulation taken from Alterman et al. (1974) predicts splitting effects to first order in ellipticity and second order in rotation.

$$\omega_e^m = (1 + \alpha_e + m\beta_e + m^2\gamma_e)$$

$$\alpha_e = A \left(\frac{\Omega}{\omega_e}\right)^2 + B\varepsilon$$

$$\beta_e = C \left(\frac{\Omega}{\omega_e}\right)$$

$$\gamma_e = D \left(\frac{\Omega}{\omega_e}\right)^2 + E\varepsilon$$

$$\omega_e^m = \text{split peak frequency}$$

- m = number of the split peak
 Ω = angular frequency of the earth's rotation
 ω_e = eigenfrequency of S or T
 \mathcal{E} = effect of earth's ellipticity
 A, B, C, D, E = constants

The centre frequency of a group of split peaks will differ by ' Ω ' from the frequency of an unsplit peak. Also, because of the effect of ' m^2 ', splitting will be asymmetric around the central peak ($n=0$). For lower order modes, the rotation effect is much greater than the ellipticity effect, so that the first order splitting effect in ellipticity is of the same magnitude as the second order splitting effect in rotation. For the higher order modes, this equivalence does not hold. Lateral heterogeneities can also give rise to splitting or widening of spectral lines, but the effects cannot be well predicted or quantized.

Up to the present, only conventional power spectral techniques have been used in the study of free oscillation splitting. MEM seems to be a logical choice in studying these effects because of the higher resolution and optimally smooth nature of the MEM power spectrum. Bolt and Currie (1975) and Ulrych and Bishop (1975) have shown the improvement in frequency resolution when using MEM. Bolt and Currie (1975) studied the torsional eigenfrequencies recorded at Trieste after the 1960 Chilean earthquake, and reported an increase in precision and number of peaks detected.

5. CORE UNDERTONES

One of the aims of this project was to look once again for core mode oscillations in the frequency range 0.0 to 1.0 cycles per hour. Slichter (1961) reported a spectral peak at .698 cycles per hour in the record of the 1960 Chile event. He also predicted that this particular mode should show spectral splitting peaks at .741 and .659 cycles per hour. The 1964 Alaska earthquake yielded no such peaks, and it is now generally believed that the peak reported in 1961 was not valid. It has been shown (Crossley, personal communication 1976) that the period of the Slichter mode is very model dependent, and the correlation between Slichter's observation and predicted periods is very low.

Spheroidal undertones can only exist in a sub-adiabatic core, as any radial particle motion is possible only when the medium is gravitationally stable. Rotational coupling between torsional and spheroidal modes restricts the theoretical range of the undertone periods to between 0 and 12 hours. At longer periods, starting at about 72 hours, Rossby waves can theoretically exist (Crossley 1975).

The most interesting of core undertones is the Slichter mode, which is a translational motion of the solid inner core driving a return motion in the fluid outer core. Jackson and Slichter (1974) believe they could detect such a motion if it produced a signal of 0.08 microgals on a Lacoste-Romberg gravimeter at the South Pole. This signal amplitude corresponds to a core motion of 6 centimeters with an inner-

outer core density contrast of 0.3 g/cm^{-3} . This minimum detectable signal would be correspondingly larger for stations at other locations on the earth. The observation of a core undertone such as the Slichter mode would be extremely useful in accurately determining the density contrast between the inner and outer core.

At this time it is unknown whether core undertones do exist, and whether they are observable phenomena. This lack of knowledge is due to three factors:

1. The level of excitation of core modes is believed to be quite low (Smith 1974).
2. Undertones are non-degenerate with respect to the azimuthal order number 'm'. The number of undertones is therefore '2n+1' greater than the corresponding overtones, making identification of individual modes difficult (Crossley 1975).
3. It is possible that many of the undertones will have periods packed around an upper limit of 12 hours. This limit is based upon calculations done by Crossley (1975) who used a formulated computing scheme to arrive at this result. This 12 hour period corresponds to that of the semi-diurnal tide, and so power from this tidal peak will tend to obscure the spectral record.

II. THEORETICAL BACKGROUND

1. CLASSICAL SPECTRAL ESTIMATION

Orthodox methods of spectral estimation often make unrealistic assumptions about the extension of the sampled process beyond the windowed region. The maximum entropy method of spectral estimation was developed specifically to obviate this restrictive supposition. The two 'classical' methods of obtaining a power spectrum are outlined below.

A. Periodogram

A function $f(t)$ can be expanded in a Fourier series if $f(t)$ is piecewise continuous in the interval $-T/2 \leq t \leq T/2$ and is periodic with period T . Then $f(t)$ can be expressed as a sum of sine and cosine functions.

$$f(t) = 1/2a_0 + \sum_{n=1}^{\infty} (a_n \cos \omega_n t + b_n \sin \omega_n t)$$

$$a_n = 2/T \int_{-T/2}^{T/2} f(t) \cos \omega_n t \, dt \quad n=0, 1, 2, \dots$$

$$b_n = 2/T \int_{-T/2}^{T/2} f(t) \sin \omega_n t \, dt \quad n=1, 2, 3, \dots$$

$$a_0 = \text{D.C. level}$$

The amplitude spectrum for the process $f(t)$ is given as

$$|F_n| = \sqrt{a_n^2 + b_n^2}$$

Due to its conditions of existence, the periodogram method assumes a periodic extension of the data beyond the sampled region.

B. Autocorrelation function

Weiner (1930) first showed the relationship between the autocorrelation function in the time domain and the power spectrum in the frequency domain. The first step in obtaining a power spectrum using this method is to obtain a suitable estimate of the autocorrelation function $R(t)$, where $R(t) = 0$ for $|t| > N$. This is equivalent to saying that an infinite non-zero autocorrelation function $R(t)$ is multiplied by some weighting function $W(t)$ where $W(t) = 0$ for $|t| > N$. The product $R(t)W(t)$ is then transformed to the frequency domain. The estimated spectrum is therefore the convolution of the Fourier transform of the weighting function with the true spectrum. Considerable work has been put into trying to design the best possible weighting function and its transform. There are two difficulties involved in the design, the first being the tradeoff that exists between resolution and variance in the frequency domain, and the second being the requirement that the spectrum be non-negative. As Burg (1975) points out, although window theory has a certain neatness to it, it is an artifice imposed by the assumption that $R(t) = 0$ for $|t| > N$.

"If one were not blinded by the mathematical elegance of the conventional approach, making unfounded assumptions as to the value of unmeasured data, and changing data values that one knows would be totally unacceptable from a common sense, and hopefully a scientific point of view"¹.

2. MAXIMUM ENTROPY METHOD

A. Information and Entropy

Burg's rationale in developing the theory of the maximum entropy method (MEM), was, that since there is an infinite set of non-negative power spectra that correspond to a given autocorrelation function, the best spectrum would be the one that corresponds to the most random time series. The concept of maximum entropy spectral analysis is based upon theoretical developments made in statistical mechanics and information theory. One of the great advantages of the MEM technique, is its ability to resolve closely spaced spectral lines in a much better manner than conventional methods.

From a statistical viewpoint, MEM can be shown to correspond to a situation with the most random behaviour. Following Ulrych and Bishop (1975) it can be seen that if there are 'M' different things ' m_i ' which could possibly occur, all with probabilities ' p_i ', then if all the ' p_i 's'

¹ J. P. Burg, Maximum Entropy Spectral Analysis, Ph.D. Thesis, Stanford University 1975.

are the same, then no information about the system has been gained. If one of the 'p_i's is different, then some information about the process has been acquired. A relationship between information and probability can be expressed as

$$I = k \log(1/P_i)$$

k = 1 when log is base 2.

If the occurrences are summed over a long period T then

$$I_{TOTAL} = k(P_1 T \log(1/P_1) + P_2 T \log(1/P_2) + \dots)$$

The average entropy given by Shannon (1948) is

$$\begin{aligned} H &= I_{TOTAL} / T \\ &= k \sum_{i=1}^M P_i \log(P_i) \end{aligned} \quad \text{II-1}$$

If all the 'P_i' but one are equal to zero, and this exception is equal to one, then H = 0. Again, all knowledge about the process is available, and there is no uncertainty in the system. If H is greater than zero, a measure of uncertainty is available. The entropy rate or entropy per unit sample is defined as

$$\bar{h} = \lim_{N \rightarrow \infty} H / (N+1)$$

and can be shown to be proportional to

$$\int_{-f_N}^{f_N} \ln P(f) \, df \quad \text{II-2}$$

$P(f)$ = power spectrum
 f_N = Nyquist frequency

B. Maximum Entropy Solution

To solve the maximum entropy variational problem, the following argument is taken from Burg (1975).

The function $P(f)$ that maximizes equation II-2 must be obtained so that the constraint equations

$$R(n) = \int_{-f_N}^{f_N} P(f) \exp(i2\pi fn \Delta t) \, df \quad (-N \leq n \leq N) \quad \text{II-3}$$

are satisfied. $R(n)$ is the autocorrelation function. Another condition is the Fourier transform relationship between the autocorrelation and the power spectrum.

$$P(f) = 1/2f_N \sum_{n=-\infty}^{\infty} R(n) \exp(-i2\pi fn \Delta t) \quad \text{II-4}$$

The constraint equation II-3 will be satisfied if the $R(n)$ in equation II-3 are equivalent to the $R(n)$ in equation II-4. To solve this problem, Lagrangian multipliers can be used, but what follows is a simpler derivation.

Substituting II-4 into II-2 gives

$$h \propto \int_{-f_N}^{f_N} \ln \left[\frac{1}{2f_N} \sum_{n=-\infty}^{\infty} R(n) \exp(-i2\pi f n \Delta t) \right] df \quad \text{II-5}$$

Maximizing II-5 with respect to $R(n)$ results in

$$h \propto \frac{1}{2f_N} \int_{-f_N}^{f_N} P^{-1}(f) \exp(-i2\pi f s \Delta t) df = 0 \quad \text{II-6}$$

for $|s| > N$

where $P^{-1}(f)$ is the inverse of the power spectrum $P(f)$.

Expanding $P^{-1}(f)$ in terms of a Fourier series gives

$$P^{-1}(f) = \sum_{n=-\infty}^{\infty} \lambda_n \exp(-i2\pi f n \Delta t)$$

$$\therefore P(f) = \frac{1}{\sum_{s=-N}^N \lambda_s \exp(-i2\pi f s \Delta t)} \quad \text{II-7}$$

II-7 is the same equation that would result from the variational solution, where the λ 's are the Lagrangian multipliers. From II-6 it can be seen that $\lambda_n = 0$ for $|n| > N$. The next task is to express the λ 's in a suitable form. Two methods are presented, one an analytical integration scheme, and the other a z-transform argument.

C. Analytical Integration

Substituting equation II-7 into equation II-3 gives

$$\int_{-f_N}^{f_N} \frac{\exp(i2\pi f n \Delta t)}{\sum_{s=-N}^N \lambda_s \exp(-i2\pi f s \Delta t)} df = R(n) \quad (-N \leq n \leq N) \quad \text{II-8}$$

Letting $z = \exp(-i2\pi f \Delta t)$ which is the normal z-transform equivalence it can be shown that

$$\begin{aligned}
 dz &= -i2\pi\Delta t \exp(-i2\pi f \Delta t) df \\
 &= -i2\pi\Delta t z df \\
 \text{and } df &= -dz/i2\pi\Delta t z.
 \end{aligned}$$

Equation II-8 can now be written as

$$1/2\pi i \Delta t \oint z^{-n-1} / \sum_{s=-N}^N \lambda_s z^s dz = R(n) \quad \text{II-9}$$

This integration curve is counterclockwise around the unit circle in the complex z plane. From II-7 and the principle of polynomial factorization it is possible to say that

$$\begin{aligned}
 \sum_{s=-N}^N \lambda_s z^s &= [P_N \Delta t]^{-1} [1 + a_1 z + \dots + a_N z^N] [1 + a_1^* z^{-1} + \dots + a_N^* z^{-N}] \\
 &= [P_N \Delta t]^{-1} \sum_{s=0}^N a_s z^s \sum_{s=0}^N a_s^* z^{-s} \\
 P_N &> 0 \\
 a_0 &= 1
 \end{aligned} \quad \text{II-10}$$

Substituting II-10 into II-9 results in an expression for $R(n)$.

$$R(n) = \frac{P_N}{2\pi i} \oint \frac{z^{-n-1}}{\sum_{s=0}^N a_s z^s \sum_{s=0}^N a_s^* z^{-s}} dz \quad -N \leq n \leq N \quad \text{II-11}$$

Since $R(n) = \int_{f_N}^{f_N} P(f) z^{-n}$ and if II-11 is summed over a_n^* so that

$$\sum_{n=0}^N a_n^* R(n-r) = \frac{P_N}{2\pi i} \oint \frac{z^r z^{-n-1} \sum_{n=0}^N a_n^*}{\sum_{s=0}^N a_s z^s \sum_{s=0}^N a_s^* z^{-s}} dz$$

it is possible to write

$$\begin{aligned} \sum_{n=0}^N a_n^* R(n-r) &= \frac{P_N}{2\pi i} \oint \frac{z^{r-1} \sum_{n=0}^N a_n^* z^{-n} dz}{\sum_{s=0}^N a_s z^s \sum_{s=0}^N a_s^* z^{-s}} \\ &= \frac{P_N}{2\pi i} \oint \frac{z^{r-1}}{\sum_{s=0}^N a_s z^s} dz \quad r > 0 \end{aligned} \quad \text{II-12}$$

Knowing that $\sum_{s=0}^N a_s z^s$ is analytic for $z \leq 1$, and for $r > 1$, z^{r-1} is analytic for $z \leq 1$, it is evident that

$$\oint [z^{r-1} / \sum_{s=0}^N a_s z^s] dz = 0 \quad \text{for } r \geq 1$$

and also that

$$\sum_{n=0}^N a_n^* R(n-r) = 0 \quad \text{for } r \geq 1 \quad \text{II-13}$$

Now that the case for $r \geq 1$ has been solved all that need be done is obtain a solution for the $r = 0$ case. Since

$$[1/2\pi i] \oint [f(z)/z] dz = f(0)$$

it can be shown that

$$1/2\pi i \oint \left(\sum_{s=0}^N a_s z^s \right)^{-1} / z dz = f(0)$$

where $f(z) = \left(\sum_{s=0}^N a_s z^s \right)^{-1}$. a_0 has been already defined as '1', so that $f(0) = 1$. Therefore II-12 becomes

$$\sum_{n=0}^N a_n^* R(n-r) = P_N \quad \text{for } r = 0 \quad \text{II-14}$$

Taking the complex conjugates of II-13 and II-14 we get

$$\sum_{n=0}^N R(n-r) a_n = P_N \quad r = 0 \quad \text{II-15}$$

$$\sum_{n=0}^N R(n-r) a_n = 0 \quad r \geq 1 \quad \text{II-16}$$

An expression for the power $P(f)$ can also be written by substituting II-10 into II-7 to give

$$P(f) = P_N \Delta t / \sum_{s=0}^N a_s z^s \sum_{s=0}^N a_s^* z^{-s} \quad \text{II-17}$$

which can be rewritten in the familiar form

$$P(f) = P_N / (2f_N |1 + \sum_{s=0}^N \gamma_s \exp(-i2\pi f s \Delta t)|^2) \quad \text{II-18}$$

D. Z-transform approach

An alternative method to obtain equations II-15 and II-16 is through a z-transform approach. Substituting II-14 and II-10 into II-6 gives

$$\begin{aligned} P_N \Delta t / \sum_{s=0}^N a_s z^s \sum_{s=0}^N a_s^* z^{-s} \\ = (1/2f_N) \sum_{r=-\infty}^{\infty} R(r) z^r \end{aligned} \quad \text{II-19}$$

Multiplying by $\sum_{n=0}^N a_n^* z^{-n}$ gives

$$\begin{aligned}
P_N / \sum_{s=0}^N a_s z^s &= \sum_{n=0}^N a_n^+ z^{-n} \sum_{r=-\infty}^{\infty} R(r) z^r \\
&= \sum_{n=0}^N a_n^+ z^{-n} \sum_{r=-\infty}^{\infty} R(n-r) z^{n-r} \\
&= \sum_{r=-\infty}^{\infty} \left[\sum_{n=0}^N a_n^+ R(n-r) \right] z^{-r}
\end{aligned}
\tag{II-20}$$

When $s = 0$ then

$$P_N = \sum_{n=0}^N a_n^+ R(n-r) \tag{II-21}$$

and when $s > 0$, powers of z do not match so that

$$0 = \sum_{n=0}^N a_n^+ R(n-r) \tag{II-22}$$

Taking the complex conjugates of II-21 and II-22, equations II-15 and II-16 are again obtained. Writing II-15 and II-16 in matrix form gives

$$\begin{array}{cccc|cc}
R(0) & R(1) & \dots & R(N) & 1 & E_N \\
R(1) & R(0) & \dots & R(N-1) & a_1 & 0 \\
\cdot & \cdot & \cdot & \cdot & \cdot & \cdot \\
\cdot & \cdot & \cdot & \cdot & \cdot & \cdot \\
R(N) & R(N-1) & \dots & R(0) & a_N & 0
\end{array}
\tag{II-23}$$

which is the equation for obtaining the N -th point prediction filter. From II-18 it can be seen that to obtain a spectral estimate $P(f)$, all that is required is a prediction error filter and the error power of prediction. These two values are given by equation II-23.

E. Heuristic Solution

From Ulrych et al. (1973) a heuristic solution to the maximum entropy problem can be replicated. If there exists a time series $x(t)$ which has a Fourier transform $X(\omega)$, there is some filter $i(t)$ that whitens $x(t)$. The maximally white time series that corresponds to a particular power spectrum has already been shown to be the one that exhibits maximum entropy. If the transfer function of $i(t)$ is $I(\omega)$, then $|X(\omega) I(\omega)|$ equals a constant 'k'. Also

$$|X(\omega)|^2 = k^2 / |I(\omega)|^2$$

is a power estimate. Any stochastic, non-deterministic, stationary time series can be represented as a moving-average process.

$$x(t) = \sum_{s=0}^{\infty} b_s e_{t-s}$$

$$b_0 > 0$$

$$b_0^2 + b_1^2 + b_2^2 + \dots < \infty$$

$$e_t = \text{a white noise series.}$$

Therefore $x(t)$ is the convolution of some filter or wavelet $b(t)$ with a white noise series $e(t)$. $b(t)^{-1}$ is the filter that whitens $x(t)$. In other words, if $a(t) * b(t) = \delta(t)$, then $x(t) * a(t) = e(t)$. $a(t)$ is a deconvolution or spiking filter and can be determined from

$$R a = 1$$

II-24

R is an N by N autocorrelation matrix

$a = a_1, a_2, \dots, a_n$ is the prediction error filter

$$1 = (1, 0, 0, \dots, 0)$$

The prediction filter $\gamma(t) = \delta(t) - a(t)$ so II-24 can be written as

$$R \gamma = P_N$$

$$\gamma = 1, -a_1, -a_2, \dots, -a_n$$

$$P_N = (P_N, 0, 0, \dots, 0)$$

$$P_N = r_0 + \sum_{i=1}^{N-1} r_i \gamma_{i+1} = \text{error power of prediction.}$$

From the power estimate

$$|X(\omega)|^2 = k^2 / |I(\omega)|^2$$

it can be seen that

$$P(f) = P_N / |1 + \sum_{k=1}^N \gamma_k \exp(-i2\pi fk)|^2$$

which is equivalent to equation II-28.

From the above discussion, the fundamental difference between MEM and conventional power spectral analysis can be seen. Maximum entropy spectral analysis gives the spectrum of a model that fits or approximates a fit to the process, a sample of which is represented by the data. Conventional

fourier transform methods, on the other hand, obtain the spectrum of the sample.

3. LEVINSON RECURSION

Burg developed a solution to equation II-23 based upon the Levinson recursion algorithm. The solution is also consistent with the concept of maximum entropy. The accuracy of Burg's method is greater than that of the normal Levinson method, and it is also executed about 1/3 faster. The development is shown below.

A prediction filter is run over the data set in both the forward and reverse directions, and the power output from this operation is minimized. The filter is not run off the ends of the data, and so no assumptions about the continuation of the data outside the sampling interval are made. This is the major feature that is related to maximizing the entropy of the process.

For the two point filter $(1, \gamma)$, the power output from running the filter over the data is

$$P_2 = 1/2 (N-1) \left\{ \sum_{i=1}^{N-1} (x_{i+1} + \gamma x_i)^2 + \sum_{i=1}^{N-1} (x_i + \gamma x_{i+1})^2 \right\}$$

The value of P_2 can be shown to be a minimum when

$$\gamma = 2 \frac{\sum_{i=1}^{N-1} (x_i x_{i+1})}{\sum_{i=1}^N (x_i)^2}$$

For the two point case, equation II-23 is written as

$$\begin{vmatrix} R(0) & R(1) \\ R(1) & R(0) \end{vmatrix} = \begin{vmatrix} 1 & \gamma \\ \gamma & 1 \end{vmatrix} = \begin{vmatrix} P_2 \\ 0 \end{vmatrix}$$

γ is obtained from equation II-25. The first autocorrelation value $R(0)$ is estimated by $R(0) = 1/N \sum_{i=1}^N (x_i)^2$, and so $R(1)$ can be calculated from $R(1) = -\gamma(R(0))$, and P_2 can be obtained from $P_2 = R(0) (1 - \gamma^2)$.

For the three point filter $(1, \gamma_1, \gamma_2)$ the power output after running the filter over the data is

$$P_3 = (1/2(N-2)) \sum_{i=1}^{N-2} \{ (x_{i+2} + x_{i+1}\gamma_2 + x_i\gamma_3)^2 + (x_i + x_{i+1}\gamma_2 + x_{i+2}\gamma_3)^2 \}$$

When γ_2 is set equal to $\gamma(1 + \gamma_3)$, where γ is the filter coefficient obtained for the two-point case, then the value of γ_3 that minimizes P_3 can be obtained. The filter $\{1, \gamma(1 + \gamma_3), \gamma_3\}$ will also be minimum phase. Equation II-23 for the three point case is written as

$$\begin{array}{r}
 | R(0) \quad R(1) \quad R(2) | \quad | 1 | \quad | 0 | \\
 | R(1) \quad R(0) \quad R(1) | \quad | \gamma | + \gamma_3 | \gamma | = \\
 | R(2) \quad R(1) \quad R(0) | \quad | 0 | \quad | 1 |
 \end{array}$$

$$\begin{array}{r}
 | P_2 | \quad | \Delta_2 | \quad | P_3 | \\
 | 0 | + \gamma_3 | 0 | = | 0 | \\
 | \Delta_2 | \quad | P_2 | \quad | 0 |
 \end{array}$$

$$\Delta_2 = R(2) + R(1)\gamma$$

$$\gamma_3 = -\Delta_2/P_2$$

$$P_3 = P_2(1 - \gamma_3^2)$$

The advantage of this recursive method is that only one variable, in this case γ_3 , has to be adjusted so as to obtain the minimum power output. The recursion is continued until the desired filter length is obtained. The values for the prediction filter $(1, \gamma_1, \gamma_2, \dots, \gamma_N)$ and the error power of prediction P_N , are then plugged into equation II-18 to obtain an estimate of the power $P(f)$. As Lacoss (1971) and Burg (1972) pointed out, the power estimate $P(f)$ is actually a spectral density estimate. If a more reliable estimate of the spectrum (in terms of relative peak amplitudes) is required, the maximum entropy estimate should be integrated.

4. AUTOREGRESSIVE MODELS AND MEM

One of the critical factors in determining the maximum entropy spectrum is deciding upon which length filter

operator should be used in the spectral estimate calculation. Too high an order leads to instability fairly quickly, whereas too low an order gives a poorly resolved estimate. In some cases prior knowledge of the spectrum (through conventional methods) can be very useful in picking a filter order. Due to the work of VandenBos (1971), who showed the equivalence of autoregressive time series modelling and the principle of MEM, the large quantity of literature on autoregressive modelling can be applied to the filter length estimation problem. In particular the works of Akaike (1969, 1970) and Gersch (1970) are worth noting. The autoregressive model for an order M , is written

$$x_t = \sum_{i=1}^M d_i x_{t-i} + a_t \quad \text{II-26}$$

and it can be seen that the present value $x(t)$ of the time series is being produced from the known past values

$x_{t-1}, x_{t-2}, \dots, x_{t-M}$. a_t is an additive white noise series called the innovation and has zero mean and a variance of σ_a^2 . If the z-transform of II-26 is taken, the result can be written as

$$X(z) = X(z) [d_1 z + d_2 z^2 + \dots + d_M z^M] + A(z)$$

and therefore

$$|X(z)|^2 = |A(z)|^2 / |1 - d_1 z - d_2 z^2 - \dots - d_M z^M|^2 \quad \text{II-27}$$

Equation II-27 can be rewritten as

$$P(f)_{A.R.} = 2\sigma_a^2 / |1 - \sum_{j=1}^M \alpha_j \exp(-i2\pi fj)|^2$$

which is equivalent to II-18, the expression for the maximum entropy spectrum. With the equivalence of autoregressive modelling and MEM shown, the final prediction error criterion of Akaike can be used to help determine the filter order. The FPE is defined as the mean square prediction error.

$$FPE = E [(x_t - \hat{x}_t)^2] \quad \text{II-28}$$

\hat{x}_t = estimated prediction of x_t

The FPE can be shown to be (Ulrych and Bishop 1975)

$$FPE_M = \{N + (M-1)/N - (M+1)\} S_M^2$$

M is the order of filter

S_M^2 is the minimum residual sum of squares

$$= \left[\sum_{t=M+1}^N (x_t - \alpha_1 x_{t-1} - \alpha_2 x_{t-2} - \dots - \alpha_M x_{t-M})^2 \right]^2$$

In many cases the FPE criterion gives an excellent idea of the filter length, but for the data being studied in this project, it was found not to be as useful. In numerous examples a guess of the optimum order was made, in some cases after several test runs were performed. M was never taken to be greater than $N/2$ where N is the length of the data set.

5. TIME ADAPTIVE MEM

As well as handling stationary time series, maximum entropy can be expanded into the realm of non-stationarity in space and time. The use of time-adaptive MEM was considered here as a possible means of identification of the noise bursts in the data. These glitches can be thought of as reverberant peaks superimposed on a non-stationary time series. Time adaptive MEM is a deconvolution scheme that designs a prediction error filter in order to locate areas of unpredictability. Seismic arrivals in reflection records, and the noise glitches in this data set, can both be thought of as regions of unpredictability. The deconvolved record should show spikes corresponding to the location of the glitches, and after this identification has been made, the noise regions can be removed by some predictive method.

Normal time adaptive schemes are handled by time gates, and two possible approaches can be used.

1. The autocorrelation lags for each gate can be calculated, the prediction error filters can be determined from these lags using the Levinson recursion algorithm, and the filters can then be applied to the data.
2. The Burg approach can be used to calculate the prediction error operators in the time gates, and the filter can be applied to the data.

Burg (1971) has developed an alternative to the time gating approach, where the prediction error coefficients are continuously updated as the filter is run across the data. This eliminates the problem of picking time gates to cover only stationary data segments.

A brief description of the processing scheme follows. The parameters discussed are described in the comment section of the program listed in APPENDIX 1. A variable NWARM controls the length of a warmup segment of data. A prediction error operator is calculated on this 'stationary' data segment in the same manner as for the normal Burg technique where the filter length is set equal to 'LCN + 1' points. This filter is then run over the first 'NWARM' points to find the prediction error of the 'NWARM + 1' point.

The filter is now recomputed using only the 'LCN' points of the segment from 'NWARM - LCN + 1' to 'NWARM + 1'. The prediction error for the 'NWARM + 2' point is then found. The process is continued until the end of the data segment is reached. If the parameter 'IFLGAP' is greater than 1, then only every 'IFLGAP' point is used in the calculation of the filter and the determination of the prediction errors. After the prediction error trace for every 'IFLGAP' point has been calculated, intermediate prediction error values are computed. There is also a parameter 'NZC' which controls the number of reflection coefficients set to zero. This has the effect of creating a filter that predicts further than unit distance, while still maintaining minimum phase requirements.

As discussed earlier, the optimum prediction error filter is the one with the minimum output power as it is run over the data. For the time adaptive case, the minimum average squared power must be set by the constant updating of the filter coefficients. A recursive scheme as outlined for the stationary MEM is utilised to obtain the $N+1$ point filter from the N point filter. Only one parameter C_j is adjusted to minimize the average squared error. C_j corresponds to a reflection coefficient in an ideally layered medium. Burg (1972) has shown that the average power is

$$P_j = \{1/(2N)\} \sum_{j=1}^N [F_j(k) + C_j B_j(k)]^2 + [C_j F_j(k) + B_j(k)]^2$$

which is the sum of the squared forward and backward prediction errors. The value of C_j which minimizes the power P_j is given as

$$C_j = -2 \sum_{j=1}^{N-1} [F_j(k) B_j(k)] / \sum_{j=1}^N [F_j(k)^2 + B_j(k)^2] \quad |C| < 1$$

which is the negative average cross-power of the forward and backward prediction error, divided by the averaged auto-powers of the forward and backward prediction errors. To handle nonstationarity the cross-powers and auto-powers are weighted so that the statistics close to the point predicted

will be more important than statistics further away.

The weighting is exponential and is both time and space variable

$$\text{Weight}(k,m) = \exp(-k \Delta T/\tau_r - m/\tau_x)$$

τ_r = relaxation time (seconds)

τ_x = relaxation distance (traces)

The relaxation time is 1/e the decay time. Since there is a tradeoff between speedy adaption and accurate computation of C_j , the use of MEM is particularly advantageous in that it allows calculation of coefficients on short data segments. A Fortran IV listing of the program is included in Appendix #1.

III. DATA ANALYSIS PROCEDURES

As discussed in Chapter II, two major problems exist with the time series under investigation. One is the fact that the onset of the free oscillation information in this data corresponds to the beginning of the record. The second difficulty is the presence of high amplitude noise glitches which occur in the filtered records. Both of these problems can be overcome by use of prediction filters designed with the Burg algorithm.

1. NECESSITY OF TAPERING

In order to accomplish frequency domain filtering, it is essential that the data set be zero mean and tapered in some manner before transformation to the frequency domain. Otherwise unnecessary noise power due to step discontinuities in the data will be added to the spectrum.

If a data set is not zero mean and tapered, it can be broken down into two parts, one being the signal information, and the other being a D.C. component. This D.C. signal is in effect a step function which represents unwanted information. The Fourier transform of a step function

$$u(t) = 1/2 + 1/2 \operatorname{sgn}(t)$$

$$\text{is } \mathcal{F}[u(t)] = \pi\delta(\omega) + 1/i\omega$$

Therefore a step function will add a D.C. component, as well as a frequency dependent component that is higher at low frequencies. Therefore the necessity of removing the mean and tapering the data set before transforming to the frequency domain, is clear.

2. PREDICTION

Since the free oscillation information starts at the onset of the record, any tapering will remove desired information. To eliminate this problem the data set was predicted forward and backwards in time so that necessary information was preserved. The 500 point prediction filter was designed using the Burg maximum entropy algorithm. The original 5320 points were predicted up to 8092 points, which represents an extension of the data 1386 points both forward and backwards. This record was then tapered with a 5% cosine bell taper (Figure #3).

3. FILTERING

Two filtered data sets were obtained from the predicted original data. One was a high pass filtered record with a cutoff frequency of 0.66 cycles per hour. This record was used to study the fundamental free oscillation modes and the associated spectral splitting. The second data set was a band pass filtered record with cutoffs of 0.12 and 1.20 cycles per hour. This band passed data was used for the investigation of

FIGURE 3.

Predicted gravimeter data extended forward and backward in time. Prediction filter length was 500 points and 1386 points were added in each direction. The position of the original record is indicated.

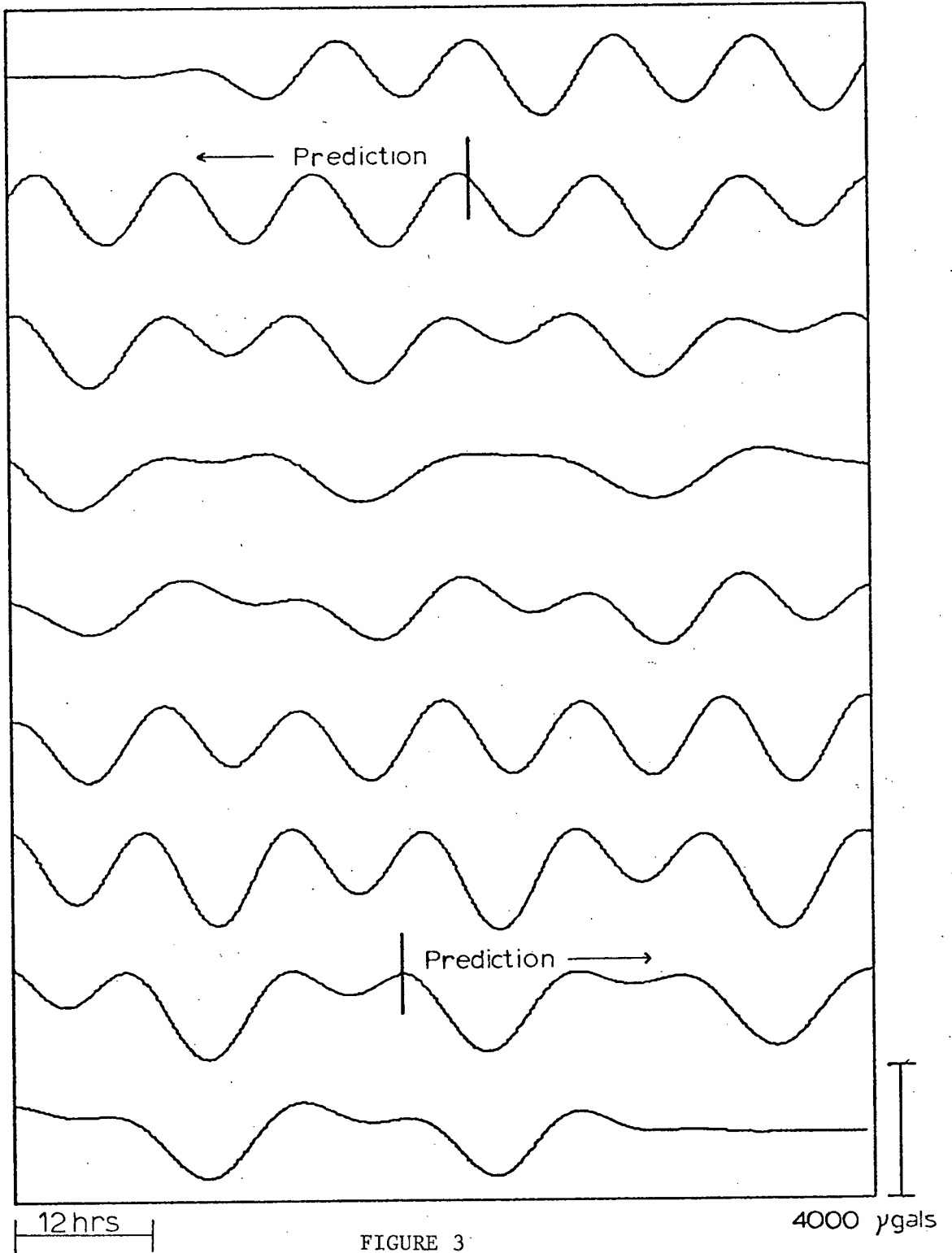


FIGURE 3

the core undertones.

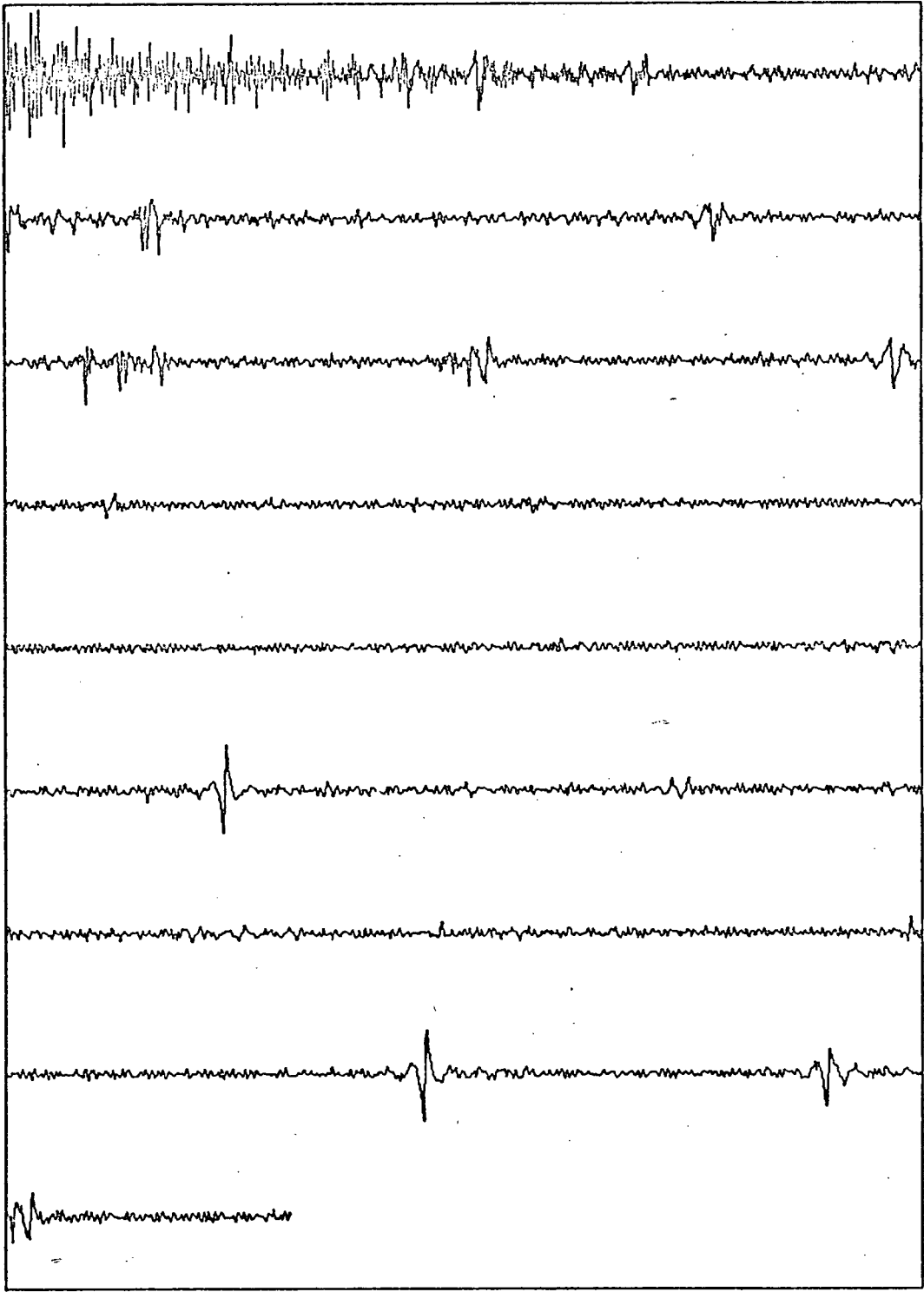
Both filtering operations were performed in the frequency domain by a smoothed boxcar multiplication operator. The sequence of filter design is as follows:

1. The boxcar function with the desired cutoffs is constructed in the frequency domain.
2. This boxcar is then transformed to the time domain and the time function is truncated and tapered to some desired length.
3. This truncated time function is retransformed back to the frequency domain, resulting in a smoothed boxcar. The amount of smoothing in the frequency domain depends upon the amount the time function has been truncated in the time domain. The longer the time domain function, the sharper the cutoff in the frequency domain.

Figure #4 is the high pass filtered predicted record and Figure #5 is the band passed predicted record. The noise glitches are immediately evident in both data sets, and can be seen to have very high amplitudes in relation to the signal. A comparison should be made between Figure #4 and Figure #6, which is the high pass filtered not predicted

FIGURE 4.

High pass filtered predicted record. The filter cutoff is at 0.66 cycles per hour. The noise glitches are immediately evident, and have a well defined character.



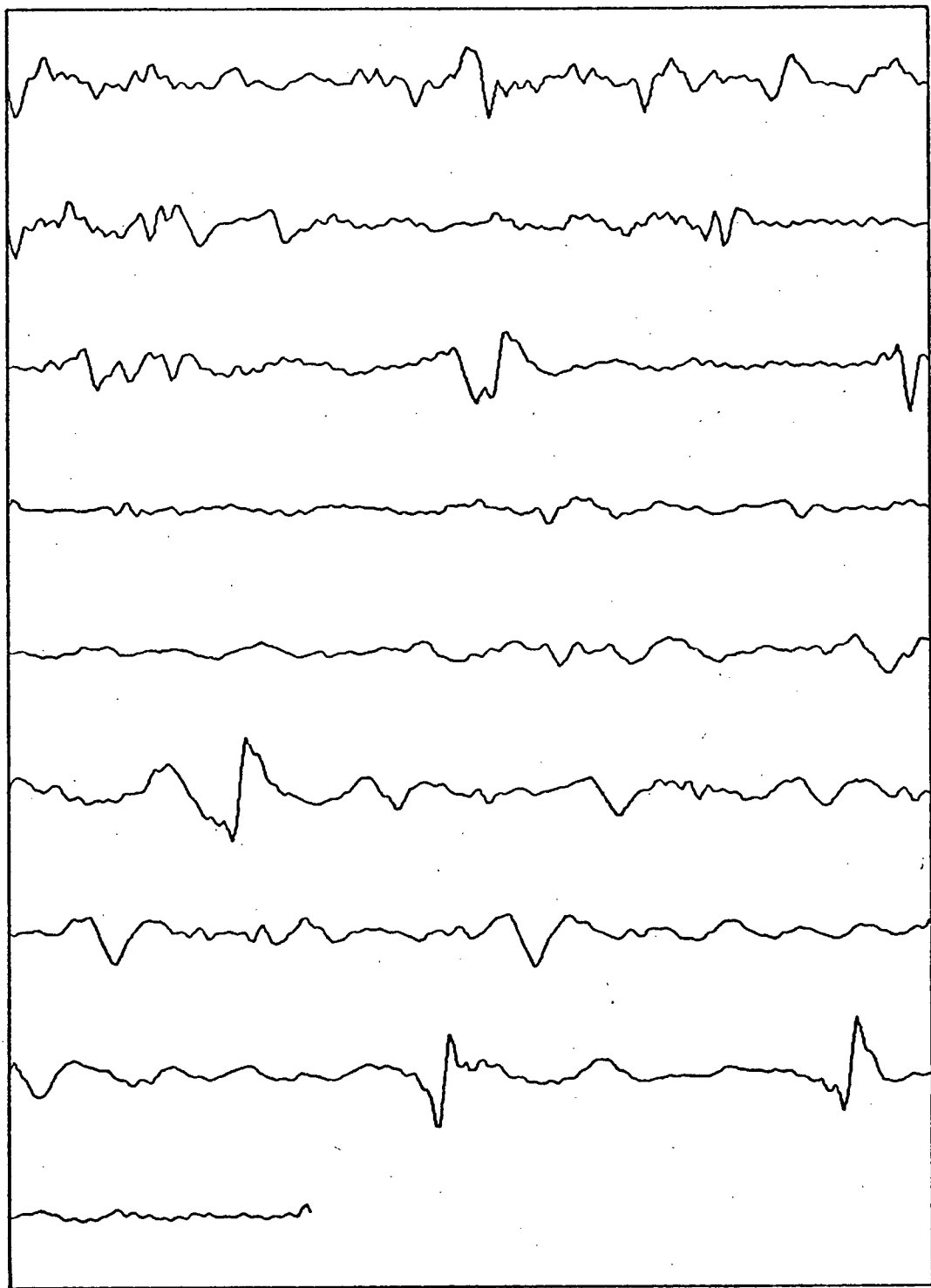
12 hrs

FIGURE 4

100 ygals

FIGURE 5.

Band pass filtered predicted record. The filter cutoffs are at 0.12 and 1.20 cycles per hour. Glitches are observable, but not as well defined as for the high passed record.



12 hrs

FIGURE 5

70 ygals

FIGURE 6.

High pass filtered unpredicted original record. The tapering, which is necessary to accomplish the filtering, is immediately evident at the onset of the record, where there is a large reduction in the signal amplitude.

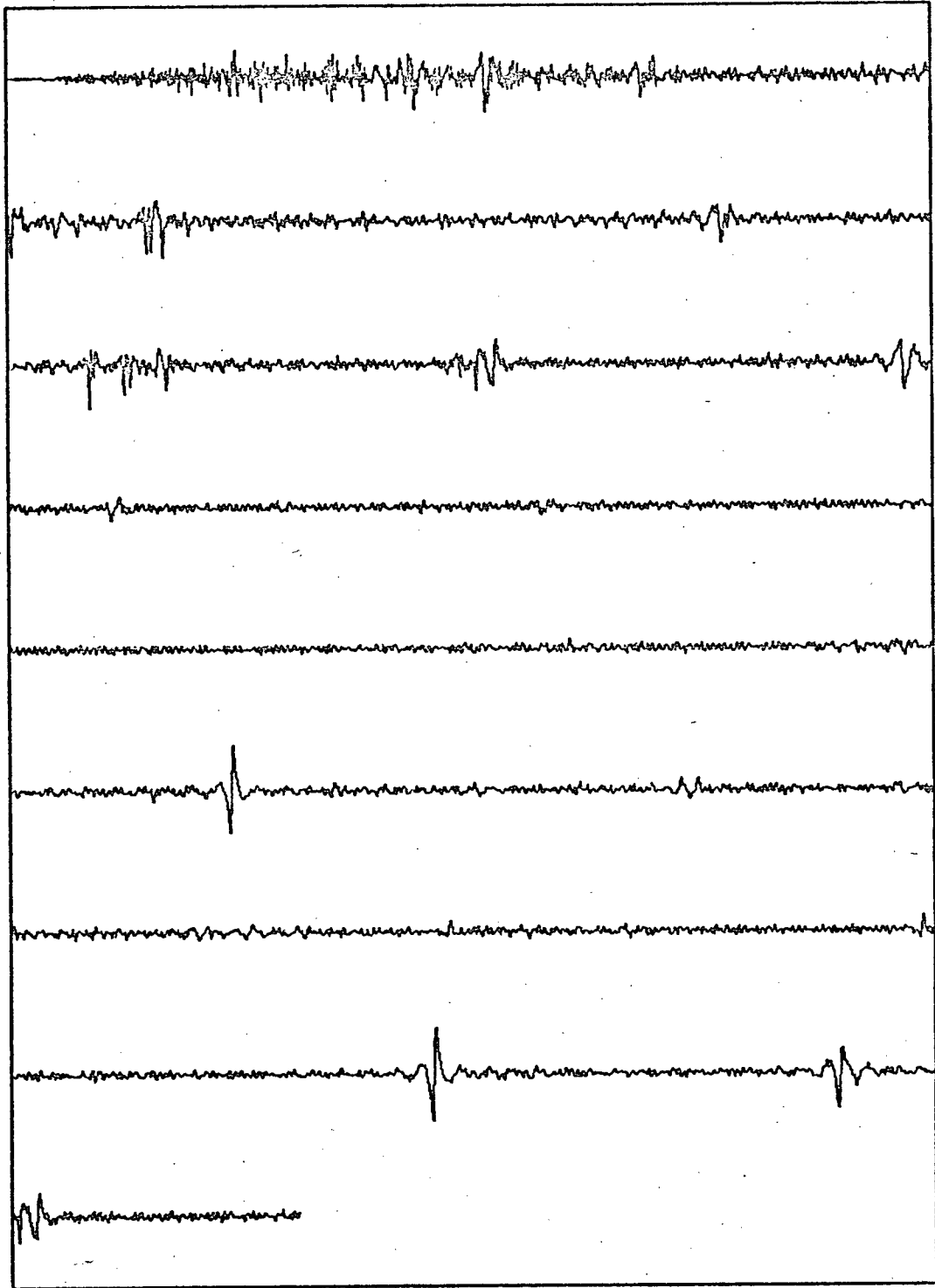


FIGURE 6

100 μ gals

Alaska record. This is the record that would result from tapering and filtering the tidal record before prediction forward and backward in time. The difference in the information available at the beginning of the record is obvious, and much better signal to noise ratios would be expected in the power spectrum.

4. DEGLITCHING

As seen on both Figures #4 and #5, high amplitude glitches are present in the filtered records. These glitches contribute a significant amount of noise in the frequency range 0.0 to 2.0 cycles per hour (Wiggins and Miller 1972).

A. Identification

The first step in elimination of these glitches is identification. For this record visual identification can isolate most of the noise areas at least for the high-passed record (Figure #4). For the band passed record, the glitches do not have the same well defined character and are harder to spot, particularly in the earlier part of the record. To aid in this identification, it was thought that it would be useful to run the time-adaptive MEM routine over the filtered records to see if regions of unpredictability were located. As mentioned in Chapter II, the glitches should show up as areas of relatively large prediction error.

After experimenting with the length of the filter

operator, and the time relaxation factor (ZTAU), respective values of 100 and 5.0 were chosen. There is no hard and fast rule for determining these values, although Burg (1972) does make some recommendations for ZTAU. Figures #7 and #8 show the prediction error traces for the high passed and band passed records. The first 100 points of each record represent a warm-up period where the filter coefficients are set to some initial value. Areas B and C on Figure #7 are also warm-up sections, as the long length of this record required its division into three segments. As hoped for, the glitches show up very well in both examples.

B. Prediction Into Gaps

In order to remove these glitches from the records, a prediction scheme based on one demonstrated by Ulrych and Clayton (1975) was used. It involves the calculation of prediction filter coefficients using the Burg algorithm. However instead of designing the filter on data only in one segment, this gap prediction method creates a filter from segments of data that are not connected. An averaging effect is thus achieved.

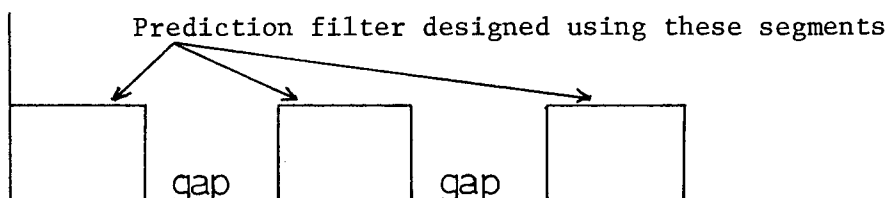
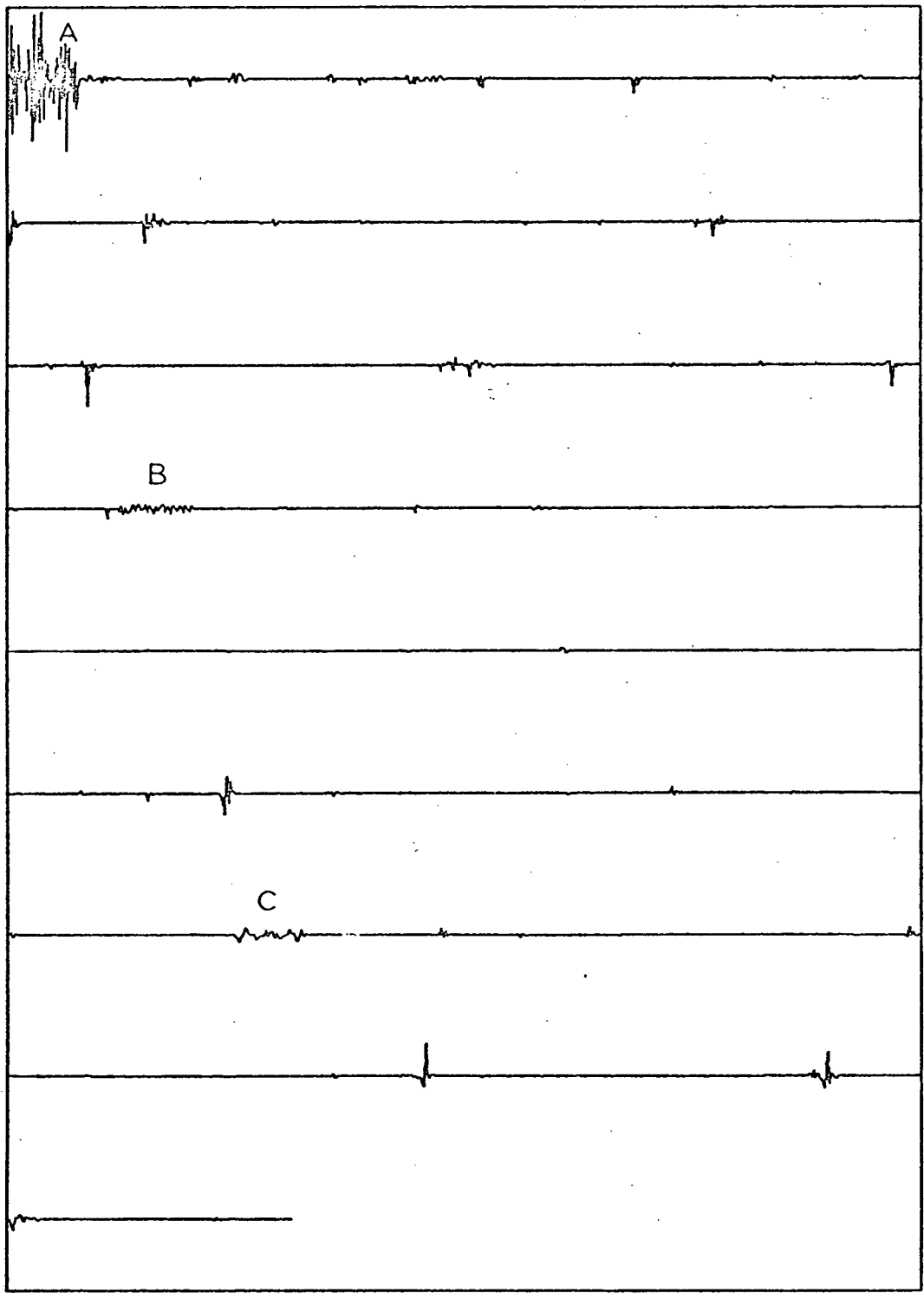


FIGURE 7.

Time adaptive prediction error trace of high pass filtered predicted data. Glitches show up as areas of unpredictability. The time relaxation factor, ZTAU, equals 5.0 and the filter length equals 100 points. Areas A, B, and C are filter warmup sections, where no prediction occurs.



12 hrs

FIGURE 7

100 μ gals

FIGURE 8.

Time adaptive prediction error trace of band pass filtered predicted data. The time relaxation factor, ZTAU, equals 5.0 and the filter length equals 100 points.

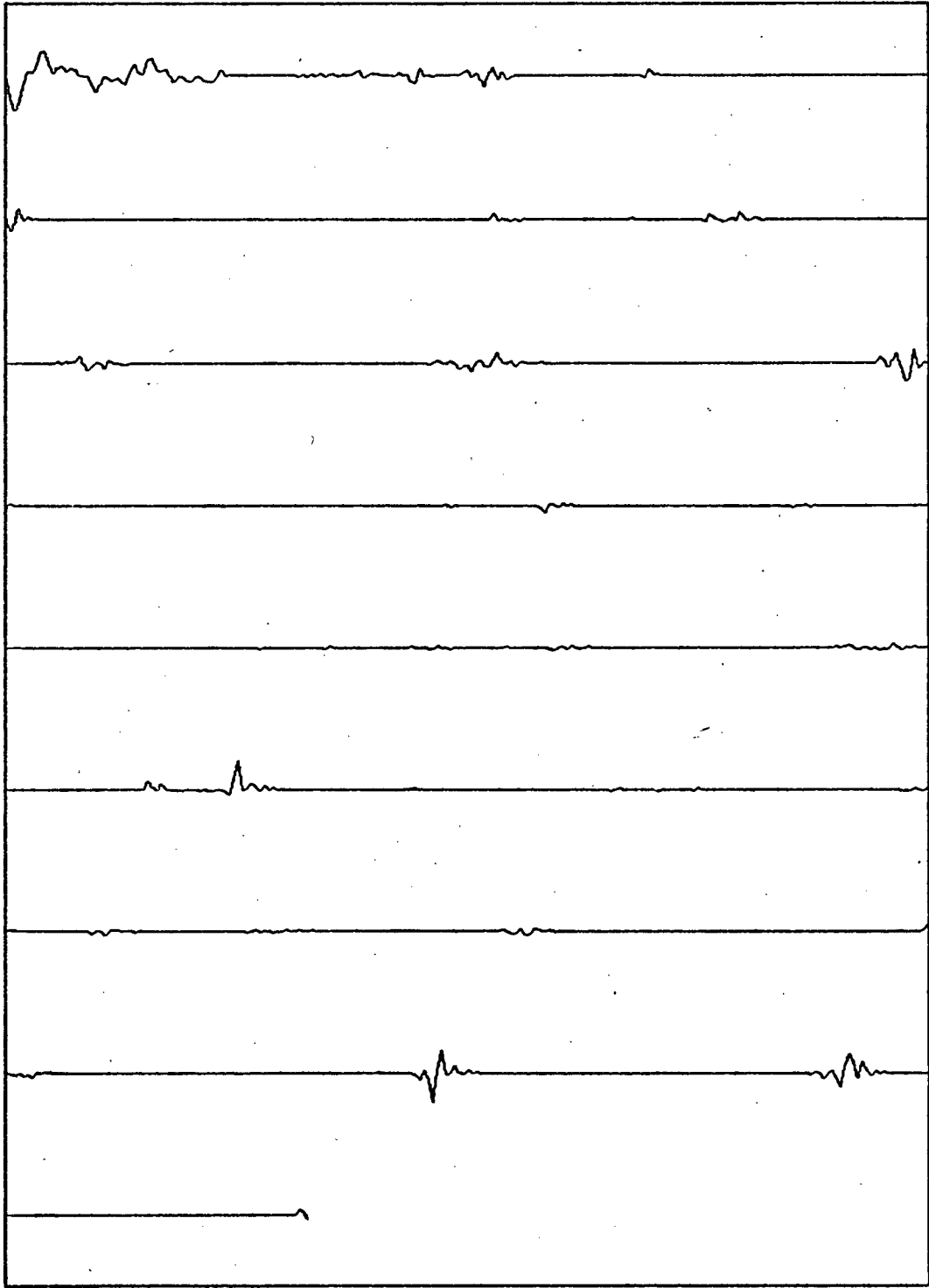


FIGURE 8

75 μ gals

Once the filter has been designed, it is run over the data such that the prediction is done into the gap from both sides. The predictions are then tapered with a ramp function and combined in a final result. In Figure #9, a harmonic signal (0.05 and 0.06 Hz.) with 20% noise is shown by the solid line. The dashed line shows the prediction of the middle 120 points of data using only information from the first and last 40 points of data. The result is quite good and studies by Ulrych and Clayton (1975) have shown that the improvement in the spectral resolution is excellent.

The results for deglitching both the high passed and band passed data sets can be seen in Figures #10 and #11. The prediction error traces for these deglitched records are shown in Figures #12 and #13. There is a remarkable improvement in the records, and this can be seen visually in both the deglitched and prediction error traces.

C. Deglitching By Envelope

An alternative method for deglitching was suggested by Wiggins (personal communication), and this technique was applied to the first 3000 points of the high passed record.

Dividing the data by the square of its envelope was thought of as a possible means of removing the high amplitudes of the noise bursts, even though the frequency content would not be altered. A modification of this scheme was applied, in that a function E' was created where

FIGURE 9.

Test case of the gap prediction routine. A mixed harmonic of 0.05 Hz. and 0.06 Hz. with 20% added noise. The solid line represents the original data, and the dotted line represents the predicted data. The first 40 and last 40 points were used to predict the middle 120 points. The filter length was chosen to be 35.

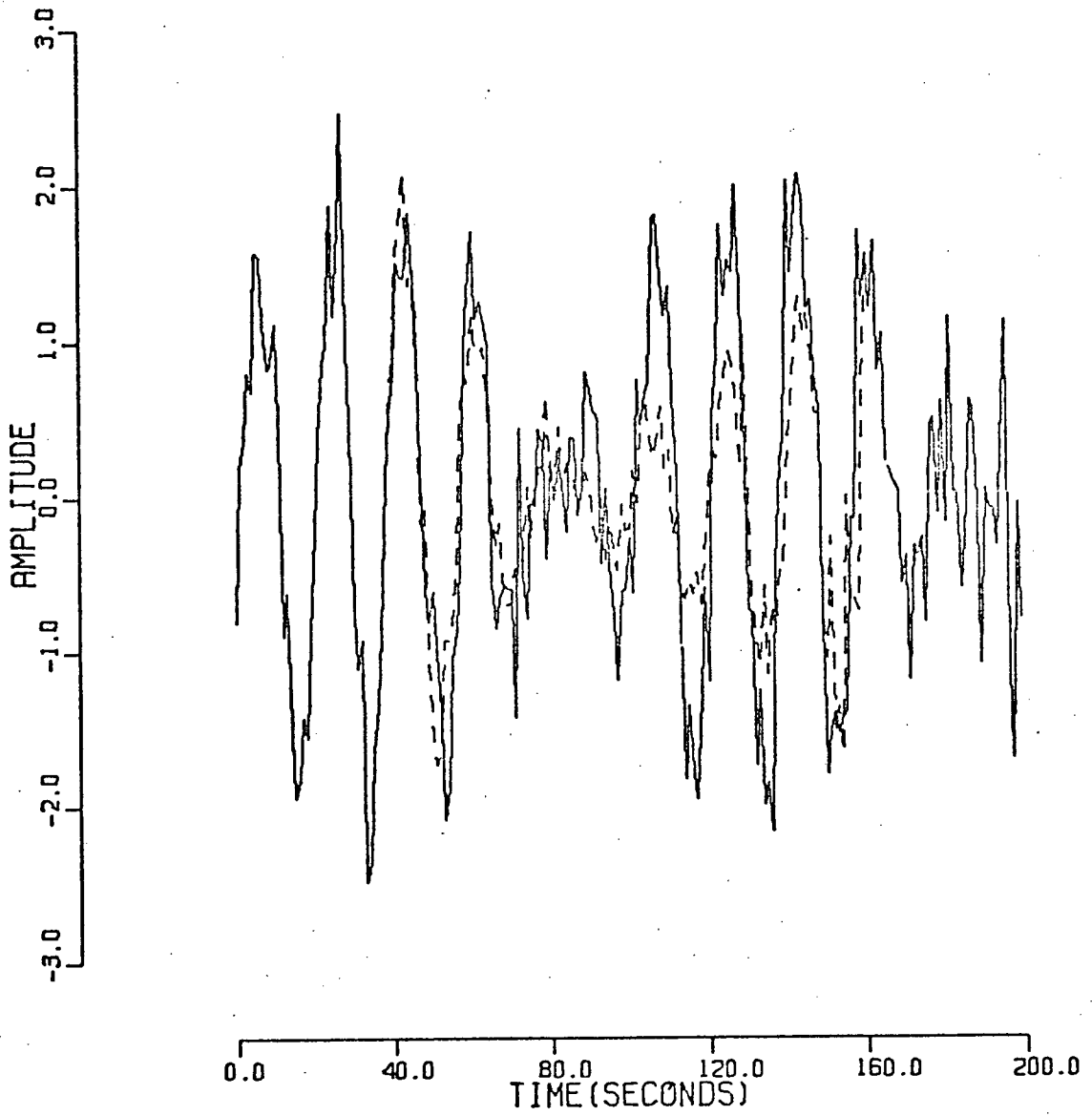
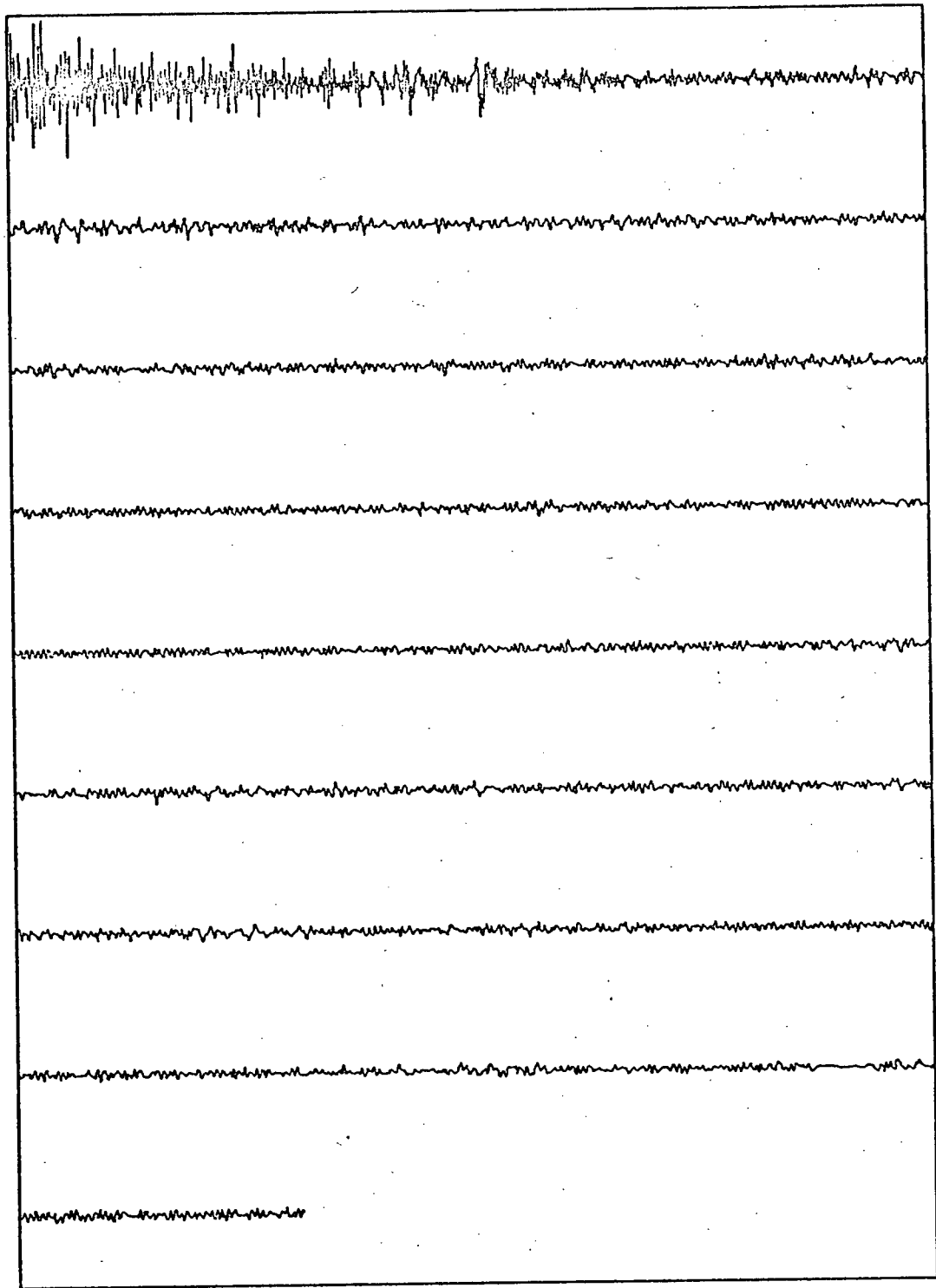


FIGURE 9

FIGURES 10 AND 11.

Deglitched high pass and band pass filtered predicted record. Glitches were identified, then predicted out using a filter operator determined from the Burg algorithm.

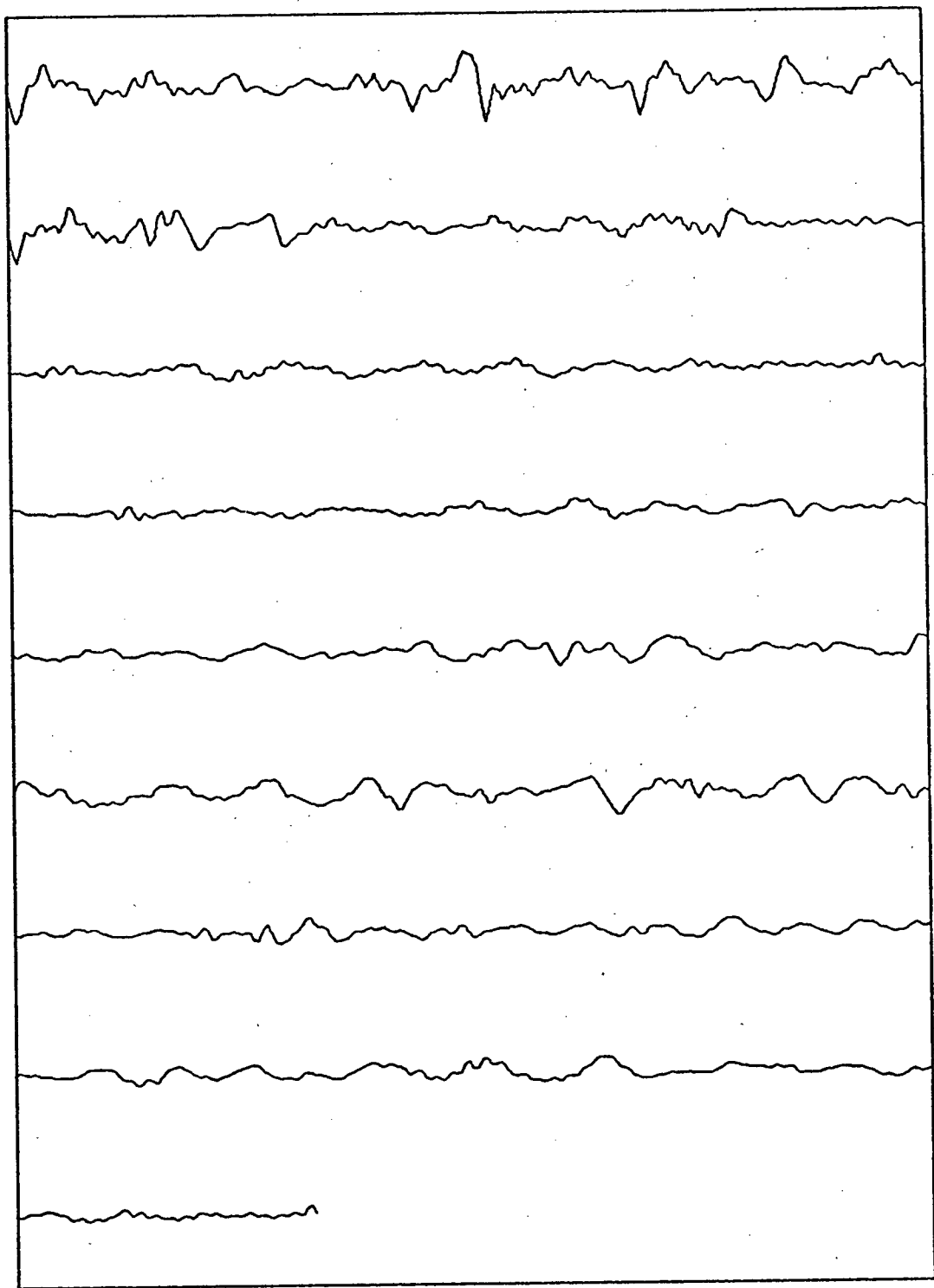


12 hrs

FIGURE 10

100 μ gals





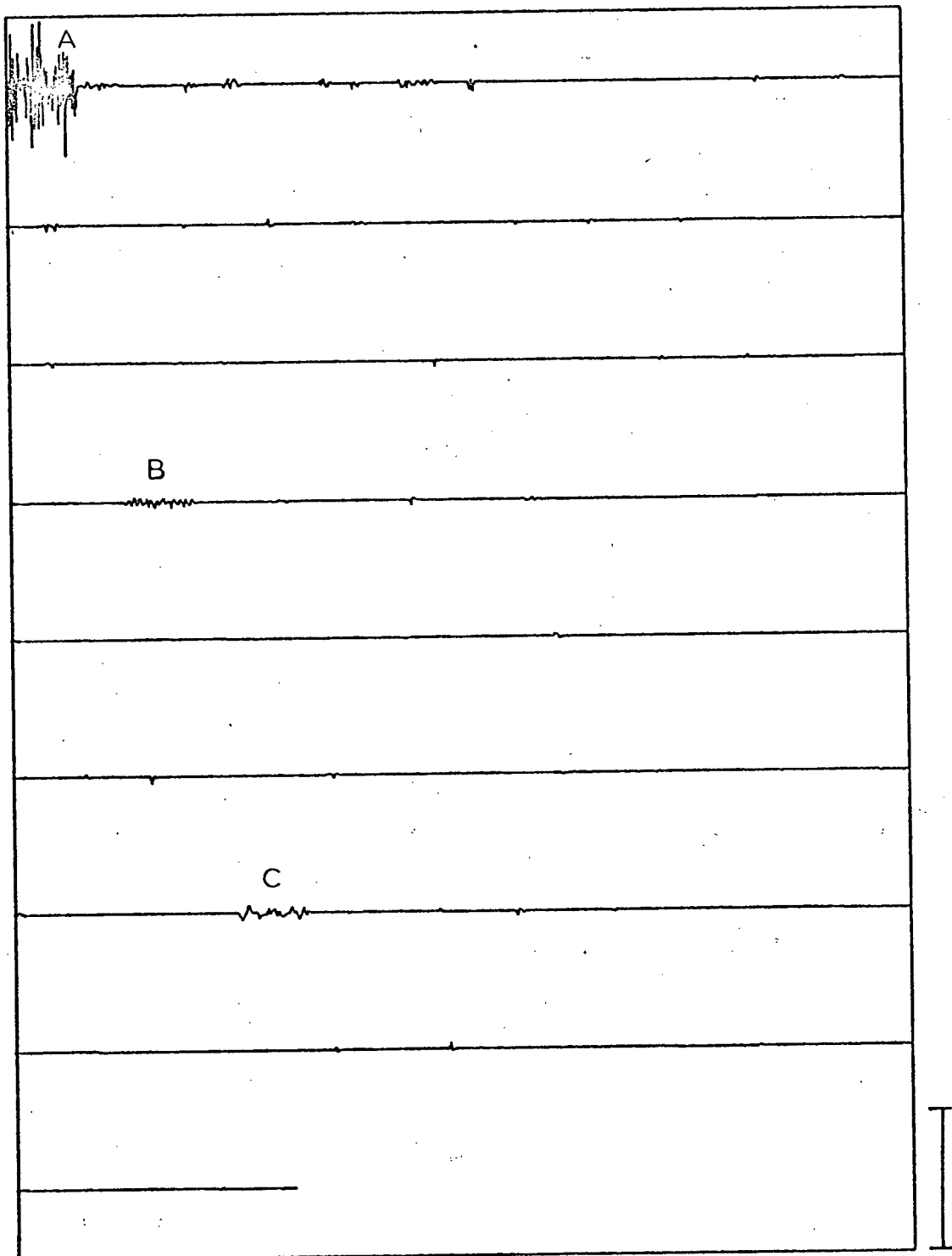
12 hrs

FIGURE 11

70 μ gals

FIGURES 12 AND 13.

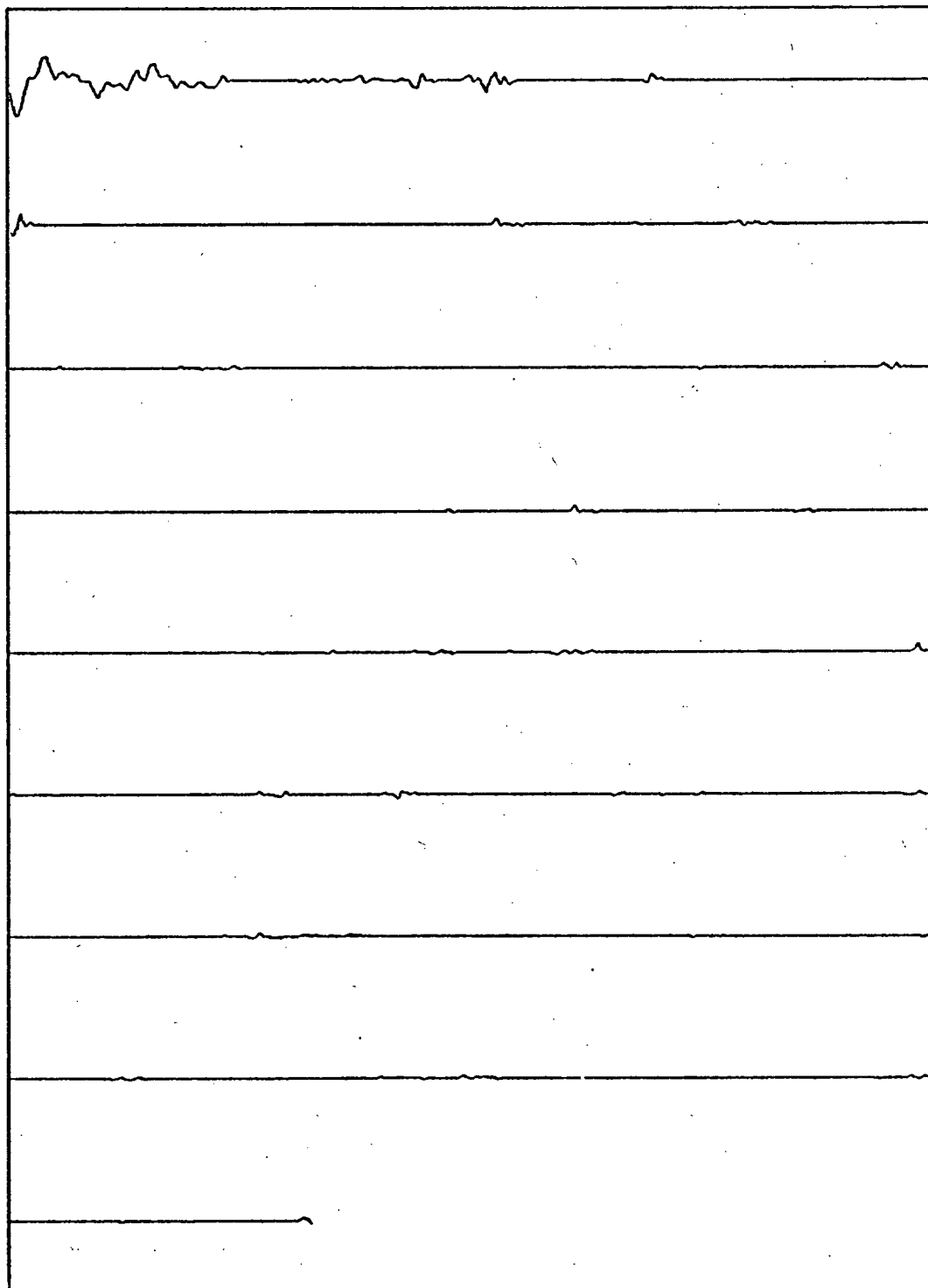
Prediction error traces of both deglitched high passed and band passed predicted records. The areas of unpredictability have been largely eliminated by the deglitching process.



12 hrs

FIGURE 12

100 ygals



12 hrs

FIGURE 13

75 μgals

$$E' = E/W.L.$$

E = envelope of the process

$W.L.$ = some predetermined water level parameter.

In this case, the water level was not constant but was weighted exponentially at the beginning of the record so as to correspond to the high signal amplitude in this section of the data. If any data fell above the water level, the function E' was set equal to $E/W.L.$ If any data value fell below the water level, the function E' was set equal to 1.0. i.e.

$$E' = 1.0 \text{ if } E' < 1.0$$

$$E' = E/W.L. \text{ if } E' > 1.0$$

The record was then divided by $(E')^2$ and the reduction in glitch amplitude was very successful (Figure #14). There is also a noticeable drop in the noise content in the frequency domain (see Chapter IV).

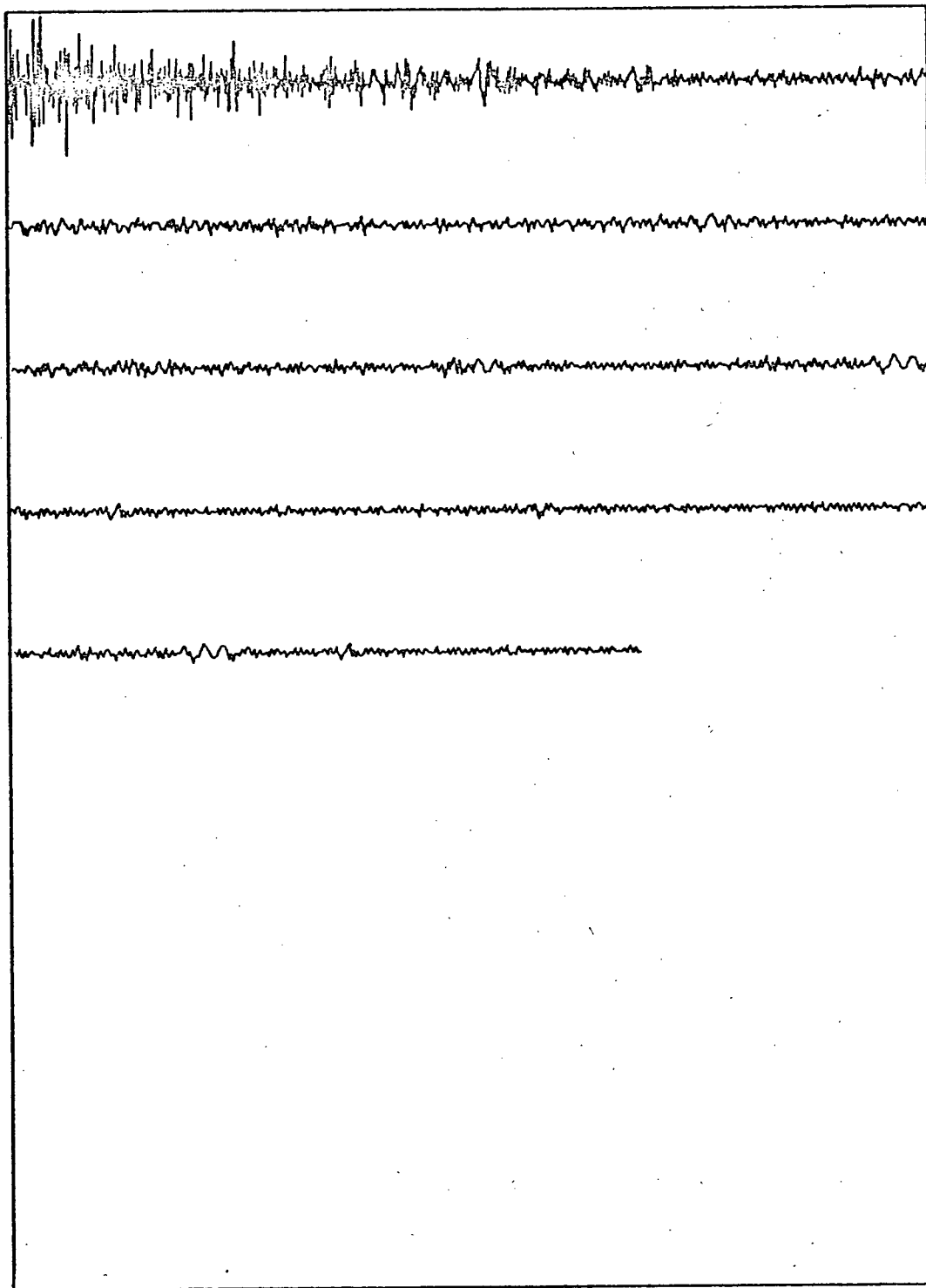
5. POWER SPECTRAL ANALYSIS

A. Periodogram and MEM Spectra

In the calculation of power spectra for this project, both conventional and MEM spectra were used. In all cases, the periodograms were not smoothed. The periodogram was

FIGURE #14.

Deglitched high passed predicted record. Deglitching was accomplished by dividing the record by the square of its envelope. The amplitudes of the glitches have been greatly reduced, but the frequency content of the glitches is still evident.



12 hrs

FIGURE 14

100 ygals

extremely useful in helping to determine the optimum order of the prediction error filter needed in the calculation of the MEM spectra, as it gave prior knowledge of the result. In almost all cases, the MEM spectra for each free oscillation mode were calculated several times using different filter orders and data lengths. In most cases the FPE gave no realistic indication of the filter order to be used.

B. Complex Demodulation

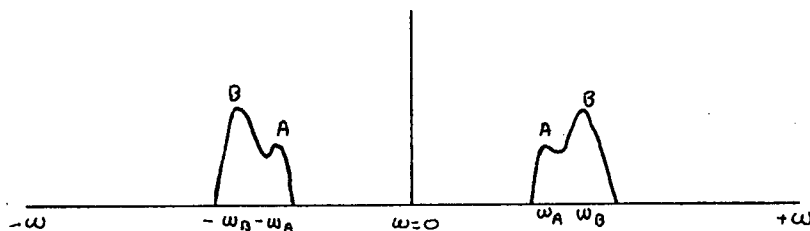
In the analysis of the spectra of individual free oscillation modes, a technique known as complex demodulation was used. This method involves a shifting of the frequency of interest down to ' $\omega = 0$ ', then low pass filtering the data, and finally resampling the data at a coarser interval. This method is particularly useful when calculating MEM spectra, as fewer points are used in the calculation of the filter coefficients. Two sources of error are thus eliminated:

1. Roundoff errors leading to inaccuracies particularly with harmonic terms.
2. Order of magnitude differences between the power of different frequency components which results in numerical instabilities (Ulrych and Bishop 1975).

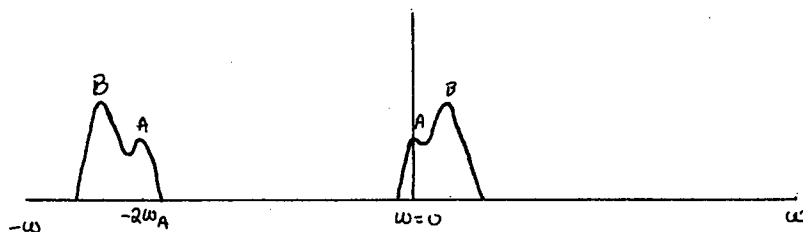
The technique of complex demodulation is expressed

schematically below.

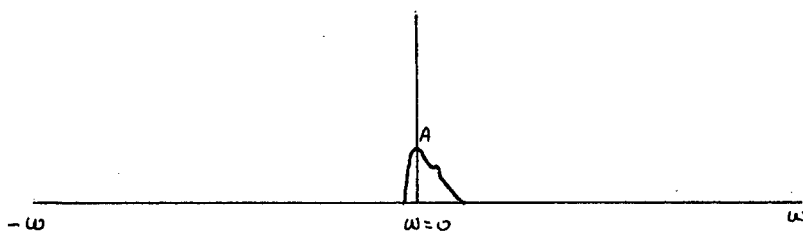
Suppose a time series $x(t)$ is comprised of two frequency bands, and it is necessary that peak 'A' be isolated.



The complex time series $C(t) = (x(t), i0)$ is multiplied by the factor $\exp(-i\omega_A n \Delta t)$, where ω_A is the angular frequency of peak 'A' and Δt is the sampling interval. This multiplication shifts peak 'A' to $\omega = 0$, and the negative peak 'A' to $\omega = -2\omega_A$.



The data can then be low pass filtered so as to only retain the frequency band around $\omega = 0$.



Resampling in the time domain can now be performed with no aliasing, and a stable MEM spectrum can be calculated for the

frequency component of interest.

This above operation can be expressed mathematically. Childers and Pao (1972) show that if a time series consists of a set of transient harmonics

$$f(t) = [e^{-(t-T)/\tau} \sin \omega_0(t-T)]$$

$$e^{-(t-T)/\tau} = \text{transient decay factor}$$

then multiplying $f(t)$ by the demodulation factor $e^{-i\omega_0 t}$ gives

$$\begin{aligned} \tilde{f}(t) &= \{ e^{-(t-T)/\tau} / 2i [e^{i\omega_0(t-T)} - e^{-i\omega_0(t-T)}] e^{-i\omega_0 t} \} \\ &= e^{-(t-T)/\tau} / 2i [e^{-i\omega_0 T} - e^{-i2\omega_0 t} e^{i\omega_0 T}]. \end{aligned}$$

This new series $\tilde{f}(t)$ has a $2\omega_0$ frequency component which can be filtered out to leave

$$\tilde{f}(t) = (e^{-(t-T)/\tau} / 2i) \{e^{-i\omega_0 T}\}$$

IV. RESULTS

1. FREE OSCILLATION MODE FREQUENCIES

The deglitched and undeglitched high pass filtered data sets were used in the examination of free oscillation multiplets and the associated splitting parameters. Periodogram and MEM spectra were calculated using various data lengths and filter orders.

The values for the splitting parameter ' β ' were calculated using the first order splitting approximation given by Backus and Gilbert (1961), where

$$\omega_m = \omega_0 + m\beta\Omega$$

ω_m = split peak frequency

ω_0 = centre peak frequency

m = splitting order number

β = splitting parameter

Ω = rotation rate of the earth

The following sections detail the measured frequency values and calculated splitting parameters for the fundamental spheroidal modes ${}_0S_2$, ${}_0S_3$, ${}_0S_4$, ${}_0S_5$, and ${}_0S_6$. Comparisons are also made between the spectra for undeglitched, deglitched, undemodulated, and unenhanced data sets. Remarks are also made about the effect of varying the filter order for

calculation of MEM spectra, and the higher resolution capability of MEM spectra as compared to periodogram spectra. In all cases, the power spectra shown were calculated from the complex demodulated data sets.

A. S_2 mode

The periodogram spectra for the undeglinted and deglinted records are shown in Figure 15a and Figure 15b. The noise levels are indicated, and the decrease in noise power was calculated to be 5 db. For the undeglinted spectrum (Figure 15a) it is only possible to identify the ± 1 peaks, whereas the deglinted spectrum (Figure 15b) shows the ± 1 peaks as well as the $+2$ peak.

Figure 15c is the periodogram power of the unenhanced (not predicted) high pass filtered record (Figure 1). This spectrum shows lower signal to noise levels than 15a, as a result of information loss at the beginning of the record. The advantage of predictive filtering in the analysis of the record can be seen.

Figure 15d is shown just as a check of the complex demodulation technique. For a periodogram there should be no difference between the spectrum calculated for the demodulated data and the one calculated for the undemodulated data. If Figures 15a and 15d are compared, this equivalence can be seen. Figures 15e and 15f show MEM spectra for the deglinted record with orders of 63 and 150 respectively. The

greater detail in 15f is the result of choosing a higher filter order. A possible -2 peak has also been identified on this plot. Figures 15e and 15f show considerably less noise, and better resolved peaks than Figure 15g, which is the MEM spectrum (order=110) for the undeglinted data set.

Interestingly enough, the MEM spectra, Figure 15h (order=45), and Figure 15i (order=55), for the first 1200 points of the record, seem to show both the ± 1 and ± 2 peaks, whereas the corresponding periodogram (Figure 15j) shows only the ± 1 peaks. This is a good example of the increased resolution capability of the MEM spectral estimation method. For the ${}_0S_2$ mode, the 'm=0' peak cannot be observed, as it corresponds to a nodal point located at Los Angeles. Therefore, the ± 1 , and ± 2 peaks are all that will be observed in this record. The frequency of the '0' peak is calculated as the average of the ± 1 peaks. Table 1 details the frequencies observed for the ${}_0S_2$ mode.

TABLE #1

<u>Periodogram</u>	<u>5320 Points</u>	<u>Undeglinted</u>	<u>15a</u>
<u>freq. (cy/hr)</u>		<u>β</u>	
+1 1.130 \pm .001		.360 \pm .007	
0 1.114 \pm .001			
-1 1.097 \pm .001		.432 \pm .007	

<u>MEM order=55</u>	<u>1200 Points</u>	<u>Undeglitched</u>	<u>15i</u>
<u>freq. (cy/hr)</u>		<u>β</u>	
+2 1.162 \pm .002		.564 \pm .008	
+1 1.134 \pm .002		.455 \pm .011	
0 1.117 \pm .001			
-1 1.100 \pm .001		.360 \pm .007	
-2 1.078 \pm .002		.444 \pm .008	

<u>Periodogram</u>	<u>1200 Points</u>	<u>Undeglitched</u>	<u>15j</u>
<u>freq. (cy/hr)</u>		<u>β</u>	
+1 1.131 \pm .001		.384 \pm .007	
0 1.115 \pm .001			
-1 1.099 \pm .002		.384 \pm .011	

<u>Average Values from MEM spectra</u>	<u>freq. (cy/hr)</u>	<u>β</u>
+2 1.160 \pm .003		.540 \pm .035
+1 1.131 \pm .002		.374 \pm .046
0 1.115 \pm .001		
-1 1.099 \pm .001		.379 \pm .020
-2 1.075 \pm .003		.480 \pm .032

Average β overall = .439 \pm .081

The errors given for the average values are standard deviations.

Gilbert and Backus (1965) gave a value of 1.116 cycles per hour for the frequency of the S_2 mode, and a value of 0.397 for the splitting parameter. Derr (1969) gave values of 1.114 cycles per hour and 0.397. These compare to the average values of 1.115 cycles per hour and 0.439 obtained in this project. However, the values for ' β ' that were calculated for each peak were not constant. As Wiggins and Miller (1972) noted, there appears to be a dependence of the splitting parameter ' β ' on the splitting order number ' m '. The latter

FIGURE 15

a.	Periodogram	5320 points	Undeglitched
b.	Periodogram	5320 points	Deglitched
c.	Periodogram	5320 points	Unenhanced
d.	Periodogram	5320 points	Undemodulated
e.	MEM order=63	5320 points	Deglitched
f.	MEM order=150	5320 points	Deglitched
g.	MEM order=110	5320 points	Undeglitched
h.	MEM order=45	1200 points	Undeglitched
i.	MEM order=55	1200 points	Undeglitched
j.	Periodogram	1200 points	Undeglitched

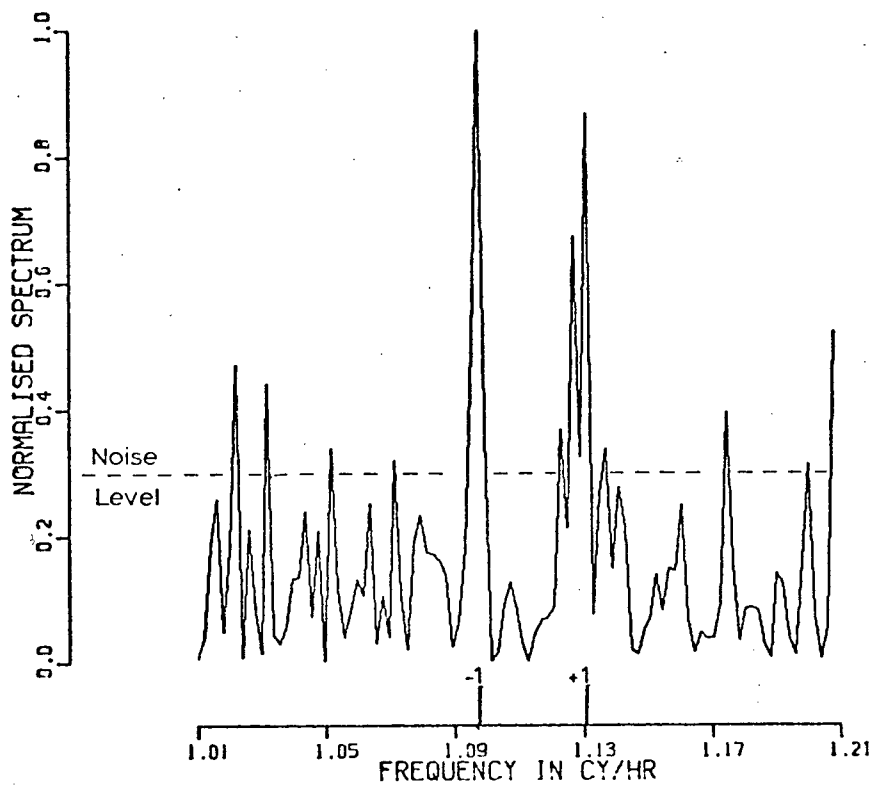


FIGURE 15a

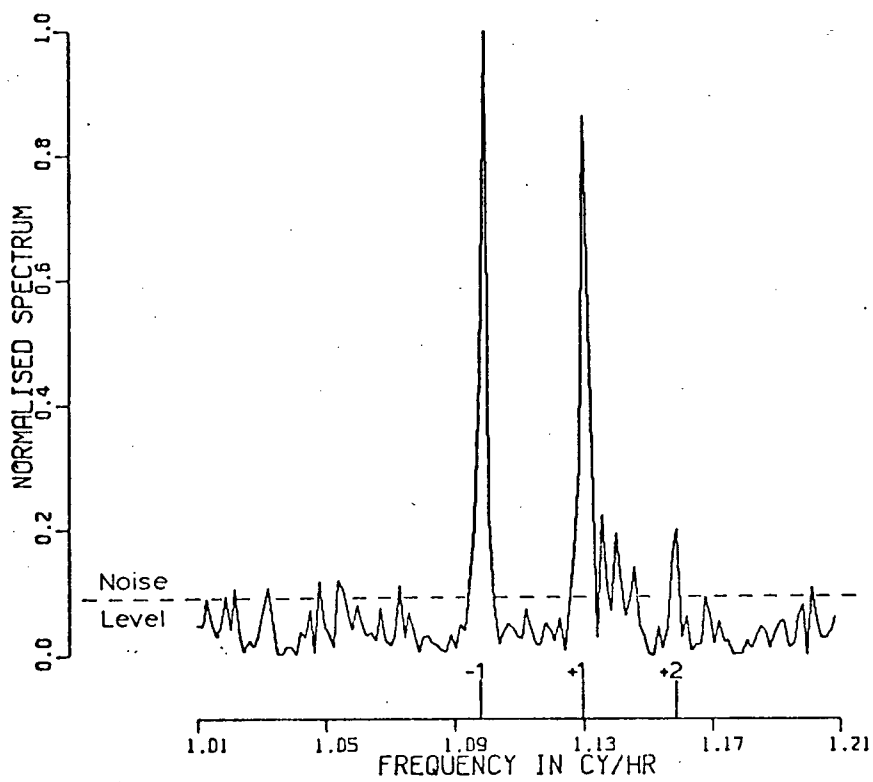


FIGURE 15b

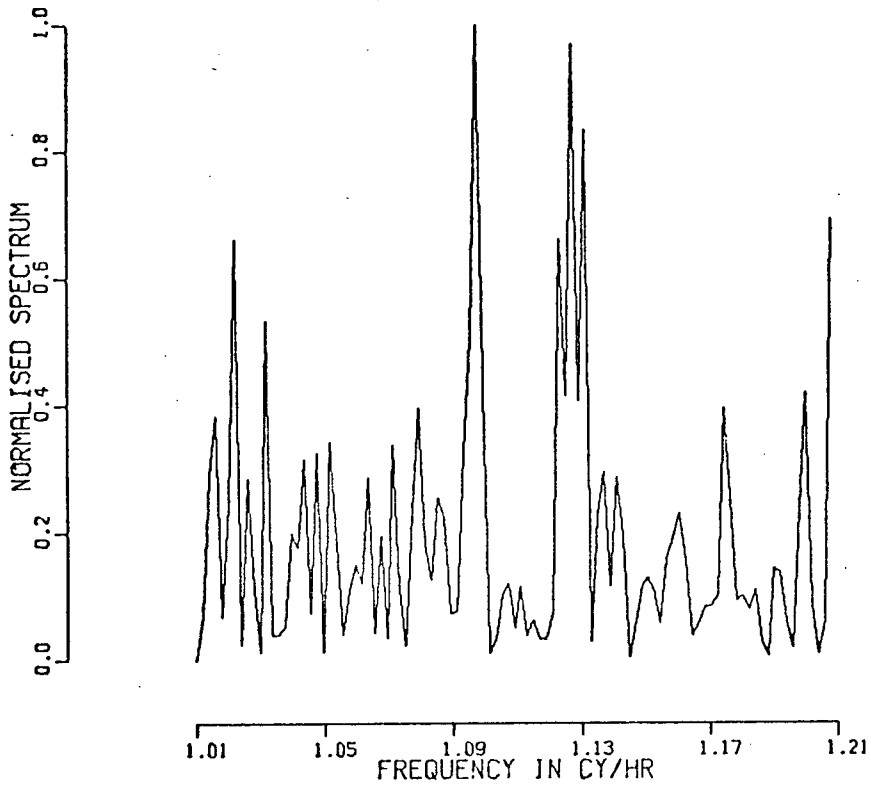


FIGURE 15c

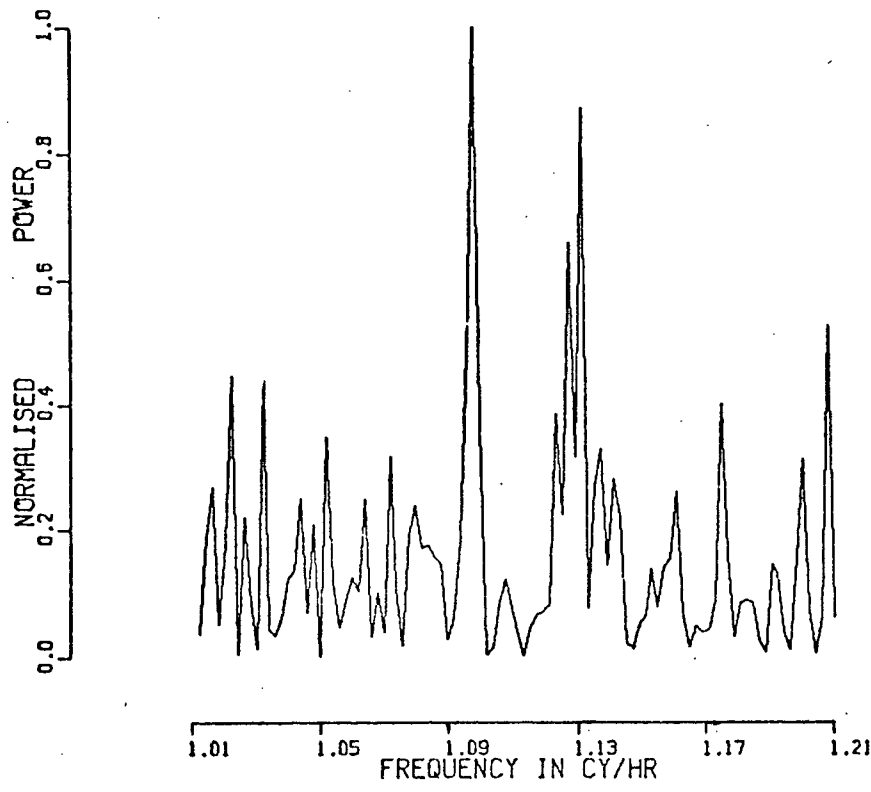


FIGURE 15d

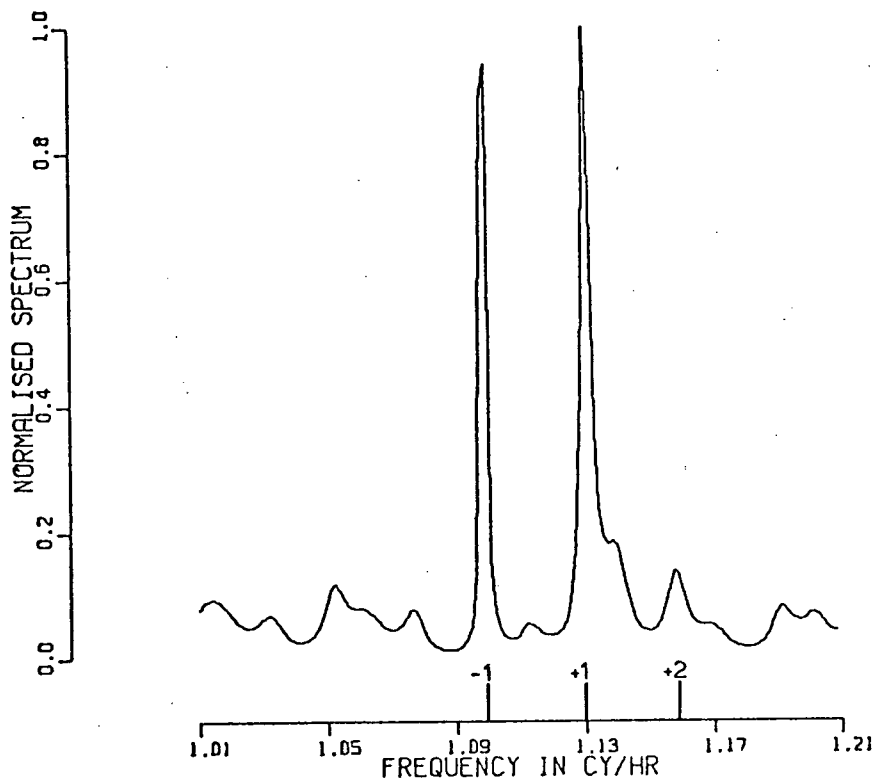


FIGURE 15e

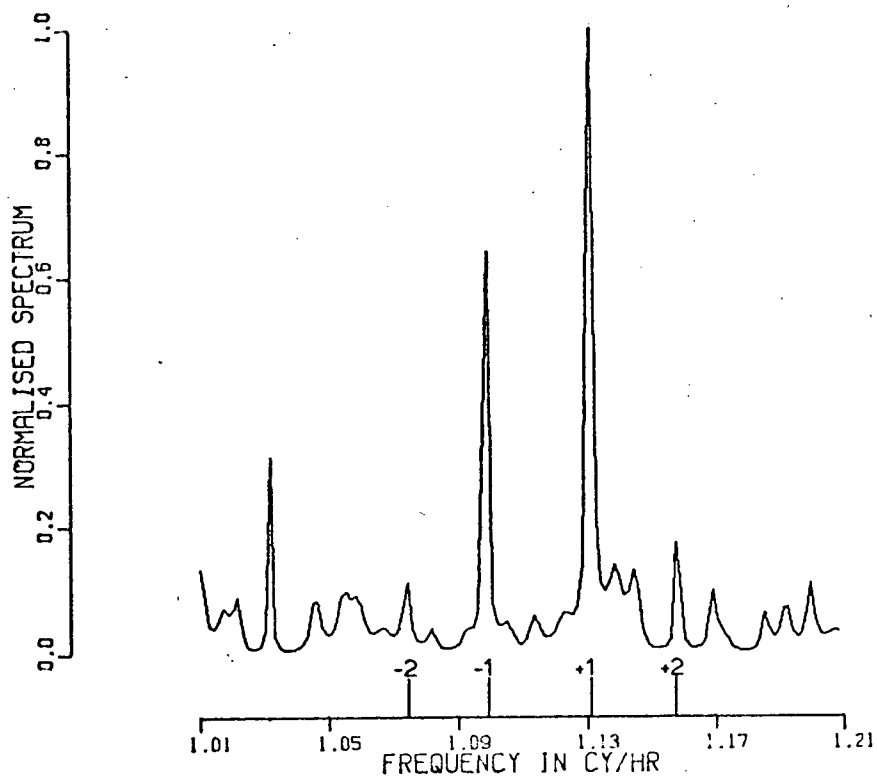


FIGURE 15f

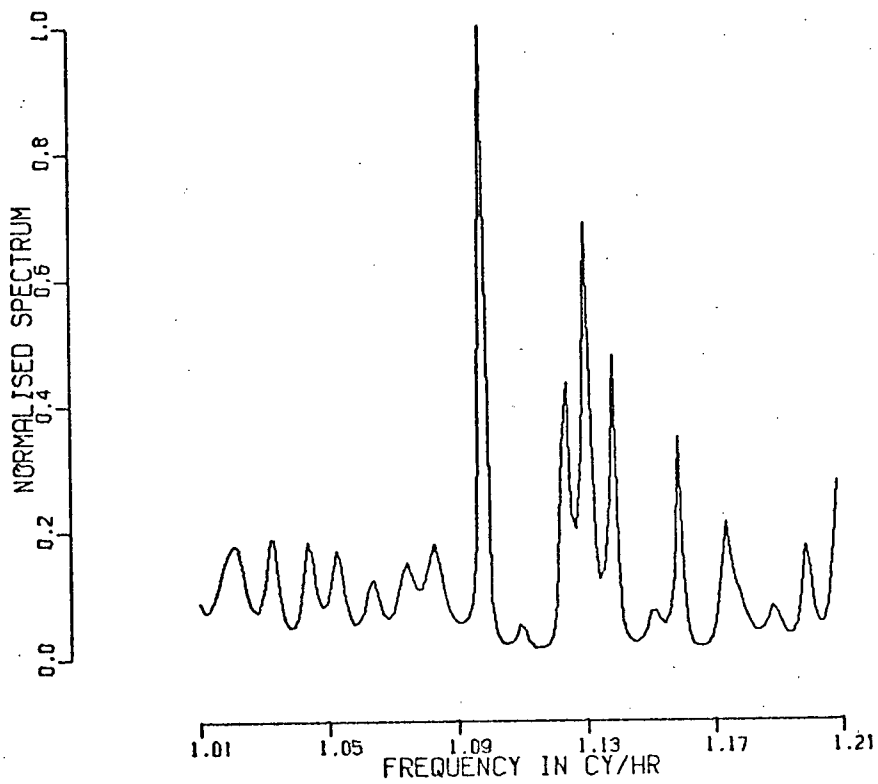


FIGURE 15g

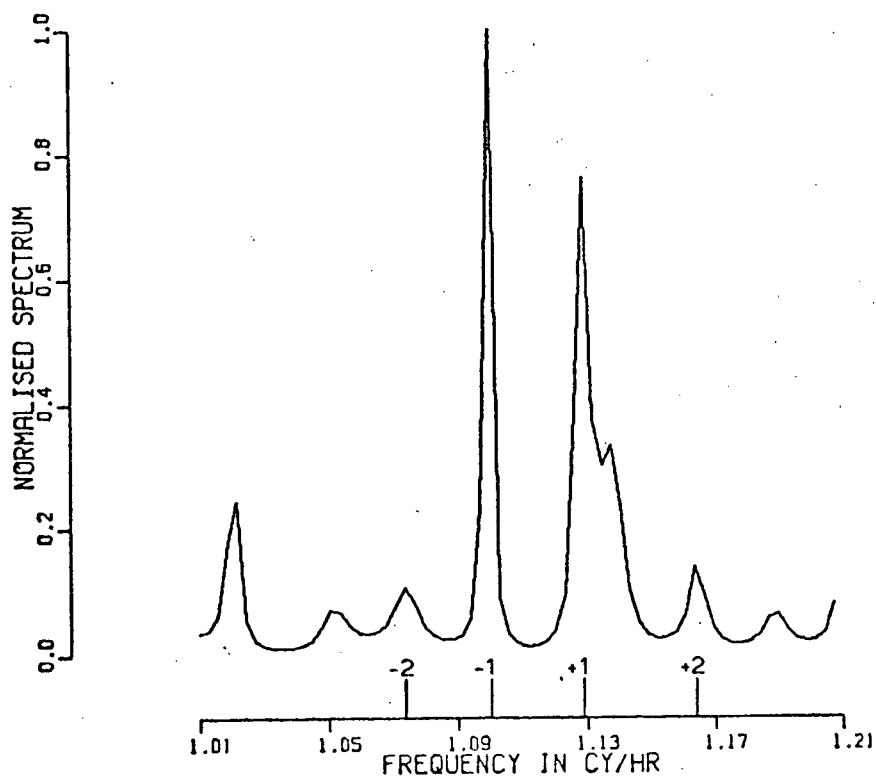


FIGURE 15h

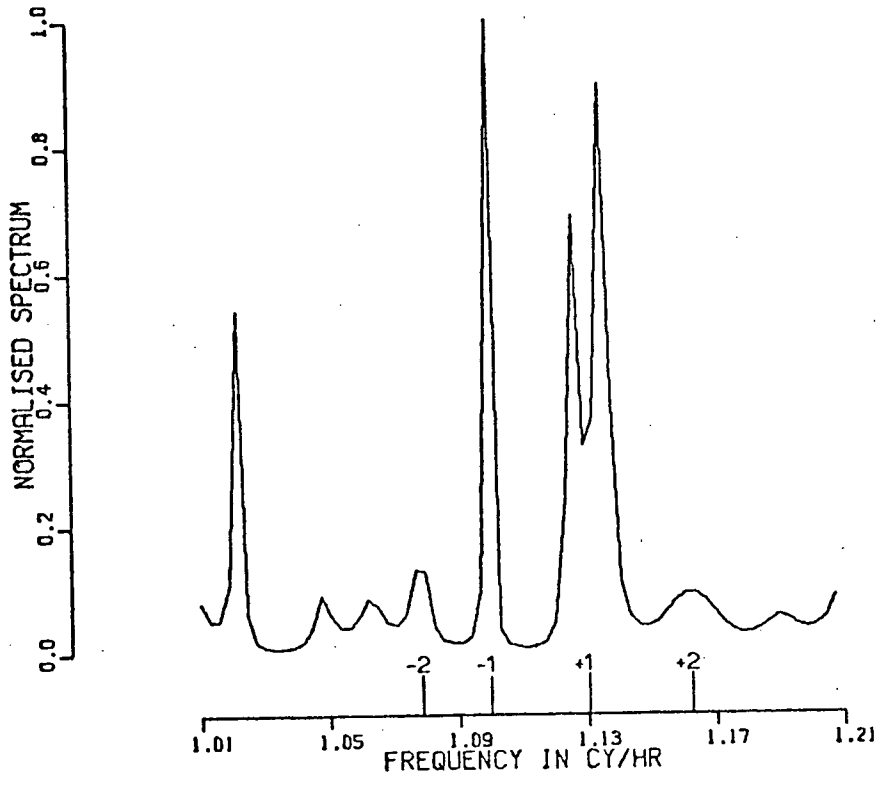


FIGURE 15i

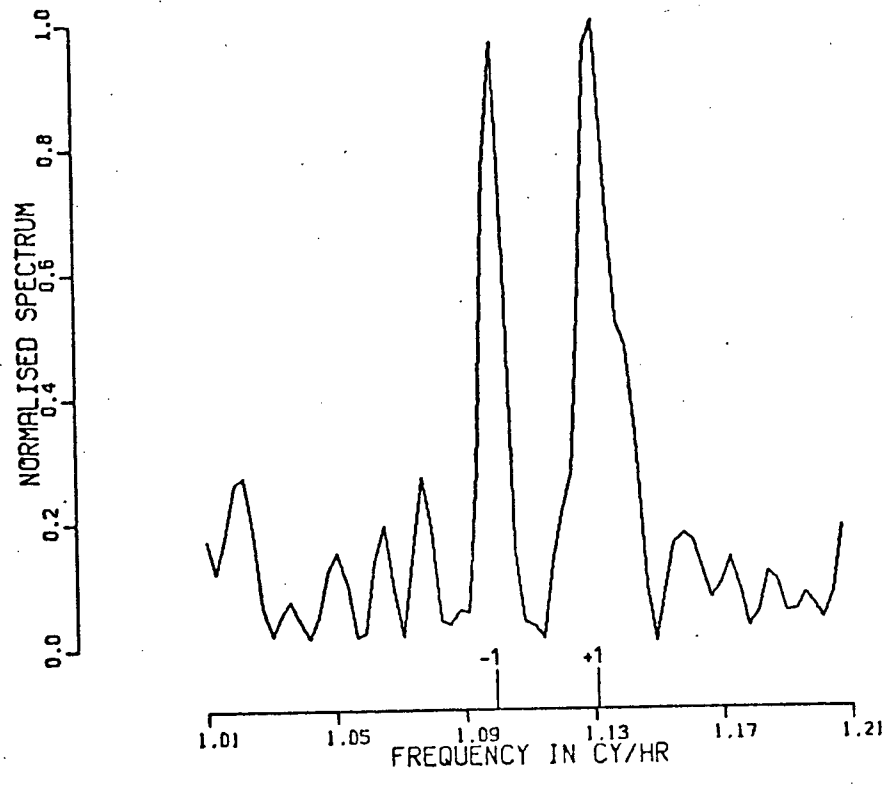


FIGURE 15j

authors gave values for ' β ' of 0.408, 0.410, and 0.522 for the -1, +1, and +2 peaks, which compare reasonably well to the values of 0.379, 0.374, and 0.540 obtained here.

B. $\circ S_3$ mode

The periodogram power spectra for the undeglinted and deglinted high passed records are shown in Figures 16a and 16b. As observed for the $\circ S_2$ mode, there is a very noticeable reduction in the noise content for the deglinted record. Figure 16c is the MEM spectrum (order=130) for the undeglinted data set, and should be compared to Figures 16d, 16e, and 16f, which are the MEM spectra for the corresponding deglinted data (orders 70, 130, and 150). The effect of varying the length of the calculated prediction operator can be seen in these last three figures, where the spectral resolution increases as the order of the filter increases. However, going to too high an order will result in an unstable spectrum. This is starting to happen with the 150 point MEM spectrum, as the noise is beginning to take on a very spiky appearance.

Deglinting the record by dividing by the square of the envelope is demonstrated in the next two figures, 16g and 16h. Figure 16g shows the periodogram power of 3000 points of undeglinted data, and 16h shows the periodogram power for the deglinted 3000 point segment. There is a noticeable reduction in the noise content using this method of removing

MEM order=130 5320 Points Deglitched 16e
freq. (cy/hr) β

+2	1.704 ± .001	.216 ± .005
+1	1.693 ± .001	.168 ± .007
0	1.686 ± .001	
-1	1.680 ± .001	.144 ± .007
-2	1.670 ± .001	.192 ± .005
-3	1.665 ± .001	.168 ± .004

MEM order=150 5320 Points Deglitched 16f
freq. (cy/hr) β

+2	1.704 ± .001	.216 ± .005
+1	1.694 ± .001	.192 ± .007
0	1.686 ± .001	
-1	1.681 ± .001	.120 ± .007
-2	1.671 ± .001	.180 ± .005
-3	1.665 ± .001	.168 ± .004

Periodogram 5320 Points Undeglitched 16g
freq. (cy/hr) β

+2	1.705 ± .001	.228 ± .005
+1	1.694 ± .001	.168 ± .007
0	1.687 ± .001	
-1	1.682 ± .001	.096 ± .007
-2	1.673 ± .001	.156 ± .005
-3	1.667 ± .002	.152 ± .006

Average Values from MEM spectra
freq. (cy/hr) β

+2	1.704 ± .001	.220 ± .007
+1	1.693 ± .001	.168 ± .033
0	1.686 ± .001	
-1	1.681 ± .001	.126 ± .024
-2	1.669 ± .002	.201 ± .020
-3	1.665 ± .001	.168 ± .009

Average β overall = .177 ± .040

Gilbert and Backus (1965) gave a value of 1.688 cycles per hour for the frequency of ${}_0S_3$ and a value of .1839 for

FIGURE 16

a.	Periodogram	5320 points	Undeglitched
b.	Periodogram	5320 points	Deglitched
c.	MEM order=130	5320 points	Undeglitched
d.	MEM order=70	5320 points	Deglitched
e.	MEM order=130	5320 points	Deglitched
f.	MEM order=150	5320 points	Deglitched
g.	Periodogram	3000 points	Undeglitched
h.	Periodogram	3000 points	Deglitched

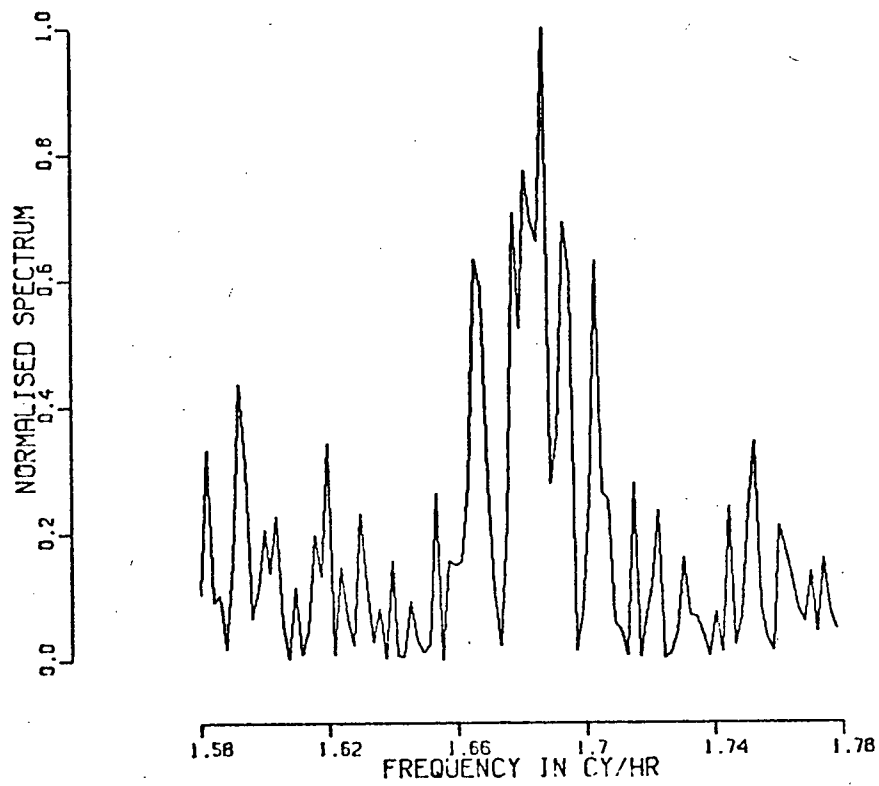


FIGURE 16a

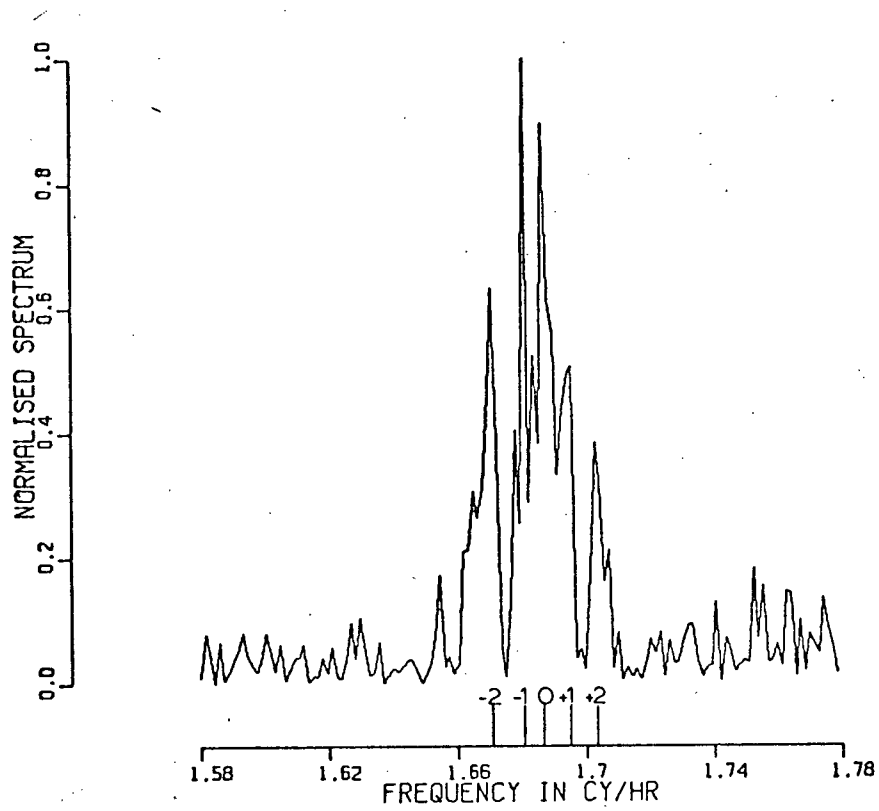


FIGURE 16b

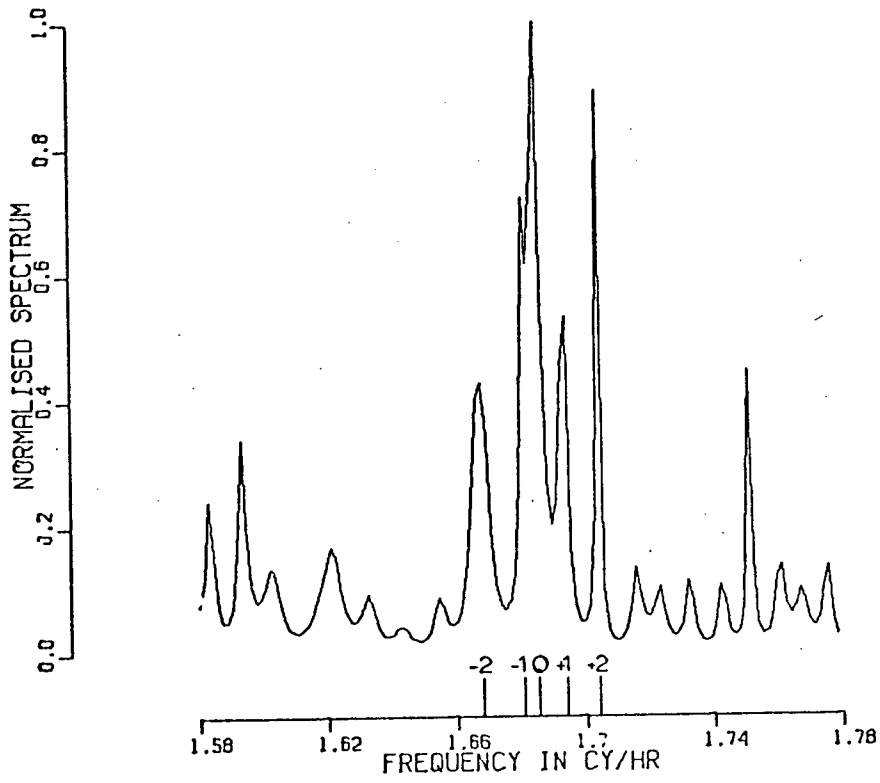


FIGURE 16c

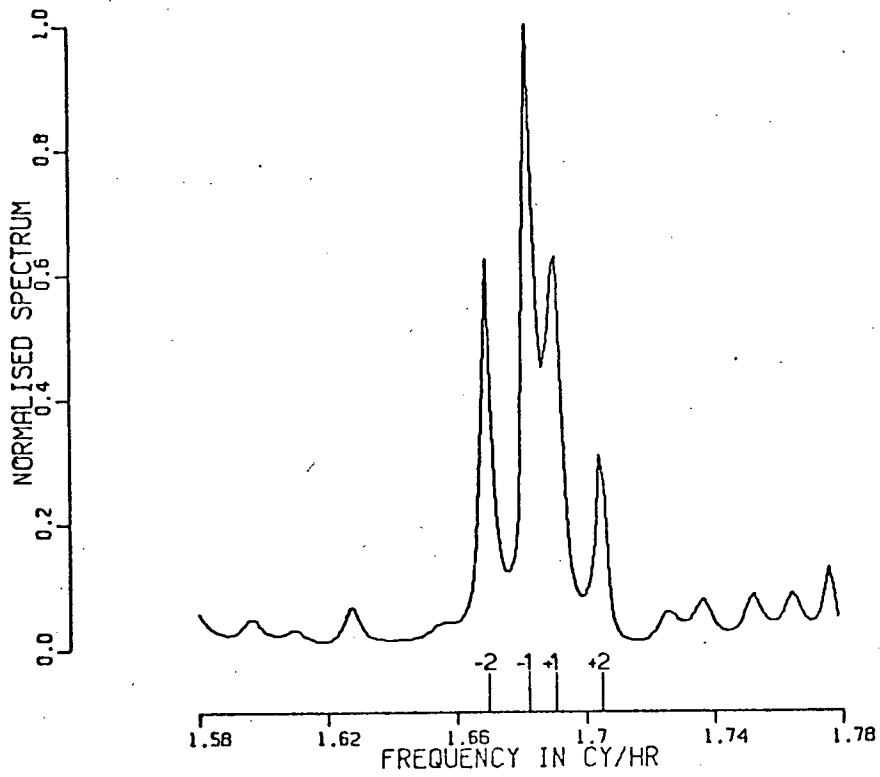


FIGURE 16d

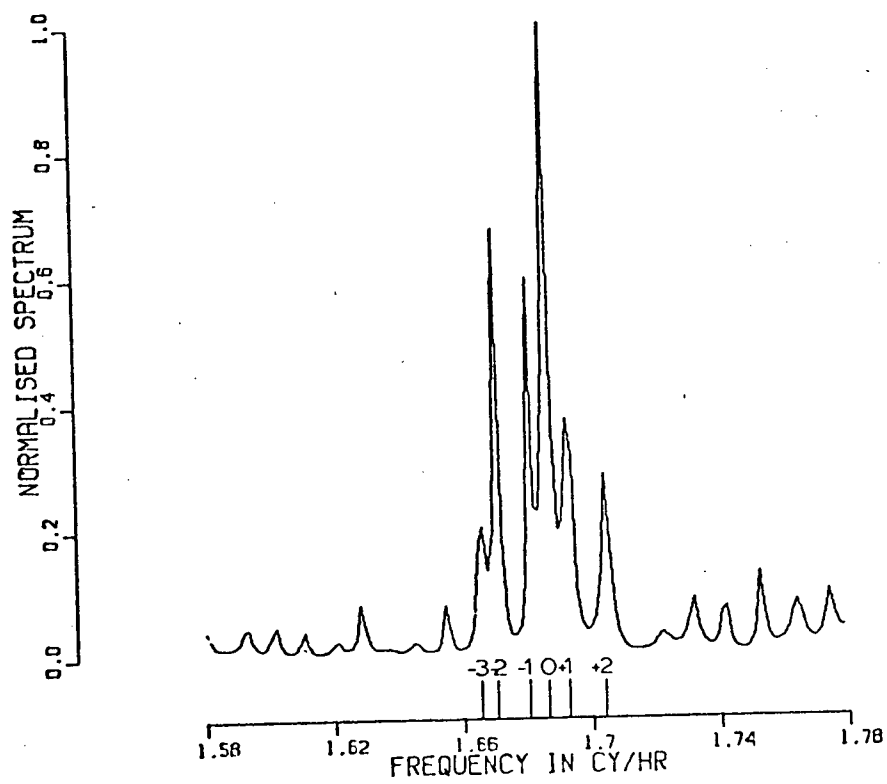


FIGURE 16e

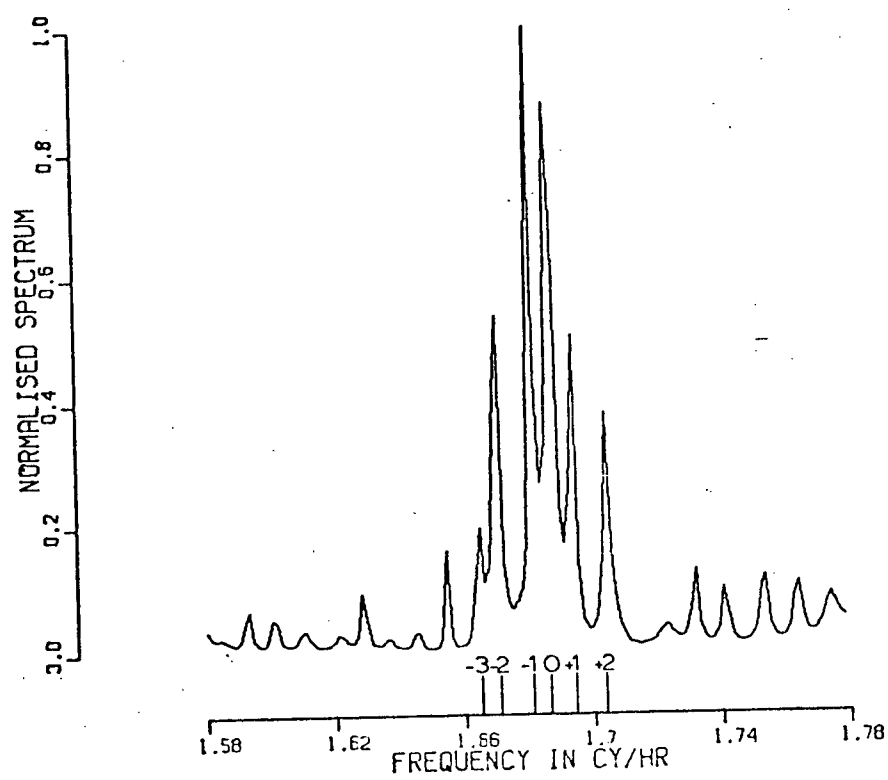


FIGURE 16f

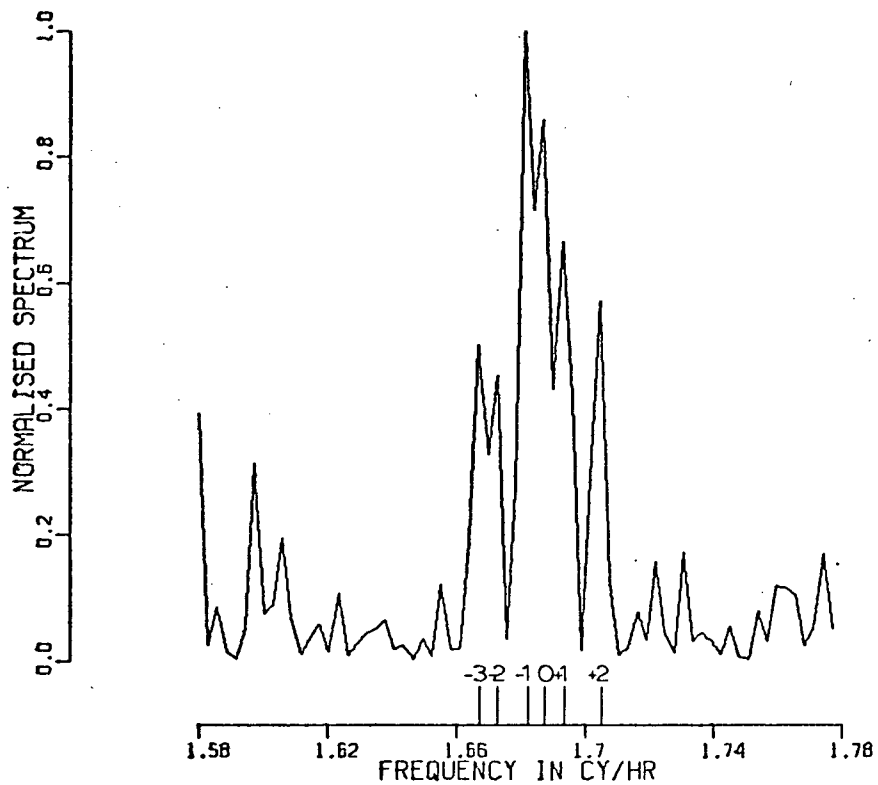


FIGURE 16g

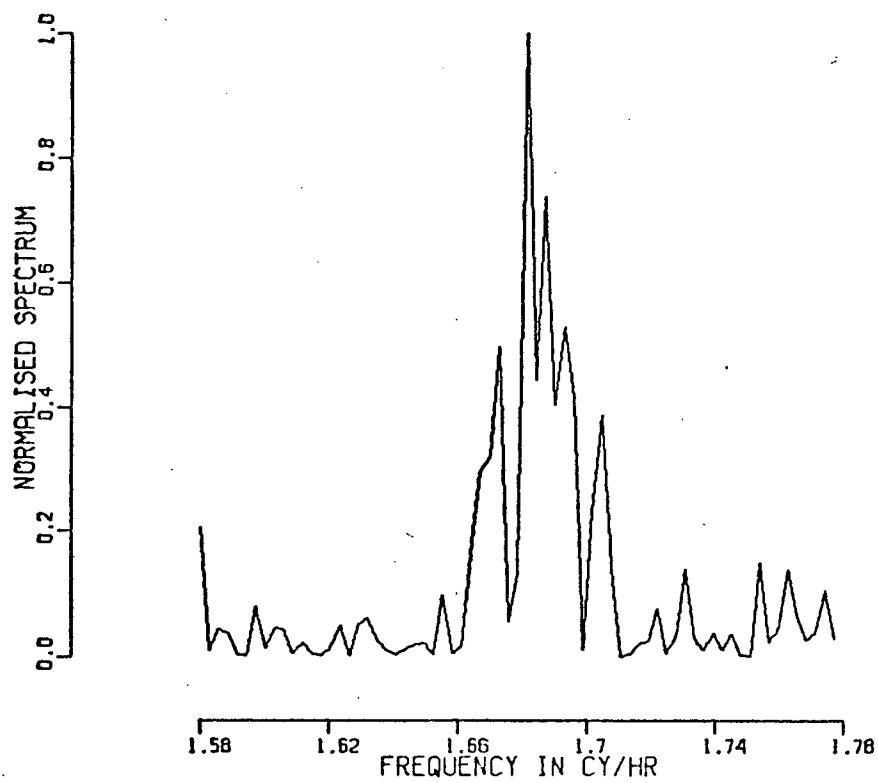


FIGURE 16h

the splitting parameter. Derr (1969) gave values of 1.687 cycles per hour and .187. These compare with the average values of 1.686 and .177 obtained in this project. A dependence of ' β ' on 'm' is again observed.

C. S₄ mode

The periodogram power spectra for the undeglitced and deglitced high passed record are shown in Figures 17a and 17b. Splitting can be observed in both, and although identification of the number of the split peaks is difficult, a fairly good explanation of the peaks has been made. Figure 17c is the periodogram spectrum of the unenhanced data, and if this is compared with Figure 17a, the advantage of extending the data set before tapering can be seen.

Figures 17d and 17e are MEM spectra of the undeglitced (order=130) and the deglitced (order=150) records. Deglitching by dividing by the square of the envelope of the record is illustrated in Figures 17f and 17g, where 17f is the periodogram power of 3000 points of undeglitced data, and 17g is the power of the corresponding deglitced data. There is however, very little difference between these two spectra, indicating that this method of removing the noise glitches is frequency dependent. Table #3 gives values for some of the observed frequency splits.

TABLE #3

Periodogram 5320 Points Deglitched 17b
freq. (cy/hr) β

+4	2.359 ± .002	.186 ± .005
+2	2.343 ± .002	.180 ± .008
+1	2.335 ± .001	.168 ± .007
0	2.328 ± .001	
-1	2.321 ± .001	.168 ± .007
-3	2.309 ± .002	.152 ± .006

MEM order=130 5320 Points Undeglitched 17d
freq. (cy/hr) β

+4	2.359 ± .001	.186 ± .003
+2	2.341 ± .001	.156 ± .005
+1	2.335 ± .001	.168 ± .007
0	2.328 ± .001	
-1	2.321 ± .001	.168 ± .007

MEM order=150 5320 Points Deglitched 17e
freq. (cy/hr) β

+4	2.359 ± .001	.186 ± .003
+2	2.341 ± .001	.156 ± .005
+1	2.333 ± .001	.120 ± .007
0	2.328 ± .001	
-1	2.321 ± .001	.168 ± .007
-3	2.310 ± .001	.144 ± .004

Average Values from MEM spectra
freq. (cy/hr) β

+4	2.359 ± .001	.186 ± .003
+2	2.341 ± .001	.156 ± .005
+1	2.334 ± .001	.144 ± .034
0	2.328 ± .001	
-1	2.321 ± .001	.168 ± .007
-3	2.310 ± .001	.144 ± .004

Average β overall = .161 ± 0.021.

The value for the $\circ S_4$ centre frequency given by

FIGURE 17

- | | | | |
|----|---------------|-------------|--------------|
| a. | Periodogram | 5320 points | Undeglitched |
| b. | Periodogram | 5320 points | Deglitched |
| c. | Periodogram | 5320 points | Unenhanced |
| d. | MEM order=130 | 5320 points | Undeglitched |
| e. | MEM order=150 | 5320 points | Deglitched |
| f. | Periodogram | 3000 points | Undeglitched |
| g. | Periodogram | 3000 points | Deglitched |

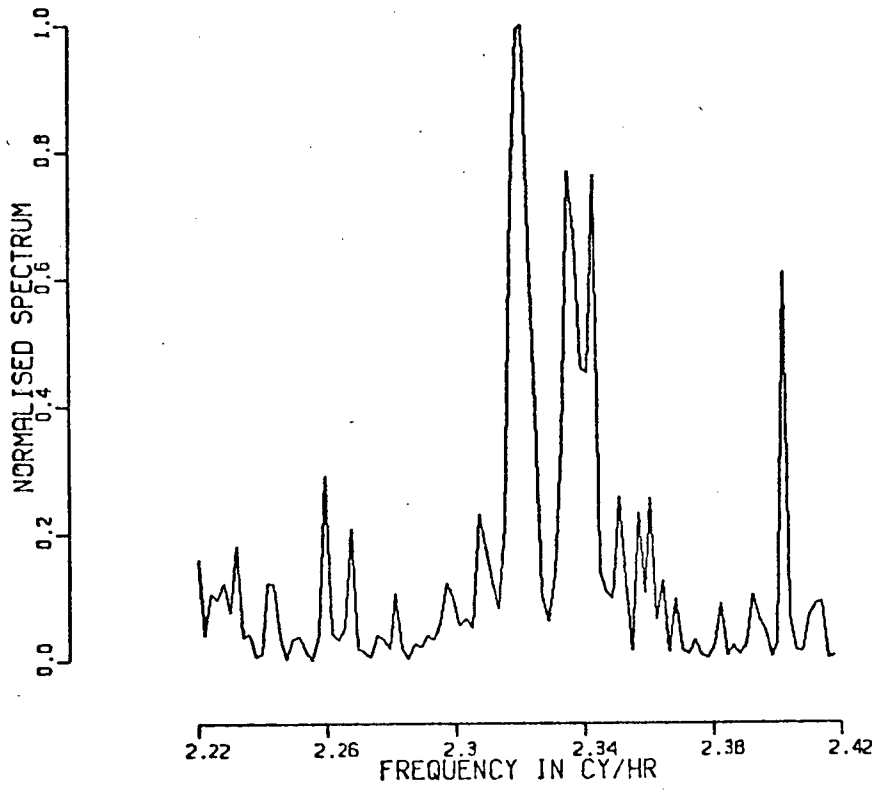


FIGURE 17a

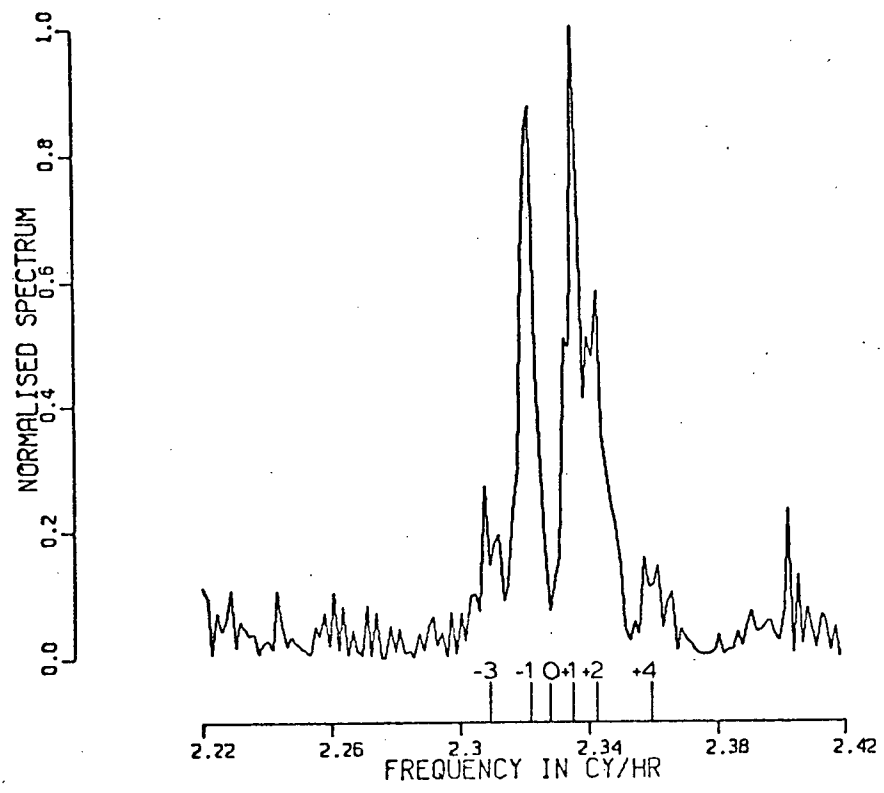


FIGURE 17b

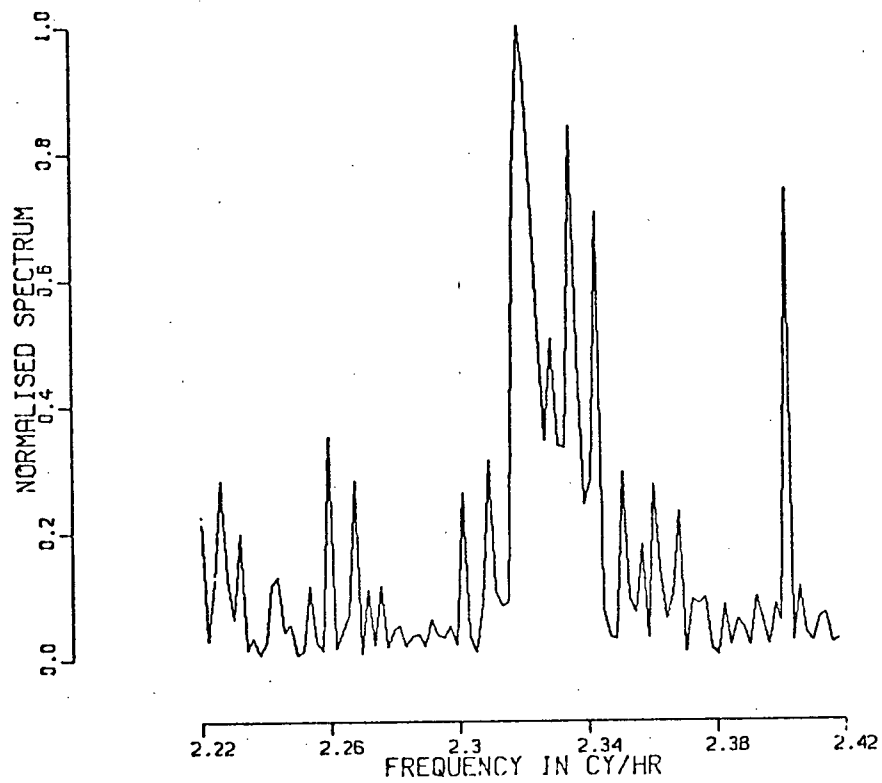


FIGURE 17c

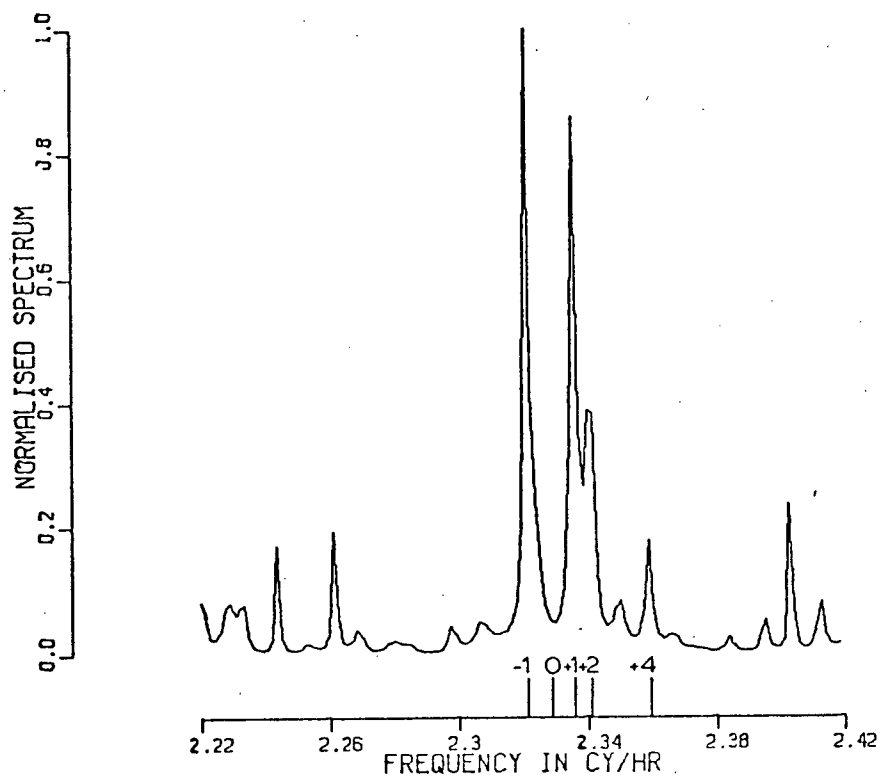


FIGURE 17d

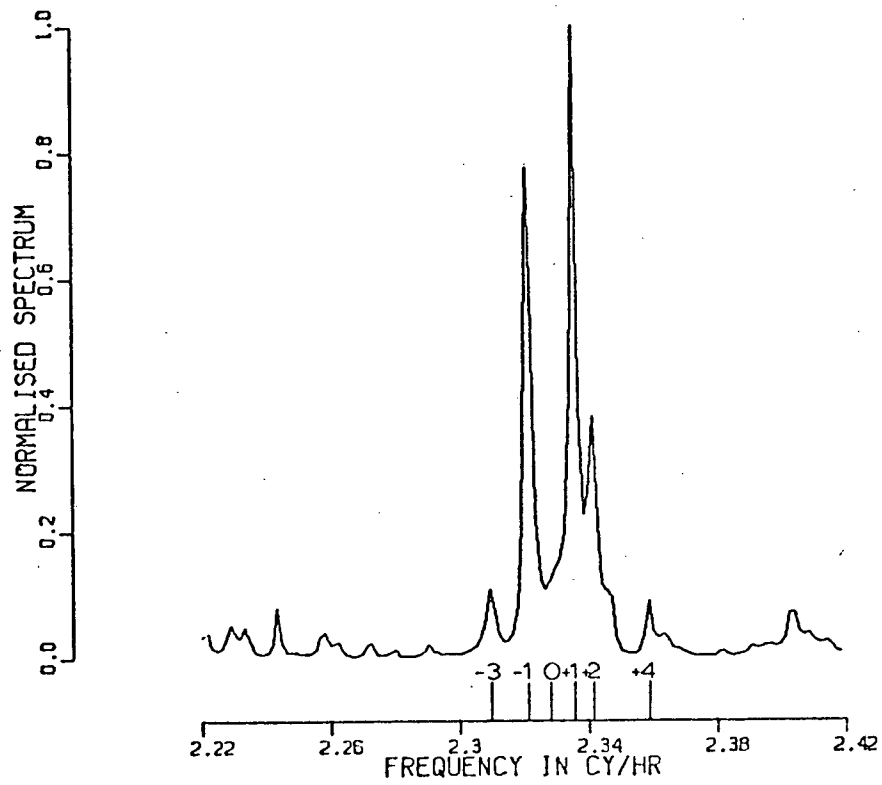


FIGURE 17e

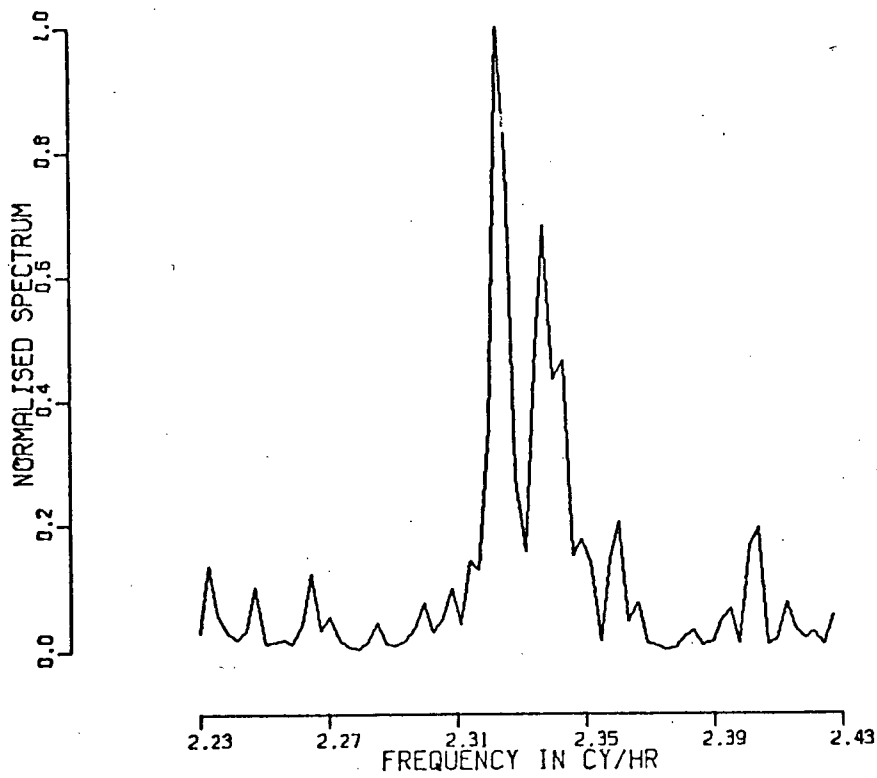


FIGURE 17f

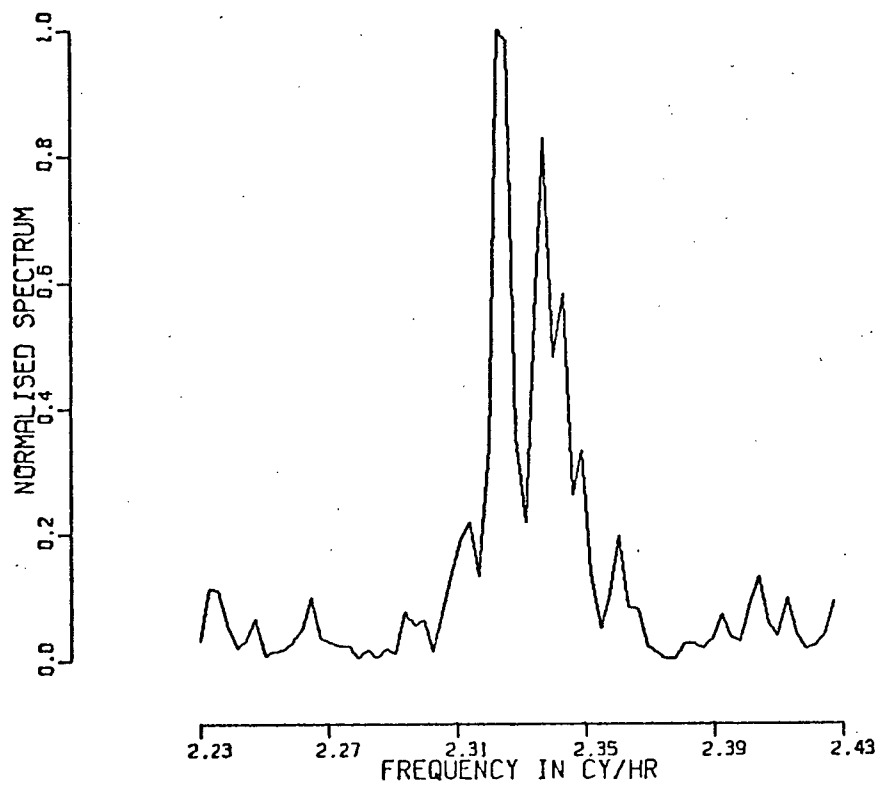


FIGURE 17g

Gilbert and Backus (1965) is 2.335 cycles per hour and Derr (1969) gave a value of 2.327 cycles per hour. Derr also gave a value of .103 for the splitting parameter which is smaller than the value of .161 obtained here.

D. ${}_0S_5$ mode

The periodogram power spectra for the undeglitched and deglitched high passed data are shown in Figures 18a and 18b. There is a noticeable improvement in the signal to noise ratio, but identification of individual peaks remains a difficult matter. In all the spectra observed, two major symmetrical splits were observed, and it is believed that these are blended +1, +2, +3 and -1, -2, and -3 spectral lines, which are not properly resolved. Therefore, for the ${}_0S_5$ mode, only the 'm=0' frequency was determined, and it was taken as the midpoint of the two major peaks on each spectrum examined.

Figure 18c is the MEM (order=130) spectrum of the undeglitched data set and Figure 18d shows the corresponding MEM (order=130) spectrum for the deglitched data. The noise reduction due to deglitching is evident in the MEM spectra as well as the periodograms. Figure 18e is the periodogram power for a 760 point undeglitched data segment. The observed frequencies for the ${}_0S_5$ mode are listed in Table #4.

TABLE #4

Periodogram 5320 Points Undeglitched 18a
freq. (cy/hr)

0 3.028 ± .002

Periodogram 5320 Points Deglitched 18b
freq. (cy/hr)

0 3.027 ± .002

MEM order=130 5320 Points Undeglitched 18c
freq. (cy/hr)

0 3.029 ± .002

MEM order=130 5320 Points Deglitched 18d
freq. (cy/hr)

0 3.028 ± .002

Periodogram 760 Points Undeglitched 18e
freq. (cy/hr)

0 3.028 ± .002

Average Values from MEM spectra
freq. (cy/hr)

0 3.029 ± .002

This average value for the centre frequency of the o_{S_5} mode compares with that of 3.034 cycles per hour given by Gilbert and Backus (1965) and 3.027 cycles per hour given by Derr (1969).

FIGURE 18

- | | | | |
|----|---------------|-------------|--------------|
| a. | Periodogram | 5320 points | Undeglitched |
| b. | Periodogram | 5320 points | Deglitched |
| c. | MEM order=130 | 5320 points | Undeglitched |
| d. | MEM order=130 | 5320 points | Deglitched |
| e. | Periodogram | 760 points | Undeglitched |

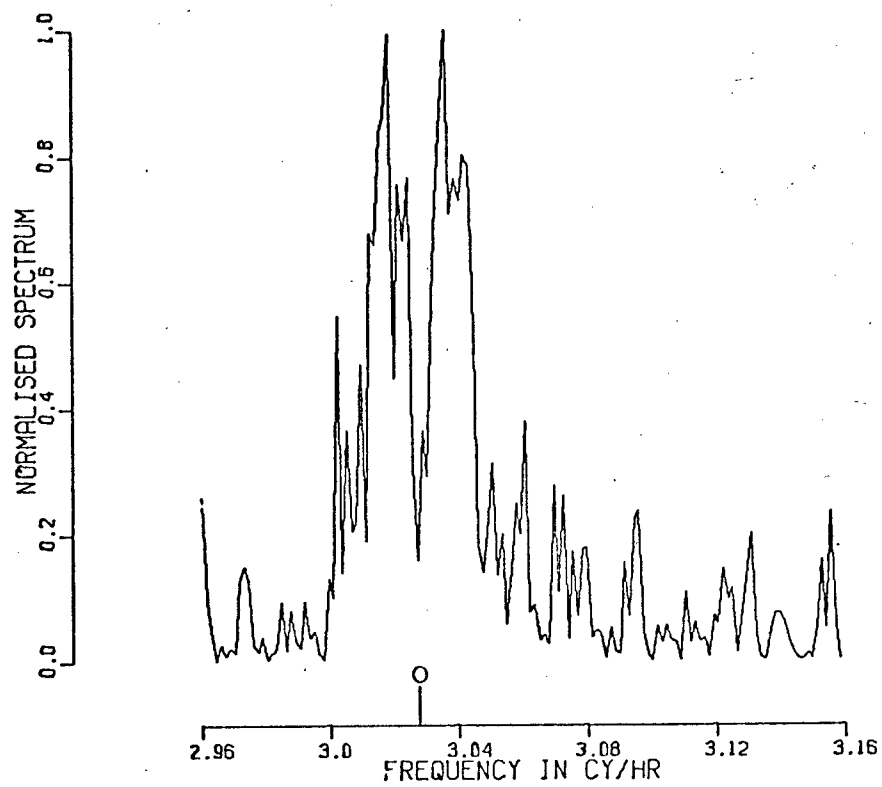


FIGURE 18a

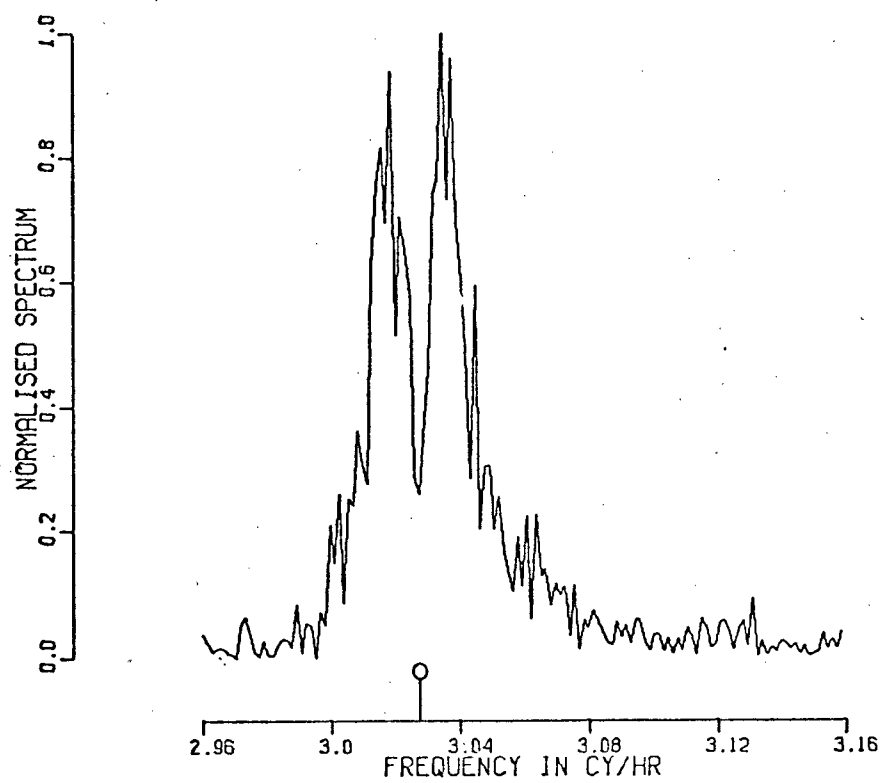


FIGURE 18b

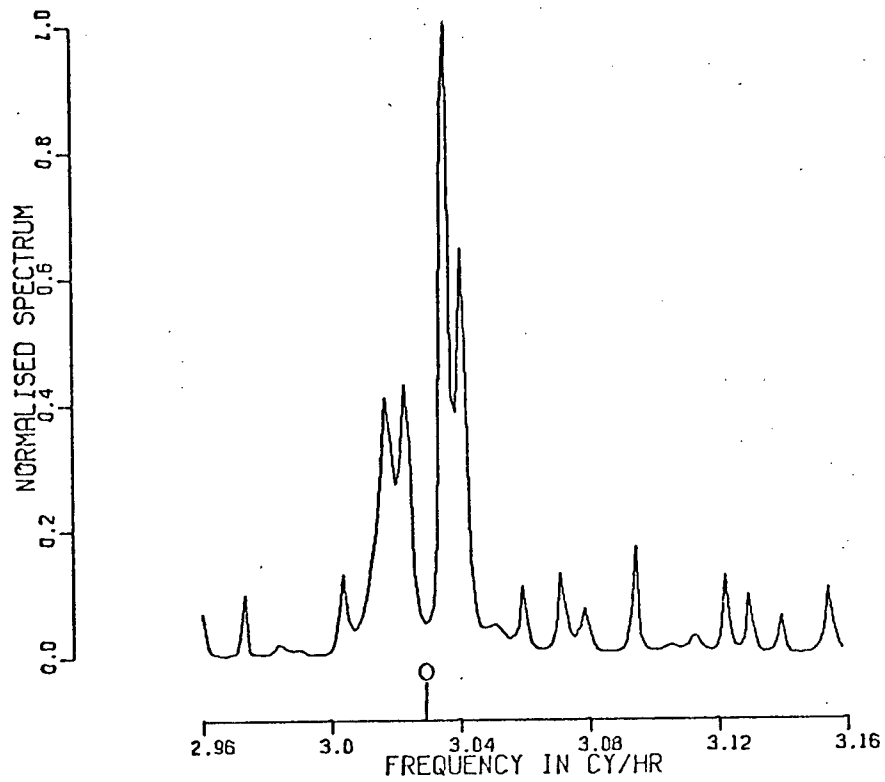


FIGURE 18c

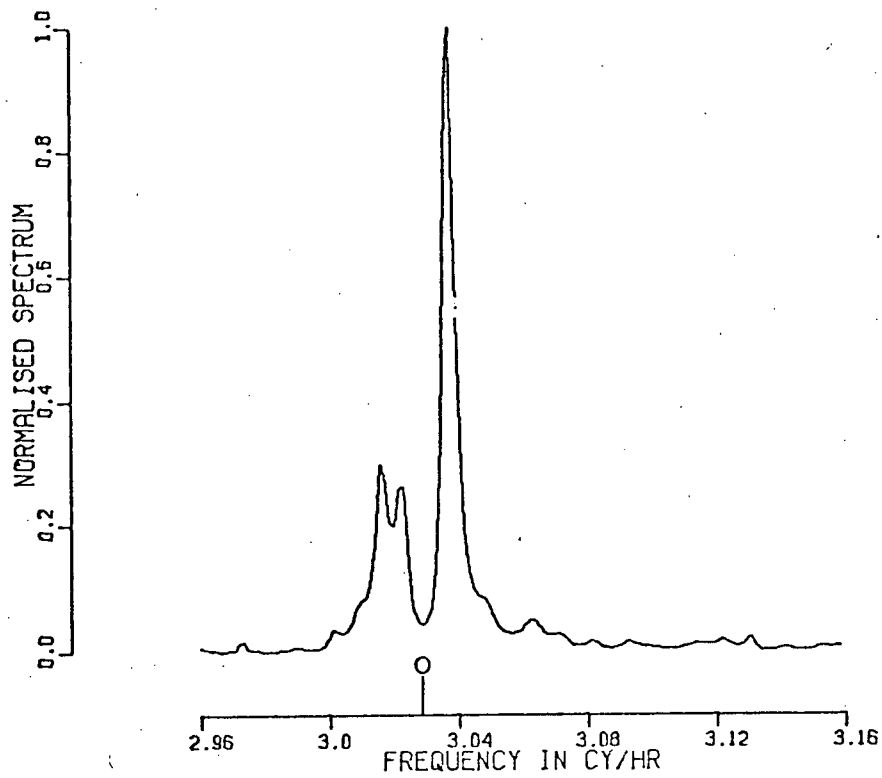


FIGURE 18d

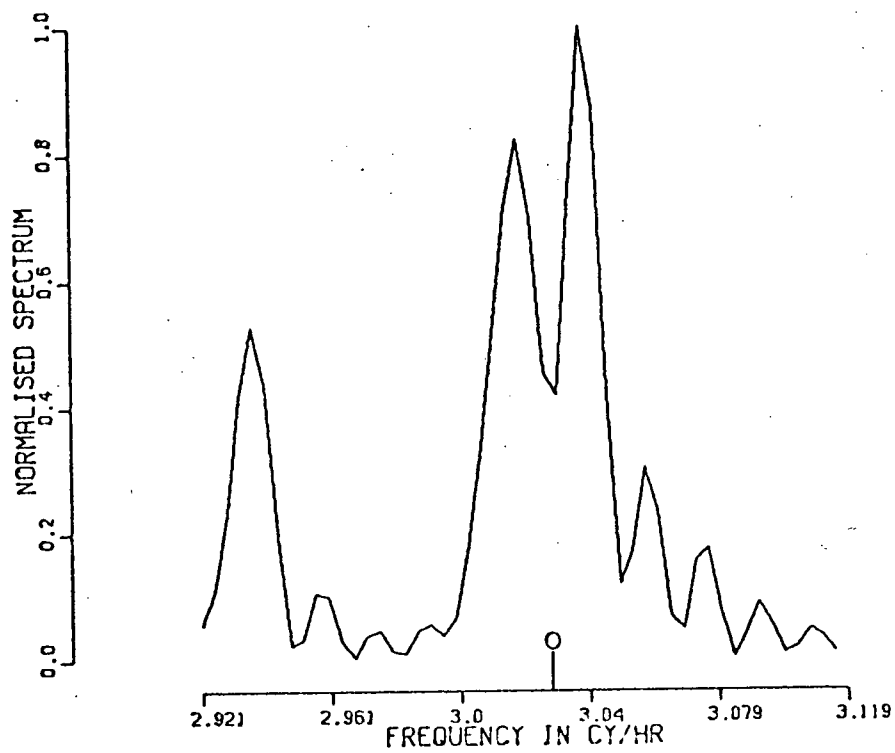


FIGURE 18e

E. ${}_0S_6$ mode

Figures 19a and 19b show the periodogram power spectra of the undeglinted and deglinted high passed data. The noise reduction due to removing the glitches is not as noticeable as for other free oscillation modes. There is some evidence for splitting in the deglinted spectrum, but the splitting number cannot be determined. Figures 19c and 19d are MEM power spectra for the undeglinted (order=110) and deglinted (order=55) records. The high resolution capability of MEM is illustrated in Figures 19e and 19f. The first is a plot of the periodogram power of a 760 point undeglinted data segment, and the second is an MEM (order=10) spectrum for the same data segment. The increased resolution is quite obvious. Table #5 gives the observed values for the ${}_0S_6$ center frequency.

TABLE #5

Periodogram 5320 Points Undeglinted 19a
freq. (cy/hr)

0 3.739 ± .004

Periodogram 5320 Points Deglinted 19b
freq. (cy/hr)

0 3.739 ± .004

MEM order=110 5320 Points Undeglitched 19c
freq. (cy/hr)

0 3.740 ± .001

MEM order=55 5320 Points Deglitched 19d
freq. (cy/hr)

0 3.740 ± .001

Periodogram 760 Points Undeglitched 19e
freq. (cy/hr)

0 3.738 ± .003

MEM order=10 760 Points Undeglitched 19f
freq. (cy/hr)

0 3.743 ± .001

Average Values from MEM spectra
freq. (cy/hr)

0 3.741 ± .002

This average value compares with the value of 3.749 cycles per hour given by Gilbert and Backus (1965) and 3.735 cycles per hour given by Derr (1969).

2. CORE UNDERTONES

A further goal of this thesis was to see if the deglitching of the band passed Alaska record could result in the identification of any free oscillation's of the earth's inner core. The period range studied was restricted to between 0.833 and 8.333 hours. 8.333 hours was chosen as the lower cutoff period, as it was felt that the overpowering

FIGURE 19

a.	Periodogram	5320 points	Undeglitshed
b.	Periodogram	5320 points	Deglitched
c.	MEM order=110	5320 points	Undeglitshed
d.	MEM order=55	5320 points	Deglitched
e.	Periodogram	760 points	Undeglitshed
f.	MEM order=10	760 points	Undeglitshed

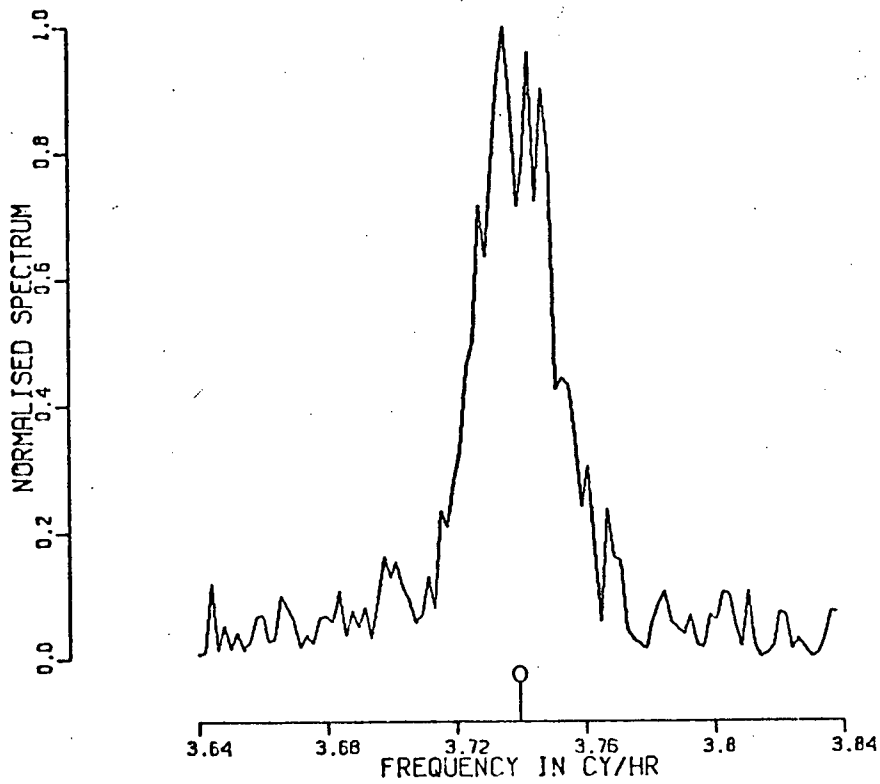


FIGURE 19a

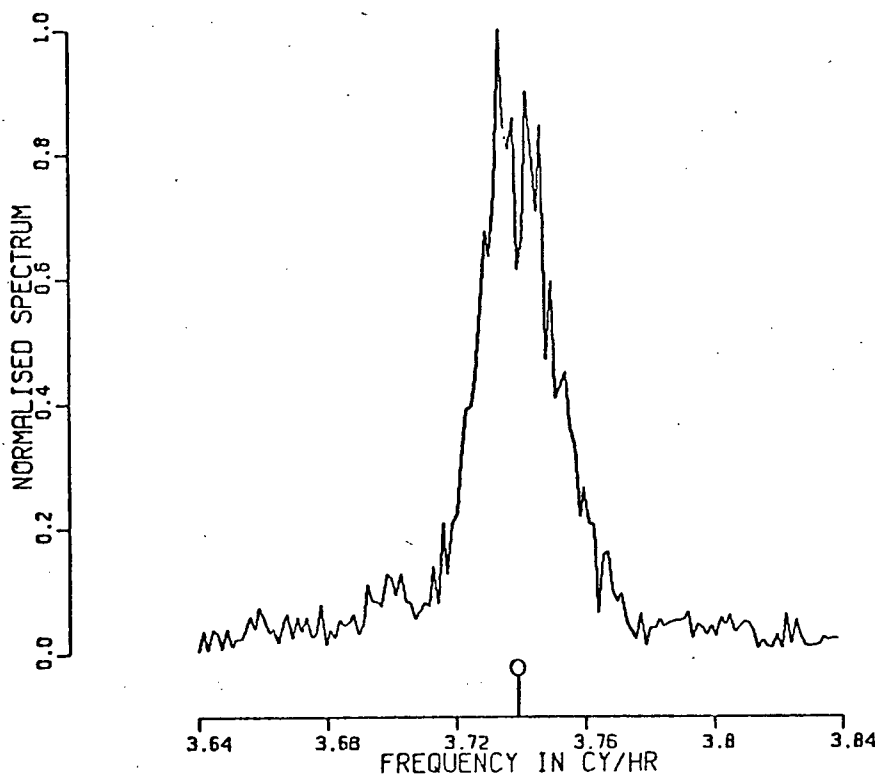


FIGURE 19b

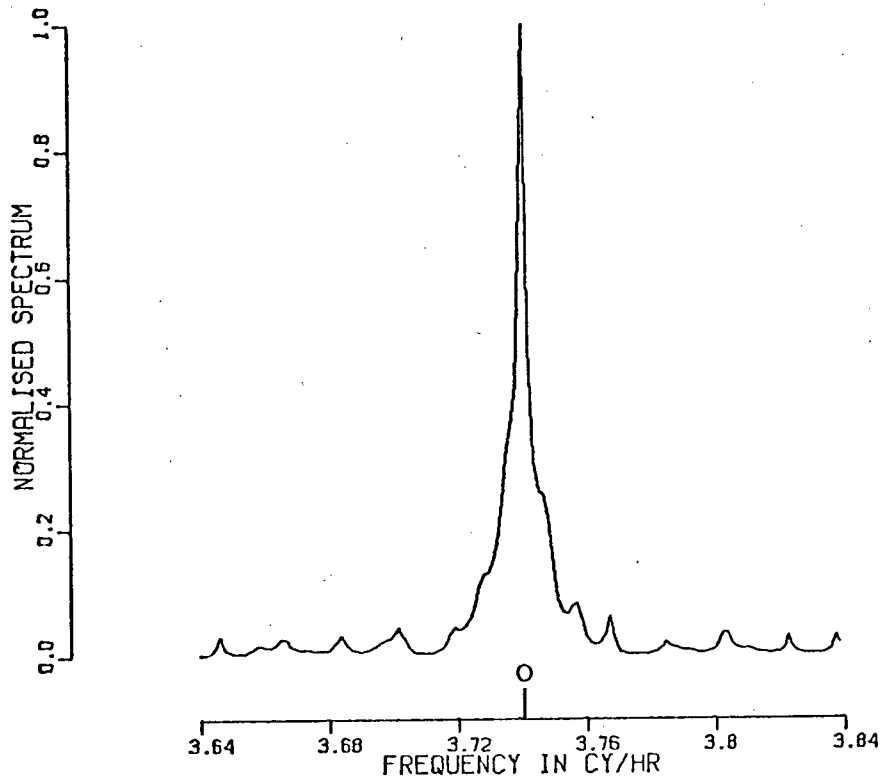


FIGURE 19c

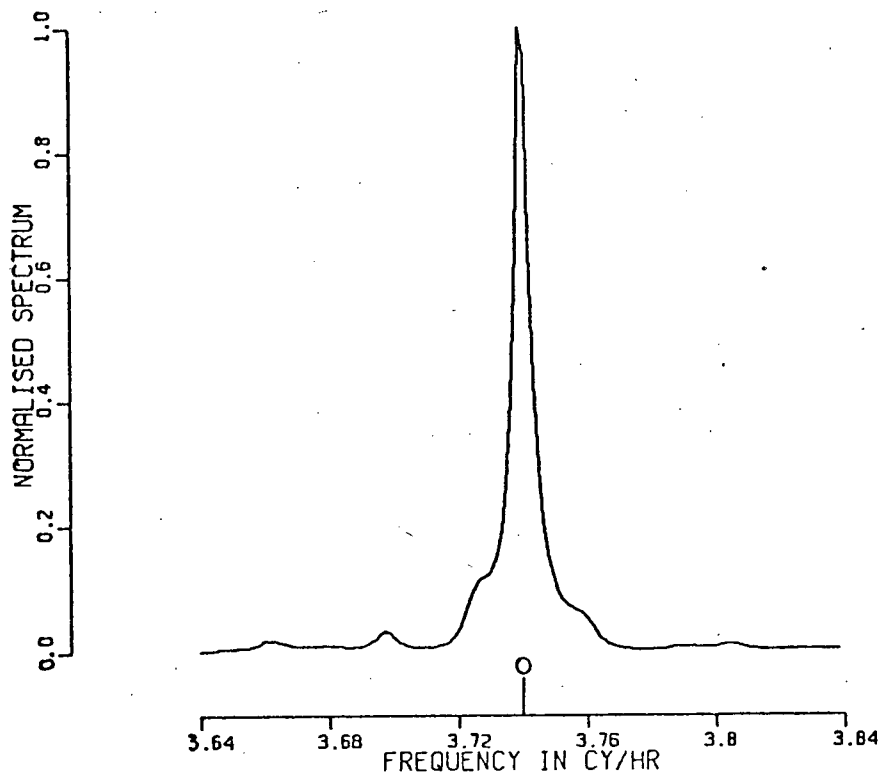


FIGURE 19d

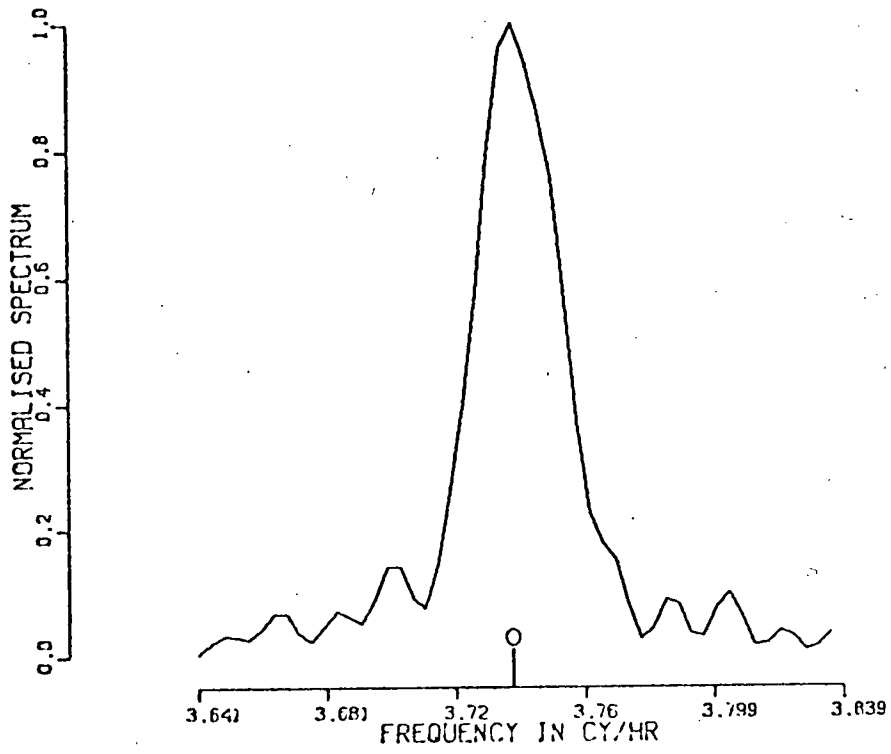


FIGURE 19e

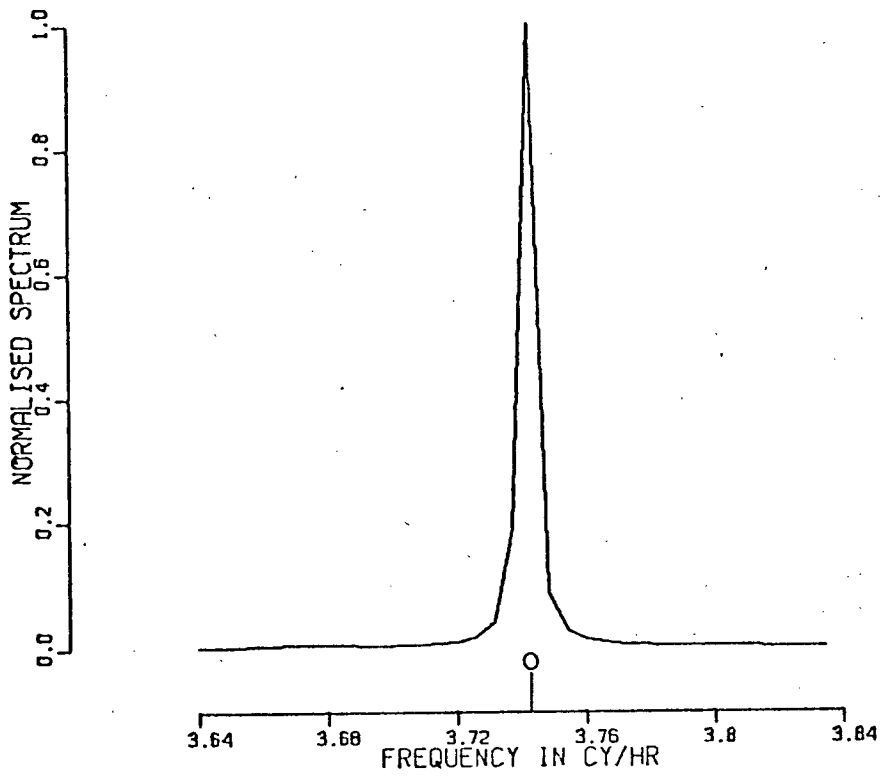


FIGURE 19f

presence of the diurnal and the semidiurnal tides would contaminate the record at longer periods.

The predicted interpolated record was bandpassed and conventional, unsmoothed periodogram power spectra were calculated both before and after removing the glitches. Figures 20 and 21 show the spectra for the undeglinted and deglinted records respectively. The location of the S mode is marked at the upper end of the frequency scale. Removing the noise bursts in the time domain resulted in an amazing reduction in the noise power in the frequency domain especially, at the lower frequencies. There are noticeable peaks in both spectra, but they become much more obvious in the spectrum of the deglinted record. The periods of these unexpected peaks are exact integer multiples of the basic lunar and solar tide, and extend up to about 0.65 cycles per hour.

An initial reaction was that these peaks were some tidal overtone effect, such as shallow water tides found in harbours and basins. However, it is very doubtful that these high order ocean tide effects will be detected by a land based gravimeter. Because of the high amplitudes of these peaks relative to σ_{S_2} , it is even more unlikely that they represent core undertone oscillations. The most reasonable explanation is that they are due to either instrument nonlinearities, or barometric pressure effects, such as those reported by Warburton et al. (1975).

The noise power for the undeglinted spectrum goes from

FIGURES 20 AND 21

Periodogram power spectra of both undeglinted (Figure 20) and deglinted (Figure 21) band pass filtered predicted record. The filter cutoffs are at 0.12 and 1.20 cycles per hour. The locations of the oS_2 free oscillation mode and the ter-diurnal tide (M3) are marked.

FIGURE 20

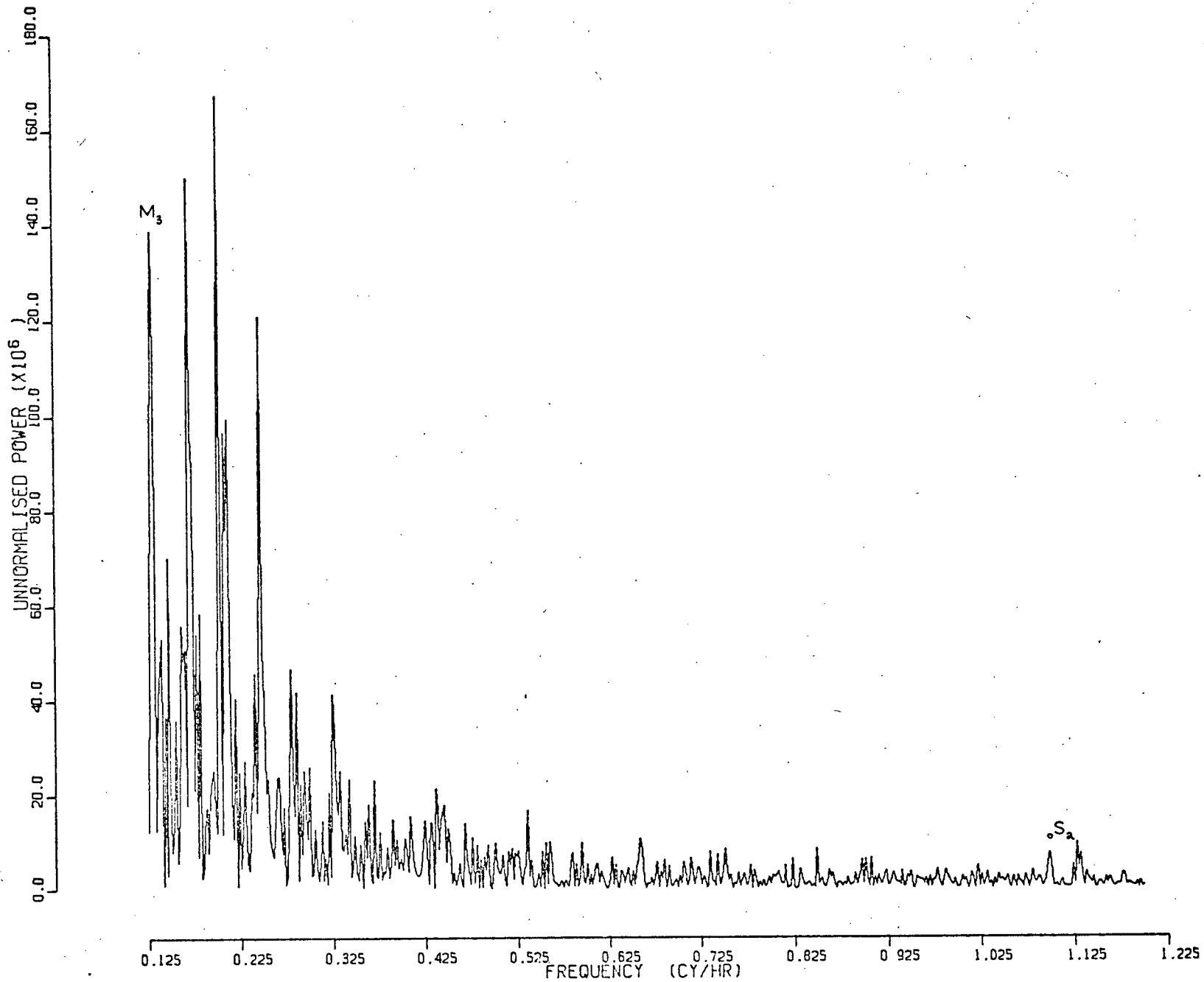
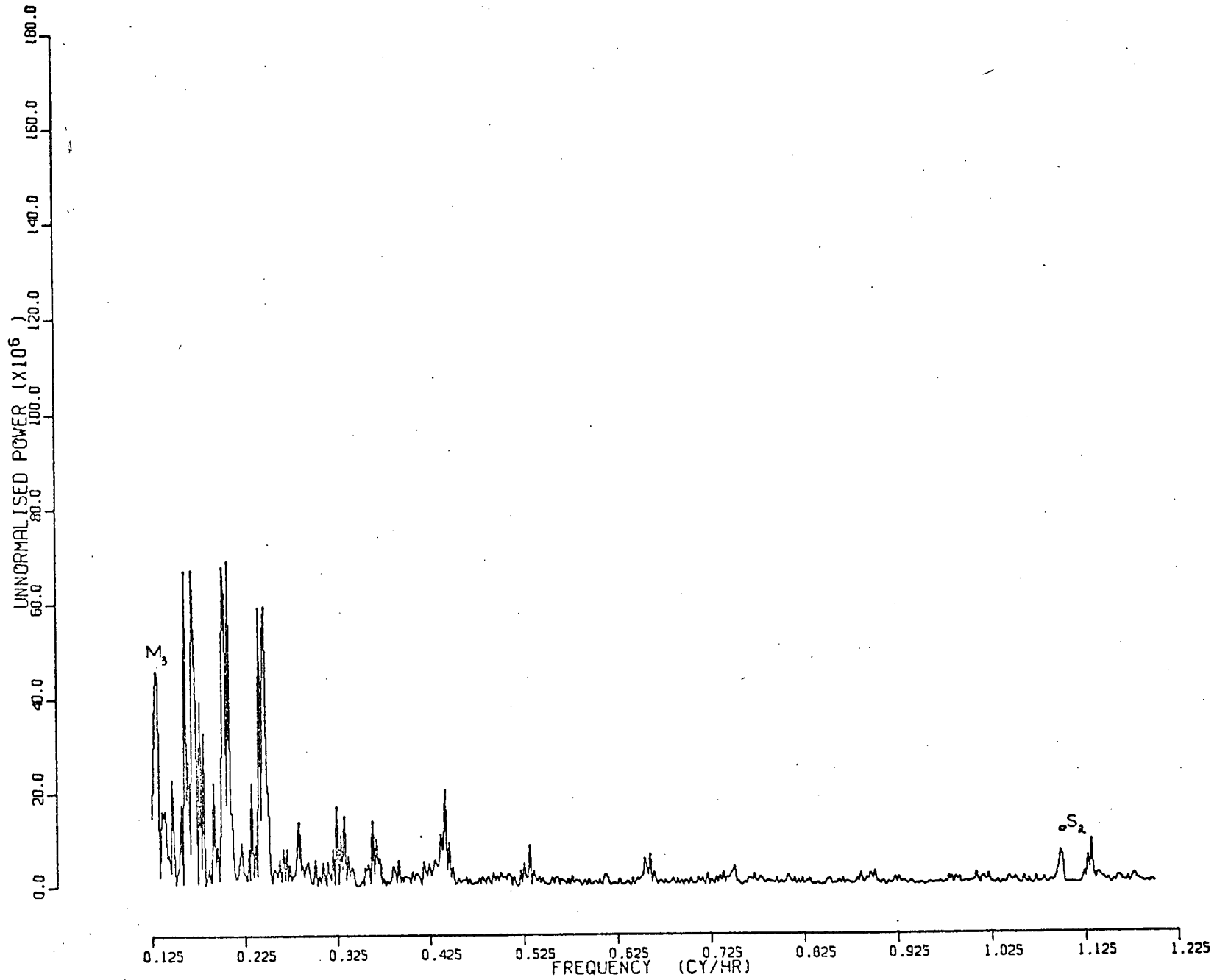


FIGURE 21



40.0 x 10⁶ at .125 Hz. to 5 x 10⁶ at .725 Hz. The noise power for the deglitched spectrum goes from 12 x 10⁶ at .125 Hz. to 2 x 10⁶ at .725 Hz. This drop in noise power is 5.2 db. at .125 Hz. and 4.0 db. at .725 Hz.

V. SUMMARY

A tidal gravimeter recording from the 1964 Alaska earthquake was subjected to various data processing techniques in an attempt to improve the quality of the record. An effort was also made to try and locate core undertone oscillations. The findings of this project can be summarized as follows:

1. A time adaptive prediction error trace provides a useful tool for identifying and locating noise bursts in time series
2. The method of removing the unwanted noise by predictive deglitching, results in an excellent improvement of the signal to noise ratio of this data set.
3. The maximum entropy method of spectral estimation gives some excellent results for the power spectra of various free oscillation modes. Unfortunately, estimation of the length of the filter operator required in the spectral calculation remains a difficult task. Prior knowledge of the spectrum through a conventional spectral technique, is very useful in aiding in the determination of the optimum filter order.

4. In several instances, the maximum entropy method of spectral estimation gave good results for the splitting of various free oscillation modes. Certainly more split peaks were observed using MEM as opposed to the periodogram approach. The central frequencies for the ${}_0S_2$, ${}_0S_3$, ${}_0S_4$, ${}_0S_5$, and the ${}_0S_6$ modes are 1.115, 1.686, 2.328, 3.029, and 3.741 cycles per hour respectively. The splitting parameters for the ${}_0S_2$, ${}_0S_3$, and ${}_0S_4$ modes are .439, .177, and .161.

5. No evidence for core undertones was discovered during the analysis of the band pass filtered record. The frequency band below 0.12 cycles per hour is strongly dominated by tidal frequencies, and the band from 0.12 to 0.65 cycles per hour is dominated by either instrument non-linearities or barometric pressure effects.

REFERENCES

- Akaike, H. 1969. Power spectrum estimation through autoregressive model fitting. Ann. Inst. Statist. Math., Vol. 21, p. 407.
- Akaike, H. 1970. Statistical predictor identification. Ann. Inst. Statist. Math., Vol. 22, p. 203.
- Alsop, A. L., G. H. Sutton, and M. Ewing. 1961. Measurement of Q for very long period free oscillations. J.G.R., Vol. 66, p. 631.
- Alterman, Z. S., Y. Eyal, and A. M. Merzer. 1974. On free oscillations of the earth. Geophysical Surveys, Vol. 1, p. 409.
- Backus, G. and F. Gilbert. 1961. The rotational splitting of the free oscillations of the earth. Proc. Nat. Acad. Sci. U.S.A., Vol. 47, p. 362.
- Backus, G. and F. Gilbert. 1967. Numerical applications of a formalism for geophysical inverse problems. Geophysic. Jour. Roy. astr. Soc., Vol. 13, p. 277.
- Benioff, H. F., B. Gutenberg, and C. F. Richter. 1954. Progress report, Seismological Laboratory, California Institute of Technology. Trans. Am. Geophys. Un., Vol. 35, p. 979.
- Benioff, H. F., F. Press, and S. Smith. 1961. Excitation of the free oscillations of the earth. J.G.R., Vol. 66, p. 605.
- Bogert, B. P. 1961. An observation of free oscillations of the earth. J.G.R., Vol. 66, p. 643.
- Bolt, B. A., and R. G. Currie. 1975. Maximum entropy estimates of earth torsional eigenperiods from 1960 Trieste data. Geophysic. Jour. Roy. astr. Soc., Vol. 40, p. 107.
- Burg, J. P. and D. C. Riley. 1971. Time and space adaptive deconvolution filter. S.E.G., Preprint.
- Burg, J. P. 1972. The relationship between maximum entropy and maximum likelihood spectra. Geophysics, Vol. 37, p. 375.
- Burg, J. P. 1975. Maximum entropy spectral analysis. Unpublished Ph.D. Thesis, Stanford.

- Childers, D. G. and Min-Tai Pao. 1972. Complex demodulation for transient wavelet detection and extraction. I.E.E.E. Trans. on Audio and Electroacoustics, Vol. AU-20, p. 295
- Crossley, D. J. 1975. Core undertones with rotation. Geophysic. Jour. Roy. astr. Soc., Vol. 42, p. 200.
- Derr, J. S. 1969. Free oscillation observations through 1968. Bull. Seism. Soc. Am., Vol. 59, p. 2079.
- Dziewonski, A. M. and F. Gilbert. 1973. Observations of normal modes from 84 recordings of the Alaskan earthquake of 1964 March 28. Geophysic. Jour. Roy. astr. Soc., Vol. 35, p. 401.
- Gersch, W. 1970. Estimation of the autoregressive parameters of a mixed autoregressive moving average time series. I.E.E.E. Trans. on Automatic Control, Vol. AC-18, p. 267.
- Gilbert, F. and G. Backus. 1965. The rotational splitting of the free oscillations of the earth. Reviews of Geophysics, Vol. 3, p. 1.
- Haddon, R. A. and K. E. Bullen. 1967. Derivation of an earth model from free oscillation data. Proc. Nat. Acad. Sci. U.S.A., Vol. 58, p. 846.
- Jackson, B. V. and L. B. Slichter. 1974. The residual daily earth tides. J.G.R., Vol. 79, p. 1711.
- Lacoss, R. T. 1971. Data adaptive spectral analysis methods. Geophysics, Vol. 36, p. 661.
- Lamb, H. 1882. Proc. Math. Soc., Vol. 13, p. 189.
- Love, A. E. H. 1911. Some problems of geodynamics, Cambridge University Press, Cambridge.
- Ness, N. F., J. C. Harrison, and L. B. Slichter. 1961. Observations of the free oscillations of the earth. J.G.R., Vol. 66, p. 62.
- Press, F. 1968. Earth models obtained by Monte Carlo inversion. J.G.R., Vol. 73, p. 5223.
- Shannon, C. E. 1948. A mathematical theory of communication. Bell. Syst. Tech. Jour., Vol. 27, p. 379.

- Slichter, L. B. 1961. The fundamental free mode of the earth's inner core. Proc. Nat. Acad. Sci. U.S.A., Vol. 47, p. 186.
- Slichter, L. B. 1967a. Free oscillations of the earth. Dictionary of Geophysics, ed. S. K. Runcorn, Pergamon Press, Oxford.
- Slichter, L. B. 1967b. Spherical oscillations of the earth. Geophysic. Jour. Roy. astr. Soc., Vol. 14, p. 171.
- Smith, M. L. 1974. The normal modes of a rotating elliptical earth. Ph.D. Thesis, Princeton.
- Ulrych, T. J., D. E. Smylie, O. Jensen, and G. K. Clarke. 1973. Predictive filtering and smoothing of short records by using maximum entropy. J.G.R., Vol. 78, p. 4959.
- Ulrych, T. J., and T. N. Bishop. 1975. Maximum entropy spectral analysis and autoregressive decomposition. Reviews of Geophysics and Space Physics, Vol. 13, p. 183.
- Ulrych, T. J., and R. W. Clayton. 1975. Time series modelling and maximum entropy. Preprint.
- VandenBos, A. 1971. Alternative interpretation of maximum entropy spectral analysis. I.E.E.E. Trans. Inform. Theory (Corresp.), Vol. IT-17, p. 493.
- Warburton, R. J., C. Beaumont, and J. M. Goodkind. 1975. The effect of ocean tide loading on tides of the solid earth observed with the superconducting gravimeter. Geophysic. Jour. Roy. astr. Soc., Vol. 43, p. 707.
- Weiner, N. 1930. Generalized harmonic analysis. Acta. Math., Vol. 55, p. 117.
- Wiggins, R. A., and S. P. Miller. 1972. New noise reduction technique applied to long period oscillations from the Alaskan earthquake. Bull. Seism. Soc. Am., Vol. 62, p. 471.

APPENDIX 1

Fortran source listing of the time adaptive maximum entropy deconvolution scheme.

SUBROUTINE BAFL(LOUT,CX,IFLGAP,LCN,NWARM,ISTR,ZTAU,XTAU,NZERO)

```

C-----SUBROUTINE BAFL-----
C
C   THE BURG ADAPTIVE FILTER LADDER: AN ADAPTIVE OR TIME
C   VARYING FIXED LEAD PREDICTION ERROR PROCESSOR
C   ADJUSTMENT OF EACH REFLECTION COEFFICIENT IS MADE EVERY
C   JUMP STATE ATTEMPTING TO MINIMIZE THE STAGE OUTPUT POWER
C
C   INPUTS
C       X(LX)=INITIAL DATA
C       LCN=LAST NON-ZERO REFLECTION COEFF.
C       IFLGAP=NUMBER OF GAPS BETWEEN FILTER COEFFICIENTS
C       SETTING IFLGAP=1 DOES NOT GAP THE SPECTRUM AND TRIES
C       TO OPERATE ON THE ENTIRE SPECTRUM.
C       NWARM=DURATION OF STATIONARY CYCLE
C       ISTRT=START OF STATIONARY GATE
C       ZTAU=TEMPORAL RELAXATION FACTOR
COMMON /BLK3/X(1774)
C       XTAU=SPATIAL RELAXATION FACTOR
C
C   OUTPUTS
C
C       X(LOUT)=FORWARD ERROR PREDICTION TRACE
C       C(LCN)=FORWARD STATE VECTOR
C       B(LCN)=BACKWARD STATE VECTOR
C       C(LCN)=REFLECTION COEFF. AT EACH STAGE
C       CX=REFLECTION COEFF. INTEGRATED IN SPACE AND TIME
C       DEN(LCN) = STAGE AUTOPOWER
C       NUM(LCN) = STAGE CROSSPOWER
C
C   CALLING BAFL FIRST SETS UP THE LOOPING AND PASSING
C   ARRAYS FOR THE PARTICULAR PROBLEM AS SPECIFIED BY
C   LCN&IFLGAP. THEN IT COMPUTES A SHORT(LENGTH=NWARM) ESTIMATE
C   OF THE REFLECTION COEFF. SERIES IN ORDER TO START THE
C   ADAPTION OUT WITH SOME REASONABLE NUMBERS
C   THEN IT LOADS UP THE CX ARRAY WITH THE INITIAL VALUES
C   AND PASSES INTO ENTRY 'BAFLGO'
C   THE USUAL ENTRY IS BAFLGO WHICH FIRST INITIALIZES THE
C   BACKWARD ARRAY THEN PASSES TO THE MAIN ROUTINE
C   THE CX SERIES IS UPDATED EVERY IFLGAP DATA POINTS AND IN THE
C   INTERMEDIATE STEPS THE OUTPUT ARE INTERPOLATED OF PROCESSED
C   AS THOUGH THE R.C. WERE STATIONARY
C   WRITTEN BY J.P. BURG
REAL NUM(200),DEN(200),B(200),F(200),C(200),EM(2000),
*EP(2000),CX(LCN,LOUT),A(200)
DATA A,B,C/600*0./
FTEST=1.
LCNP1=LCN+1
LCNP2=LCN+2
IFGM1=IFLGAP-1
LBSP=LOUT-IFLGAP
NZERP1=NZERO+1
NEND=LCN-NZERP1
DO 80 K=LBSP,LOUT
EP(K) = 0.

```

```

C          BEGIN STATIONARY WARMUP
DO 10 I=1,NWARM
EM(I) = X(I*IFLGAP+ISTRN)
10 EP(I) = X(I*IFLGAP+ISTRN)
C
DO 11 J=2,LCNP1
DEN(J) = 0.
NUM(J) = 0.
DO 12 I=J,NWARM
DEN(J) = DEN(J)+EP(I)*EP(I)+EM(I-J+1)*EM(I-J+1)
12 NUM(J) = NUM(J)+EP(I)*EM(I-J+1)
DIV=NWARM-J+1
NUM(J) = NUM(J)/DIV
DEN(J) = DEN(J)/DIV
C(J) = -2.*NUM(J)/DEN(J)
DO 11 I=J,NWARM
EPI=EP(I)
EP(I) = EPI+C(J)*EM(I-J+1)
KS=IFLGAP*LCN+1
11 EM(I-J+1) = EM(I-J+1)+C(J)*EPI
DO 8 J=1,LCN
DO 8 K=1,KS
8 CX(J,K) = C(J+1)
DO 33 J=1,LCN
33 DEN(J) = DEN(J+1)
NUM(J) = NUM(J+1)
C          END WARM UP CYCLE
C          SET RELAXATION TIMES
DLX=EXP(-1./XTAU)
DL=EXP(-1./ZTAU)
DRX=1.-DLX
DR=1.-DL
C
C-----USUAL ENTRY-----
ENTRY BAFLGD
C
C          INITIALIZE BACKWARD VECTOR
B(1) = X(KS-IFLGAP)
A(1)=1.
DO 1000 J=2,LCN
B(J) = X(KS-J*IFLGAP)
A(J) = 0.0
DO 1000 I=2,J
A(I) = A(I)+CX(J,KS)*A(J-I+1)
1000 B(J) = B(J)+A(I)*X(KS+(I-J+1)*IFLGAP)
C
C-----BEGIN MAIN LOCP-----
DO 5000 K=KS,LOUT,IFLGAP
Z=X(K)
DO 1010 J=1,NZERP1
1010 F(J) = Z
DO 2000 J=NZERP1,LCN
DEN(J) = (F(J)**2+B(J)**2)*DR+DEN(J)*DL

```

```

NUM(J) = F(J)*B(J)*DR+NUM(J)*DL
IF(FTEST.LE.1.1) CX(J,K)=-2.*NUM(J)/DEN(J)
CX(J,K) = -2.*DRX*NUM(J)/DEN(J)+CX(J,K)*DLX
2000 F(J+1) = F(J)+CX(J,K)*B(J)
X(K) = F(LCNP1)
DO 3000 JR=1,NEND
J=LCN-JR
3000 B(J+1)=B(J)+CX(J,K)*F(J)
IF(NZERO.EQ.0) GO TO 5000
DO 4000 JR=1,NZERO
J=NZERPI-JR
4000 B(J+1) = B(J)
5000 B(1)=Z
C
C-----END OF MAIN LOOP-----
C
C      NOW GO BACK TO FILL IN THE GAPS
IF(IFLGAP.EQ.1) GO TO 9050
DO 9000 L=1,IFGM1
KSTART=KS+L
DO 9000 K=KSTART,LOUT,IFLGAP
KC=K-L
Z=X(K)
DO 6000 J=1,NZERPI
6000 F(J) = Z
DO 7000 J=NZERPI,LCN
7000 F(J+1) = F(J)+CX(J,KC)*B(J)
X(K) = F(LCNP1)
DO 8000 JR=1,NEND
J=LCN-JR
8000 B(J+1) = B(J)+CX(J,KC)*F(J)
IF(NZERO.EQ.0) GO TO 9000
DO 8050 JR=1,NZERO
J=NZERPI-JR
8050 B(J+1) = B(J)
9000 B(1) = Z
9050 FTEST=FTEST+1.
RETURN
END

```